SESSION 2

CLEANING CHEMICAL PROCESSING EFFLUENTS

MONDAY: August 22, 1988
CHAIRMEN: R.T. Jubin
K.S. Murthy

MODELLING OF A SELECTIVE ABSORPTION PROCESS FOR RARE GAS REMOVAL FROM REPROCESSING OFFGAS

J. Römer, E. Henrich
Kernforschungszentrum Karlsruhe, Institut für Heisse Chemie
Federal Republic of Germany

Abstract

A mathematical model for a selective absorption process for rare gas recovery from the dissolver offgas will be presented.

The process is a conventional gas absorption-desorption procedure using circulating CCl_2F_2 solvent at cryogenic temperatures. A high product purity is achieved with an additional intermediate stripping step for the removal of coabsorbed carrier gases.

The mathematical model is based on the stage theory. The absorber and the final desorber can be described by simple equations, because the operating conditions are constant over the packed length. For the intermediate stripper the whole system of material and energy balance equations has to be solved for each stage. An iterative procedure has been developed, which allows the determination of flow and concentration profiles for each gas component. A selfconsistent temperature profile terminates the iteration.

The model requires experimental distribution data of the various gas components, operating conditions and design parameters such as the number of stages in the packed zones, which must be determined experi-mentally. Optimum operation conditions have been predicted by the model and verified in the pilot plant.

I. Description of the Separation Process

The process for the rare gas removal from reprocessing offgas, being developed in our institute, is a conventional gas absorption-desorption process at low temperature and normal pressure. The process and experimental results are described in detail elsewhere.[1]-[4] The solvent is R12, an ordinary refrigerator coolant. Figure 1. shows distribution coefficients of some gases as a function of temperature, ranging from the melting point to the boiling pointof the solvent. The carrier gases, nitrogen and oxygen are much less soluble than the heavy noble gases.

Figure 2. shows a simplified flowsheet of the process. The equip-ment consists of two nearly identical columns. The first column sel-ectively absorbs Xe at suitable temperature (see Fig. 1) and flow ratio in the absorber section. Coabsorbed carrier gas and Kr is de-sorbed in the subsequent intermediate stripper section. In the final stripper Xe is stripped from the solution by boiling. Then the sol-vent is re-cycled through a countercurrent heat exchanger to the top of the absorber. This heat exchanger reduces the cooling energy requirements.

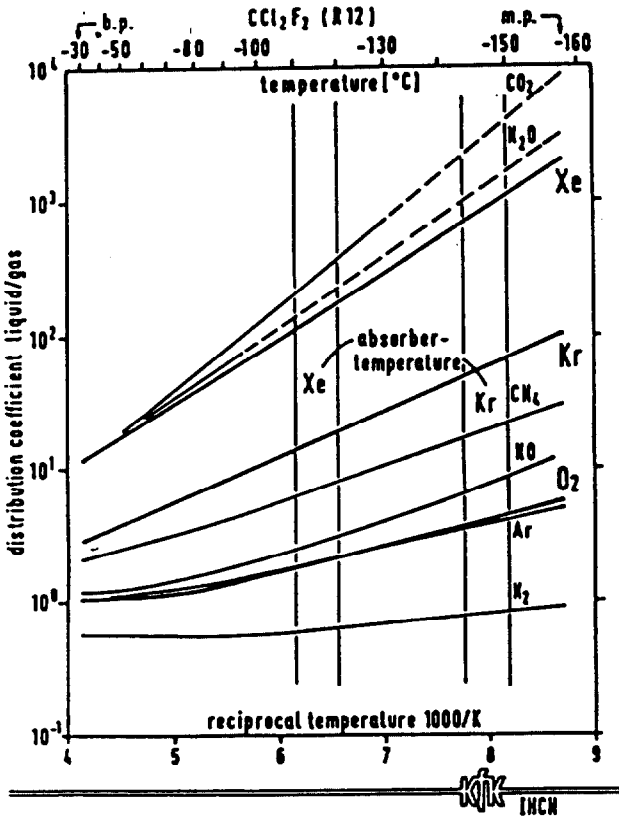

Fig.1 SOLUBILITY OF GASES IN LIQUID R12

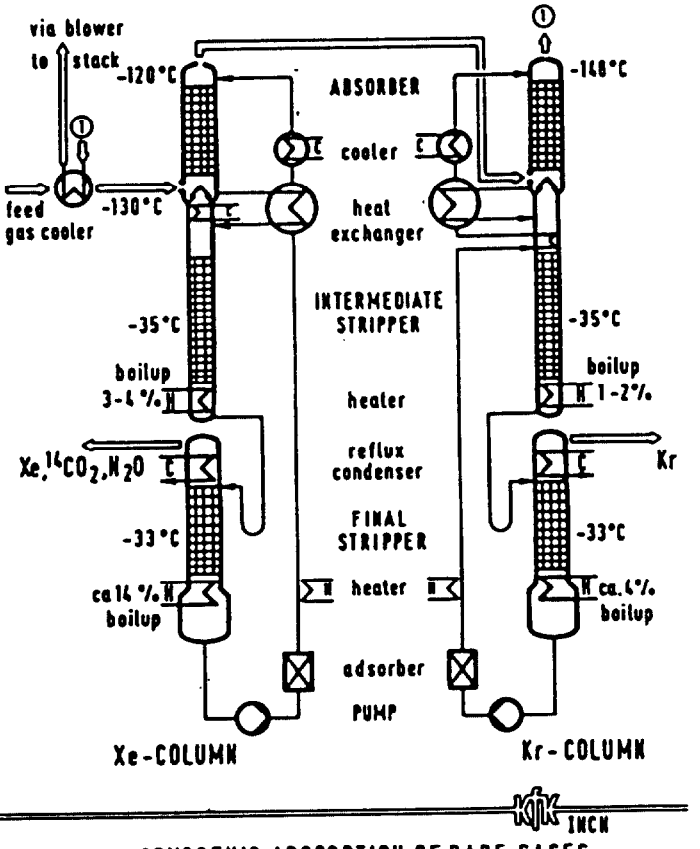

Fig.2 CRYOGENIC ABSORPTION OF RARE GASES SIMPLIFIED PROCESS FLOWSHEET

In the Kr column the same procedure is used for Kr under appropriate operation conditions. The absorber temperature is by 20°C lower and the solvent to gas flow ratio is about four times higher. This is necessary because the distribution coefficient of Kr is lower than that of Xe (Fig. 1). In contrast to the Xe column, the Kr column includes an internal heat exchanger. It acts as a small absorber sec-tion added to the top of the intermediate stripper. Desorbed Kr and the R12-vapor are hindered from reaching the absorber sump. Thus the accu-mulation of Kr and the solvent degradation is reduced and the decon-tamination factor of the column is increased.

II. Mathematical Model

Balance of Material

Stage theory has been used for modelling the process. Figure 3. gives a brief description of the condition in one stage. The basic assumption of stage theory is, that the outcoming streams are in mutual equilibrium. The amount of material exchanged between the in-coming streams is determined by the extraction factor.[1] In the ab-sorber or in the final stripper the extraction factor is nearly equal at all stages. The ratio between the inlet and outlet gas concentration of each component for a column section with n stages is calculated from the so called "Fenske equation".[1]

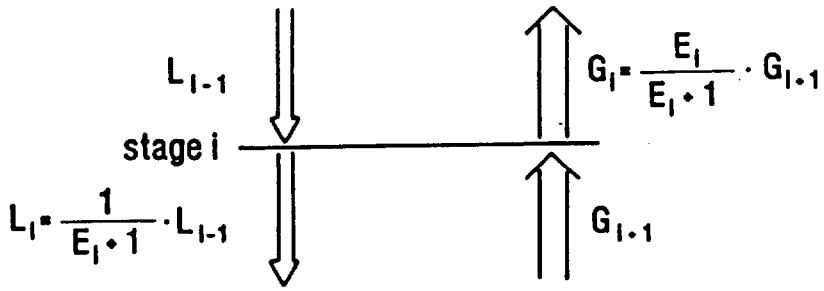

G_i = gas flow
L_i = solvent flow
E_i = extraction factor

$$E_i = \frac{L_i}{G_i} * D$$

Fig. 3 Material Streams in the Liquid and Gas Phase for one Stage

$$\frac{c_{in}}{c_{out}} = \frac{E^{n+1} - 1}{E - 1} \qquad (1)$$

c_{in}, c_{out} = inlet, outlet gas concentration
E = extraction factor

In the intermediate stripper and the internal heat exchanger the extraction factor varies within a broader range. Due to the condensation of a part of solvent vapor the extraction factor decreases from the bottom to the top.

To calculate the concentration profiles in the intermediate stripper, a n*(n+1) dimensioned, linear equation system must be solved for each gas component and each stages. The following equations [2][3] describe the internal stripper. The loaded solvent is introduced at the top and the unloaded solvent vapor stream at the bottom. The sump heater is taken as the lowest stage. The unloaded solvent vapor is introduced formally into this heater stage.

$$L_{j,m} = \frac{1 + E_{j,m+1} + E_{j,m+1} \cdot E_{j,m+2} + \ldots E_{j,m+1} \cdot \ldots E_{j,n}}{1 + E_{j,1} + E_{j,1} \cdot E_{j,2} + \ldots E_{j,1} \cdot \ldots E_{j,n}} \quad (2)$$

$L_{j,m}$ = relative flow of the gas component j from the m-th stage in the solution

$E_{j,m}$ = extraction factor of the component j on the m-th stage

$$G_{j,m} = E_{j,m} \cdot L_{j,m} \quad (3)$$

$G_{j,m}$ =relative flow of the gas component j from the m-th stage in the gas phase

The Balance of Energies

In steady state the energy of the inflowing streams is equal to that of the outflowing streams at each stage. The flow of the stripping vapor is a function of the temperature profile over the packed length. Therefore, a relation exists between the temperature profile and the extraction factor.

The energy balance equations can be simplified under the following assumptions, taking into account the low temperature variation over the packed length of the intermediate stripper:

- The system energy is given relative to the unloaded solvent at boiling temperature under the system pressure.
- The specific heat of the gases and solvent vapor are low compared with the heat of evaporation and can be neclected.
- The specific heat of the loaded solvent is approximately equal to the specific heat of the unloaded solvent, due to the low loading.
- The heat of solution of the gases and the heat of evaporation is constant over the packed length, due to the low variation of the pressure and temperature.

The following equations give the stripping vapor flow for each stage as a function of the evaporation rate, stage temperature and the sum of gas components:[4]

$$
\begin{aligned}
&i=1: && R_1 = R_H - \alpha \cdot [\delta_0 - \delta_n] - \sum_j \beta_j \cdot G_{j,1} \\
&i=2: && R_2 = R_H - \alpha \cdot [\delta_1 - \delta_n] - \sum_j \beta_j \cdot G_{j,2} \\
&i=3: && R_3 = R_H - \alpha \cdot [\delta_2 - \delta_n] - \sum_j \beta_j \cdot G_{j,3} \\
&.... && ..... \\
&i=n: && R_n := R_H - \alpha \cdot [\delta_{n-1} - \delta_n] - \sum_j \beta_j \cdot G_{j,n}
\end{aligned}
\qquad (4)
$$

R_H = rate of evaporation as vapor flow per hour

R_i = vapor flow from the i-th stage

β_j = heat of solution of gas component j normalized to heat of solvent evaporation

δ_i = temperature difference at stage i to the boiling point of the solvent

α = specific heat of the unloaded solvent normalized to heat of evaporation

$G_{j,m}$ = gas flow of component j at stage m

The total gas flow in the intermediate stripper is given by equation:(5)

$$G_m := R_m + \sum_j G_{j,m} \qquad (5)$$

G_m = the total gas flow from stage m

The temperature dependence of the distribution coefficients (Fig. 1) allows the determination of the heat of solution of each gas component. The plots of $\log(D_j)$ vs. $1/T$ are straight lines, at least in a limited temperature range, and their slopes are proportional to the heat of solution. The values given in Table 1 are given relative to the heat of solvent evaporation, which is defined as equal to 1.0. They valid for the boiling point of the solvent and their accuracy is 20 %.

Table 1. Heat of solution of some Gas Comonents

Component	N_2	O_2	Ar	Kr	Xe	N_2O	CO_2	CH_4
Heat of solution	0.0	0.0	0.1	0.3	0.5	0.55	0.6	0.2

Solving the Equation System by Iteration

The description of n stages of the intermediate stripper requires n material balance equations for each gas component plus n equations for the energy balance. For example, for five gas components in a 15 stage section a system of (5+1)x15=90 equations has to be solved. The equation system is not linear. Therefore, it is not possible to obtain a direct mathematical expression for the concentration at each stage. However, utilising the systematic interrelation between the equations, a feasable iterative procedure can be developed.

The iterative procedure is initiated with a appropriate assumed temperature profile for the intermediate stripper. During the first iteration step only the vapor flow is substituted into equation No. 4, while the gas flows are set equal to zero. In this way the first extraction factor profile is calculated. Using the material balance equations No. 2 and No. 3, the first relative gas flow profile in the liquid and in the gas phase is obtained. In the steady state, it is possible to obtain the absolute flow of the products, because the product flow entering the facility as a gas stream must be equal to the product flow in the liquid stream leaving the last stage of the intermediate stripper. The concentrations of the other gas components in the liquid stream of the first stage can be calculated from the concentrations in the loaded solvent coming from the absorber. The solvent leaves the absorber and flows through the heat exchanger,

which acts as a one stage desorber. Here the solvent is partially degased and is directed to the top of the intermediate stripper.

From this gas concentration profile a new temperature profile can be calculated, using the convential equation of the vapor pressure of the solvent. A new solvent vapor flow profile is calculated taking into account the gas concentrations, and this gives a better extraction factor profile. Now the iterative procedure is repeated until the temperature profile changes are within a limit as narrow as 10^{-3} ^{o}C.

III The Description of the Computer Code

Some Practical Approximations

To reduce the computation time, the computer modelling of the process has been simplified by the following approximations.

- In the absorber and the final stripper the solvent and gas flows as well as temperature are nearly constant over the packed height. Therefore, the simple "Fenske" equation No.1 can be used for calculate of the inlet and outlet gas concentrations.

- Each of the external heat exchangers acts as a one stage stripper operating at outlet temperature.

- The internal heat exchanger in the Kr column has a linear temperature profile over its height, as confirmed experimentally, and is integrated as the top section of the intermediate stripper.

- The coabsorbed oxygen and nitrogen carrier gases are added to the gas flow in the absorber only, because they are almost completely stripped in the intermediate stripper.

  The final stripper degases the solvent completely. Therefore, a unloaded solvent circulates to the top of the absorber. This is easily achieved in practice with a sufficiently large evaporation rate.

The Structure of the Program

The computer program has a modular structure. The calculation of the Xe and Kr columns are performed with the same program modules. Within these modules the appropriate parts are activated by pointers and flags. Fig. 4 shows the block scheme of the program.

The program starts with a block data statement, to obtain a set of independent variables for the calculation. These variables can be replaced by an alternative data set, which either is stored on a disk or is read as experimental data from our pilot plant. It is also possible to change every variable in a dialogue, if the influence of parameter variations is to be studied with the model.

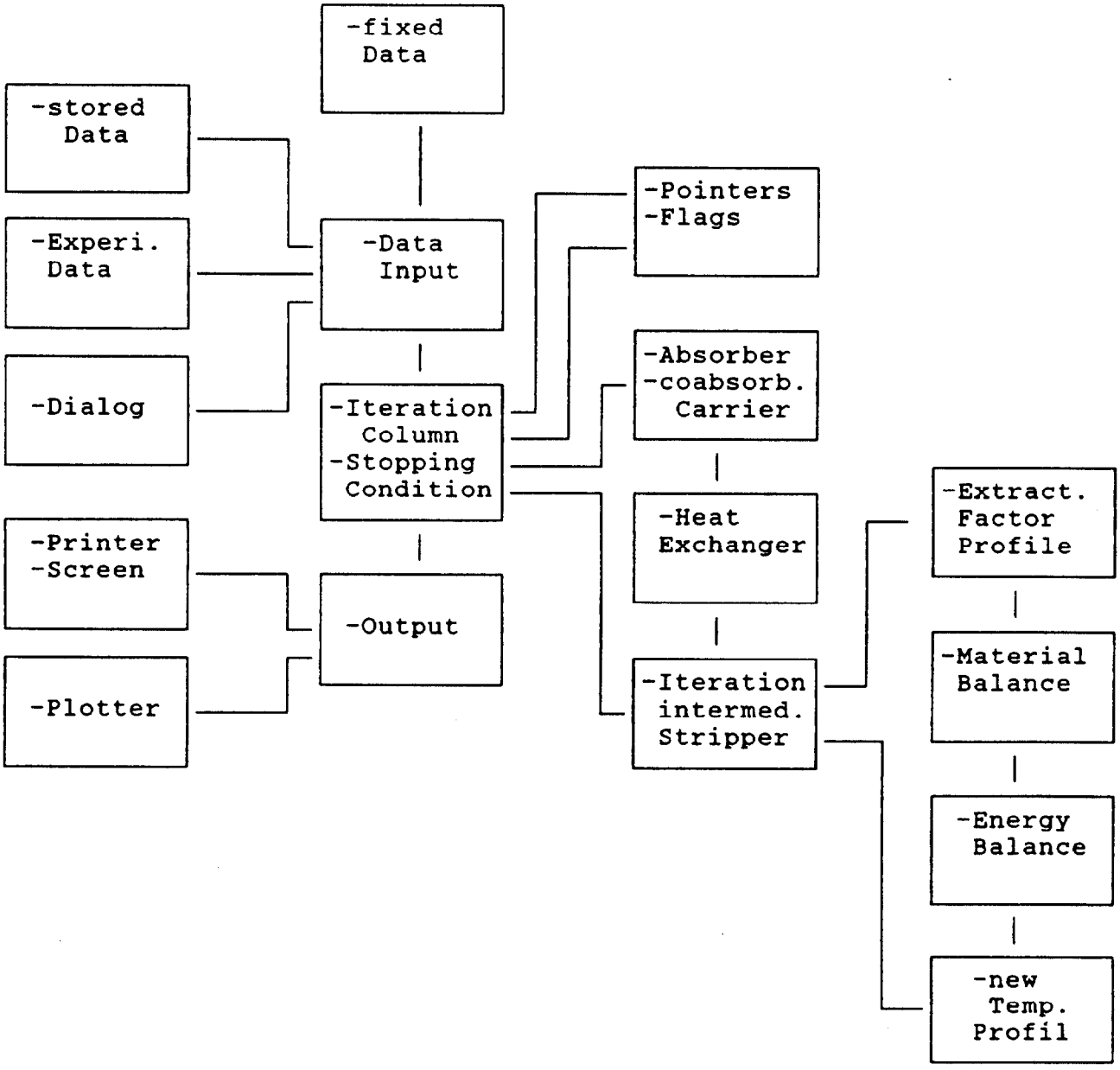

Fig. 4 Block Scheme of the Program

The Absorber

The computation starts with an iterative calculation of the co-absorbed carrier gas. So the correct liquid to gas flow ratio in the absorber column is gained. Average column temperature is used in the calculation of the mean extraction factor. This value is not changed for the subsequent iterations. This approximation is based on the assumption that the contribution of the slightly accumulating product gas to the flow ratio is negligible. After each iteration the stripped gas components leaving the heat exchanger and the intermediate stripper are added to the absorber sump. So concentrations in the gas and liquid phases are increased at this point. The iterative procedure is stopped, if the relative concentration change of the product in an iterative step is <0.1%.

The External Heat Exchanger

The loaded solvent leaving the absorber flows through the external heat exchanger and here it is heated by the recycled, unloaded solvent. During heating, a part of the absorbed gases is stripped and the vapor pressure of the liquid phase is increased. The gas and the liquid phase go co-curently through the exchanger. Therefore, the ex-changer acts as a one stage desorber.It is described by the following equations:(6)(7)(8)

$$E_j = \frac{L}{G_{tot}} \cdot D_j \qquad (6)$$

$$G_j = \frac{L_j}{E_j + 1} \qquad (7)$$

$$G_{tot} = \frac{\sum_j G_j \cdot P_{tot}}{P_{tot} - P_{R12}} \qquad (8)$$

G_{tot} = total gas flow
L_j = gas component j in the liquid phase
P_{tot} = system pressure
P_{R12} = vapor pressure of solvent

These equations have to be solved in an iterative procedure. With an assumed first gas flow an extraction factor is computed. Now the stripped fraction of the gas components can be calculated. Summation of the gas amounts gives a new gas flow, which is in equilibrium with the solvent vapor pressure. The result of a new calculation is a better extraction factor. The iteration is terminated, if the relative change of the extraction factor is <0.1%.

The Intermediate Stripper

The Xe Stripper

In the Xe section the loaded solvent leaves the heat exchanger and proceeds to the top of the intermediate stripper. A controlled electrical heater adjusts temperature of the solvent to a value between 5 - 10°C below the boiling point. Thus it is avoided, that too much vapor reaches the absorber sump. If temperature of the solvent lies too far below the boiling point, the front of the solvent vapor would be moved to the bottom of the stripper and the Xe product would be contaminated with Kr. Therefore, at this point a precise temperature control is important.

The solvent runs over the packing and is heated up by the solvent vapor, which partially condenses. The extraction factor decreases from the bottom to the top. Therefore, the material and energy balance equations Nos. 2 and 3 must be solved.

With a evaporation rate of 3-5% of the solvent flow the fraction of coabsorbed radioactive Kr is suppressed to $<10^{-8}$%.

The Kr Stripper

The distribution coefficient of Kr near the boiling point of the solvent is 4 times lower than that of Xe. Thus the rate of evaporation in the intermediate stripper sump has to be lowered to a similar ex-tent.However, the temperature difference to the boiling point of the solvent at the stripper top has now to be <2.5°C.

At this low temperature difference the high vapor pressure of the solvent results in a large amount of solvent vapor entering the ab-sorber sump. Then the vapor brings large amount of refluxed Kr, which accumulates in the sump. For that reason, an internal heat exchanger with 30% of the total exchanging area is placed before the stripper. The exchanger acts as an absorber with few stages. It is constructed from horizontal tubes, which are laid in layers in alter-nately rec-tangular directions. The whole packing of the tubes is fixed in the inner space of a square cross-section column. The tubes conduct the unloaded, recycled warm solvent. The cold solvent coming from the external exchanger flows over the tubes, in counter-current direction to the unloaded solvent. Since no heat is produced, the tem-perature profile in the exchanger should be linear. This was confirmed experimentally within an error of about 0.2°C.

Now it is possible to neglect in this part the energy equations and to solve only the material equations with fixed, linear temperature profile. The equations can be solved for both the internal and

intermediate stripper, which are treated as an integral column. Deviations of the temperature profil are taken into consideration only in the lower part of the stripper.

The Final Stripper

The loaded solvent leaving the stripper sump is directed into the final stripper. Here the vapor flux and the number of stages are high enough to strip all gas components. In the model it is assumed that an unloaded solvent comes out of the sump and enters the top of the absorber column.

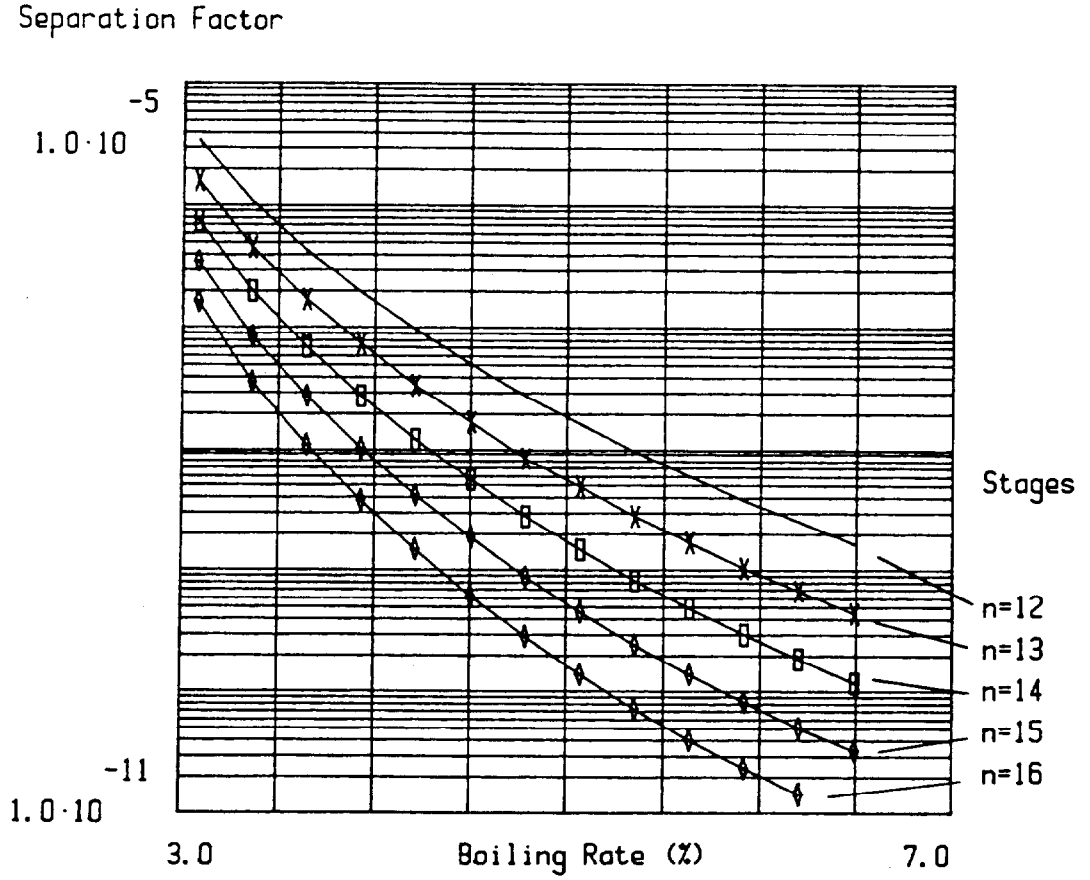

Fig. 4a The theoretical Separation Factor of the intermediate Xe Stripper in Relation to the boiling Rate and the Number of Stages

VI. The Experimental Results

The Measuring Equipment

In experimental runs the Xe and Kr product gases were mixed again and recycled into the process. This made it possible to perform the experiments with appropriately small inventories of the expensive rare gases. Methane has simular distribution coefficient to Kr and was used for the verification of the mathematical model. A methane flow of 1.0 l/h was added to the feed gas. A controlled neon gas flow of 4.0 l/h was fed into the final strippers for gas flow cal-ibration. The neon passes through the columns without any absorption analogously to the carrier gases. The composition of the gas phase in the final strippers was determined every 45 min in bypass loops. The gas phase was analyzed by gas chromatography. The rare gas free output of the facility was analyzed by mass spectrometry. Important liquid and gas flows, tem-perature and heating or cooling power supply were remotely controlled by a computer system. Data provided by about 240 control sites and particular temperature profiles were recorded in 15 min periods with the same computer system. The data, together with results of analyses were incorporated into a data bank for further use. The modelling pro-gram is able to read these data as a basis for the calculations.

The Intermediate Stripper for Xe

For verifying the model we performed some experiments in our pilot plant. The efficiency of the Xe absorption and its separation from Kr is the most important information to be predicted for the Xe column. The figure 4a gives the theoretical separation factor of Kr as function of the boiling rate in the stripper sump and in relation to the number of stages of the packing. The model predicts a separation factor ranging from 10^{-5} to 10^{-10}, made possible by the high difference at the distribution coefficients at boiling point (fig.1.). Under normal conditions the experiments give a separation factor $<10^{-6}$, due to the low sensitivity of the gas chromatographic analysis. Only under abnormal conditions, if the Kr concentration was ten times higher than the Xe concentration in the absorber sump, a separation factor of $<10^{-8}$ was found

The Intermediate Stripper for Kr

The Kr stripper with its internal heat exchanger was the most difficult part of the facility to be described by the mathematical model. The stripper must be operated so that accumulation of Kr is reduced and the R-12 vapor prevented from reaching the absorber sump. Moreover, methane is absorbed in the internal heat exchanger and its separation from Kr is suppressed. The distribution coefficients of the two components between the solvent and the gas phase at the boiling point differs only by a factor of about 1.5 (Fig. 1).

To study the behaviour of the intermediate stripper, we performed several experimental runs under different conditions. Outlet tem-perature of the internal heat exchanger and the boiling rate in the sump are the most sensitive operating parameters.

The model must know the number of theoretical stages in different parts of the facility. The number of stages can be calculated from the Fenske equation, if the decontamination factor in the absorber columns, especially in the Kr absorber, are measured at various conditions. At a known packing length in the column the stage height was calculated. Results are given in Table 2.

Table 2. Calculated Number of Stages

Xe Absorber	10	Kr Absorber	9
Xe Stripper	12	Kr Stripper	14
Xe Degaser	14	Kr Degaser	14

The internal heat exchanger differs in its design of the packing from the other columns and, therefore, the number of theoretical stages is diffcult to estimate. We tried to determine it by a comparison of ex-perimental results with theoretical calculations. Table 3 gives the ex-perimental decontamination factors of methane (CH4) and the residence time at a boiling rate of 2.0 % and 1.8 % in the intermediate stripper. All other conditions of the facility are kept equal as closely as possible. Process conditions were recorded by the data processing system and were respected in calculating the mean values given in Table 3.

Experim. Condit.	Experimental Data	Theoretical Data n=4 f=1.3	n=5 f=1.4	n=6 f=1.45
CH4 2.0%	0.64 ± 0.07 %	0.66 ± 0.1	0.51 ± 0.08	0.61 ± 0.1
time	1.2 ± 0.07 h	1.16 ± 0.05	1.2 ± 0.05	1.24 ± 0.07
CH4 1.8%	1.39 ± 0.07 %	1.93 ± 0.15	1.54 ± 0.1	2.05 ± 0.2
time	0.7 ± 0.02 h	0.61 ± 0.02	0.61 ± 0.05	0.60 ± 0.02

Table 3 Comparision between experimental and calculated results (CH_4 content (%) and resdence time (h) at a boiling rate of 2.0% and 1.8% in the intermediate stripper)

The values are the averages of 10 measurements made over a period of 8.0 hours. Standard deviation of the mean are also given in Table 3. To find the best fit of the experimental and calculated decontami-nation factors, we made computations in varying the number of stages of the internal exchanger. We also varied the distribution coefficient of methane within the limits of the experimental errors. The best fit was found with five stages and with a distribution coefficients of Kr and CH_4 differing at the boiling point by a factor of 1.4.

Figures 5 and 6 gives the calculated concentration profiles over the length of the internal heat exchanger and the intermediate stripper of the Kr section. The profiles are given for Kr loadings ranging from 50 to 500 vpm Kr. Major part of the Kr amount is found in the lower part of the stripper. The gas concentration is so high that it should cause a measurable change of the temperature profile. Such change was really found in experimental runs, and were corroborated by calcula-tions. The experimental results and calculated temperature profils are shown in Figure 7, which illustrats the good agreement between the experimental results and the calculations.

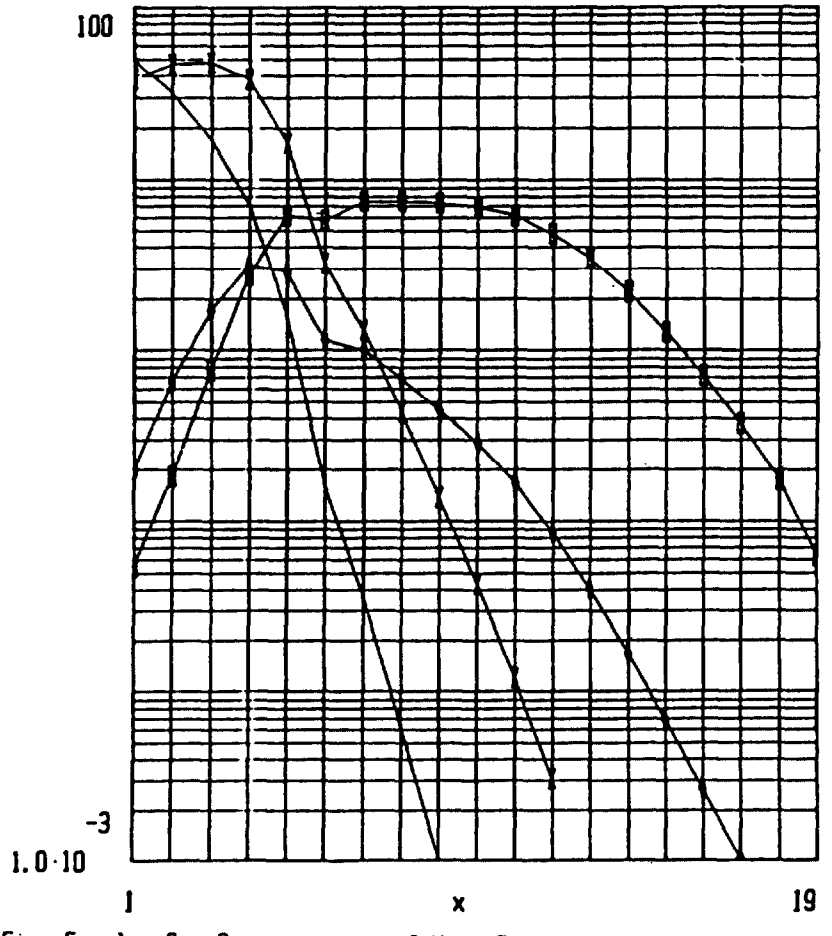

Fig. 5 calc. Gas Concentration of Heat Exchanger and Stripper (50 vpm Kr)
(—— =N2 ×—× =O2 ◇—◇ =CH4 □—□ =Kr)

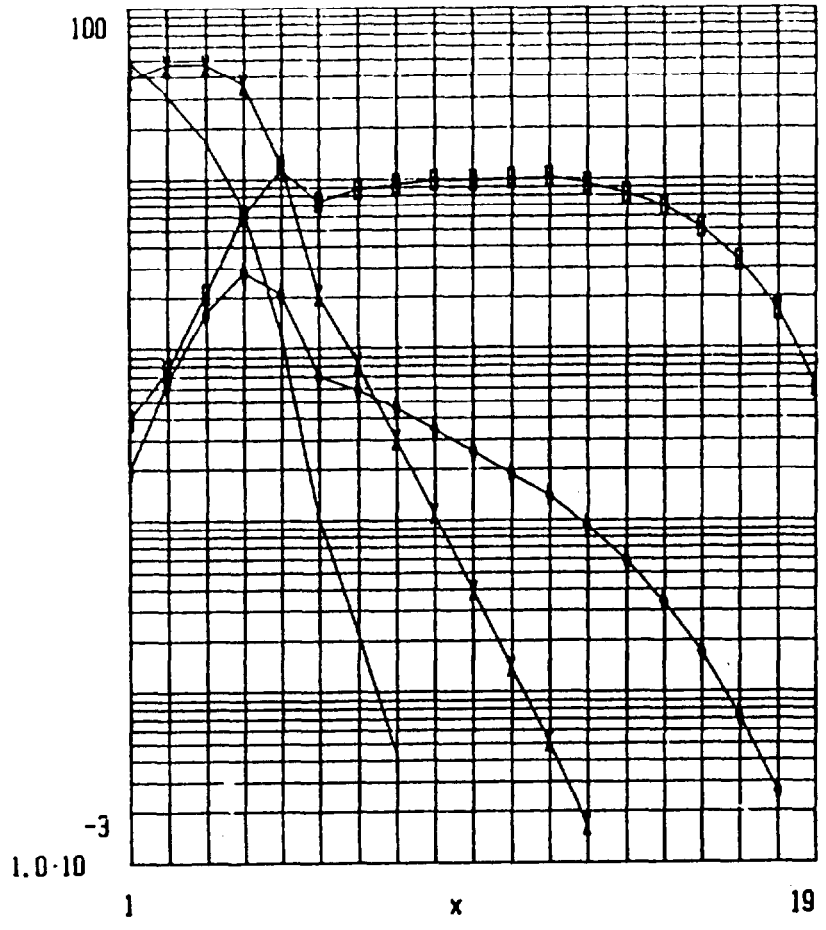

Fig. 6 calc. Gas Concentration of Heat Exchanger and Stripper (500 vpm Kr)
(——— =N2 —x—x— =02 —◇—◇— =CH4 —□—□— =Kr)

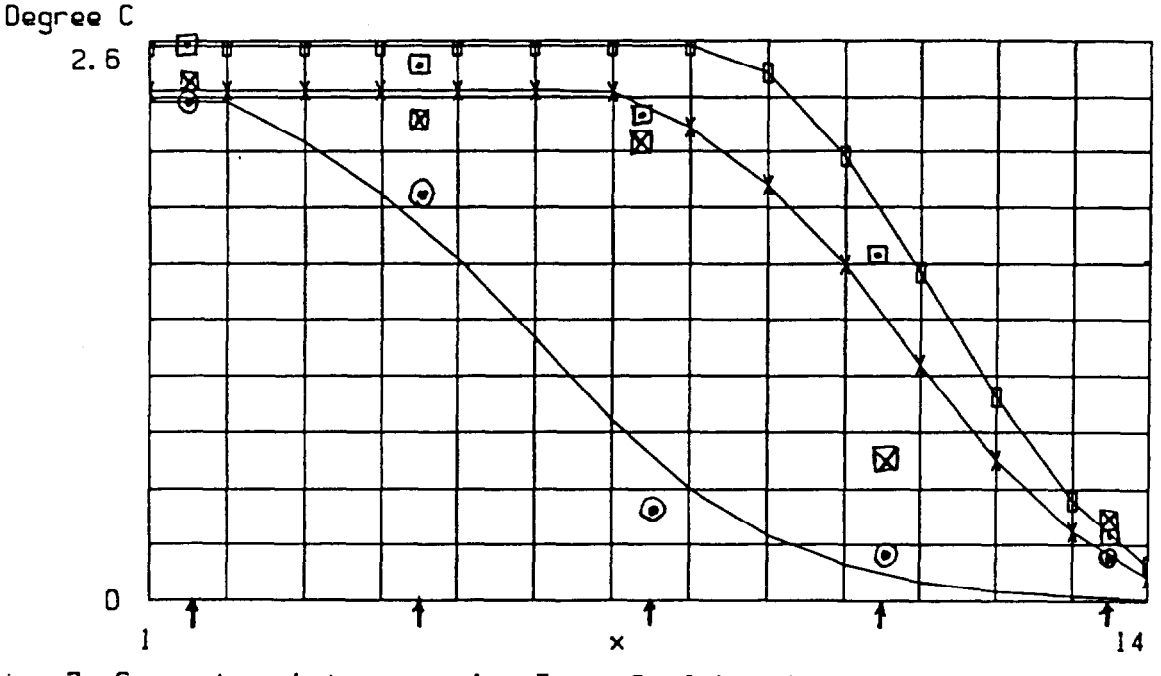

Fig. 7 Comparison between calc. Temp. Profil and exp. Values
— 30 vpm Kr —x—x— 400 vpm Kr —□—□— 630 vpm Kr
⊙ ⊠ ⊡ Exp. Values

References

(1) Henrich E.,Hüfner R.,Weirich F.,Bumiller W.,Wolff A.
Selectiv absorption of noble gases in freon-12 at low temperature and atmosperic pressure
18th DOE Nucl. Airborne Waste Management and Air Cleaning Conf.
Baltimore/USA 1984, Proceedings p. 959

(2) Henrich E. ,Hüfner R.,Weirich F.,Fritsch T.
Removal of xenon by pressureless absorption in freon-12
Proceedings LEC Specialists Meeting, Brüssel 1982

(3) E. Henrich, U, Bauder, F. Weirich
RECOD, Paris 23-27 August 1987,
Proceedings p. 553

(4) E. Henrich, R. von Ammon
Experimenteller Vergleich von zwei Verfahren zur Edelgasrückhaltung durch Rektifikation oder Absorption bei tiefer Temperatur
KFK Nachrichten Jahrg. 20 2/88 S. 104-110

DEVELOPMENT OF A CRYOGENIC ABSORPTION PROCESS FOR RARE GAS REMOVAL FROM REPROCESSING OFF-GAS

E. Henrich, F. Weirich

Kernforschungszentrum Karlsruhe, Institut für Heisse Chemie
Fed. Rep. Germany

ABSTRACT

A selective absorption process for Xenon, Krypton and 14-CO_2 removal from reprocessing dissolver off-gas has been developed. Process and equipment design has been investigated since 4 years on the cold engineering scale at 25 m^3/h gas troughput.

The rare gases are absorbed in two successive absorption columns in CCl_2F_2 solvent. The first column removes the Xe plus 14-CO_2 at about -125° C, the second column removes the Kr at about -150° C. Freezing gas components are removed in prepurification steps at temperatures below 0° C: A scrubber with circulating 4-10 M HNO_3 plus H_2O_2 removes water vapor and NO_x to less than 1000 ppm; the small remainder is removed to the trace level with a H-mordenite molecular sieve adsorber.

Essential technical and safety characteristics are: (1) the system operates at slightly subambient pressure (2) the Kr residence time is less than half an hour (3) the process is insensitive to impurities and even compatible with ozone; no preremoval of O_2 is needed.

Essential results within a suitable range of operating conditions are: (1) Decontamination factors for Xe more than 10^5, for Kr more than 10^3, (2) Product purities more than 99 %, (3) Separation factors for key-design components Xe/Kr more than 10^6, Kr/O_2 more than 10^7 and even Kr/CH_4 more than 10. (4) Predictions from a process model and experimental results are in good agreement.

The reliable and good-natured process behaviour allowed operation by automatic control without personnel overnight and the weekends. A low radiolytic solvent degradation of ca. 3 g per tonne spent fuel has been estimated from separate investigations. Experience from integrated tests with a total dissolver off-gas system and design characteristics for a larger cryogenic absorption subsystem suited for hot demonstration will also be briefly reported.

1. INTRODUCTION

In present reprocessing plants, the radioactive aerosols, iodine and the bulk of nitric oxides and water vapour are removed from the dissolver off-gas (DOG), but the gaseous fission products Xe and radiokrypton are released into the atmosphere. An additional retention of the inactive Xe, Kr-85 and eventually C-14 as CO_2 is desirable for larger reprocessing plants in the future.

The radiotoxicity of Kr-85 is low. It is a noble gas and does not concentrate in food chains or in the human body. Therefore, the radiological benefit of Kr-85 retention is only moderate. An uncontrolled release of Kr-85, halflife 10.8 y, however, causes a long-term contamination of our only natural resource of 1.1 ppmv Kr in the atmosphere. To date, 1 m^3 (STP) of air contains about 25 pCi of Kr-85 /1/, though only about 10% of the annual spent nuclear fuel arisings are reprocessed. A commercial 50 L pressurized cylinder of Kr contains already more than 100 µCi of Kr-85. There is also some concern about potential effects of an increased atmospheric ionisation.

As a precaution for the anticipated nuclear power increase in the future, our German radiation protection commission (SSK) recommends the hot demonstration of a Kr-85 management technique /2/. A socio-political contribution could be improved public acceptance of nuclear power.

Commercial utilization of about 1+m^3(STP) valuable inactive Xe per t U and some Kr-85 can be an economic incentive. This should not be neglected in a cost benefit analysis. Last not least, additional tailend steps for rare gas recovery contribute to a better and more reliable DOG purification, especially in case of minor upstream malfunctions.

During the past two decades, many cryogenic distillation, absorption and adsorption processes for routine rare gas recovery from reprocessing off-gas have been developed and proposed /3/. Additional processes create an additional hazard for the operating personnel. In the initial stages of this development work, much attention was therefore paid to the aspect, that a moderate radiological benefit for the environment should not be achieved at the expense of the operators. Some general characteristics, which are expected to contribute to technical simplification and especially to safety are as follows:

(1) Process compatibility with oxygen and even some ozone obviates the preremoval of oxygen, thus simplifying the precleaning steps.
(2) Processes without large Kr-85 inventories during normal operation or during start-up, shut-down and standby conditions are preferred, to limit the consequences of an accidental release.
(3) Operation at subambient pressure is usual in off-gas purification for safety and technical reasons, to reduce the probability of a release.

2. BRIEF DESCRIPTION OF THE TOTAL DOG SYSTEM

An integrated DOG system must be developed as a whole, to ensure mutual compatibility of the individual purification steps. Fig.1 shows a total DOG purification train for a large dissolver off-gas flow >1000 m^3 per ton of spent fuel (not per hour !!). The rather simplified first part is a conventional DOG system and routinely operated eg. in the Karlsruhe reprocessing plant (WAK). The second part in the cold box shows the newly developed tailend subsystem for rare gas and 14-CO_2 recovery.

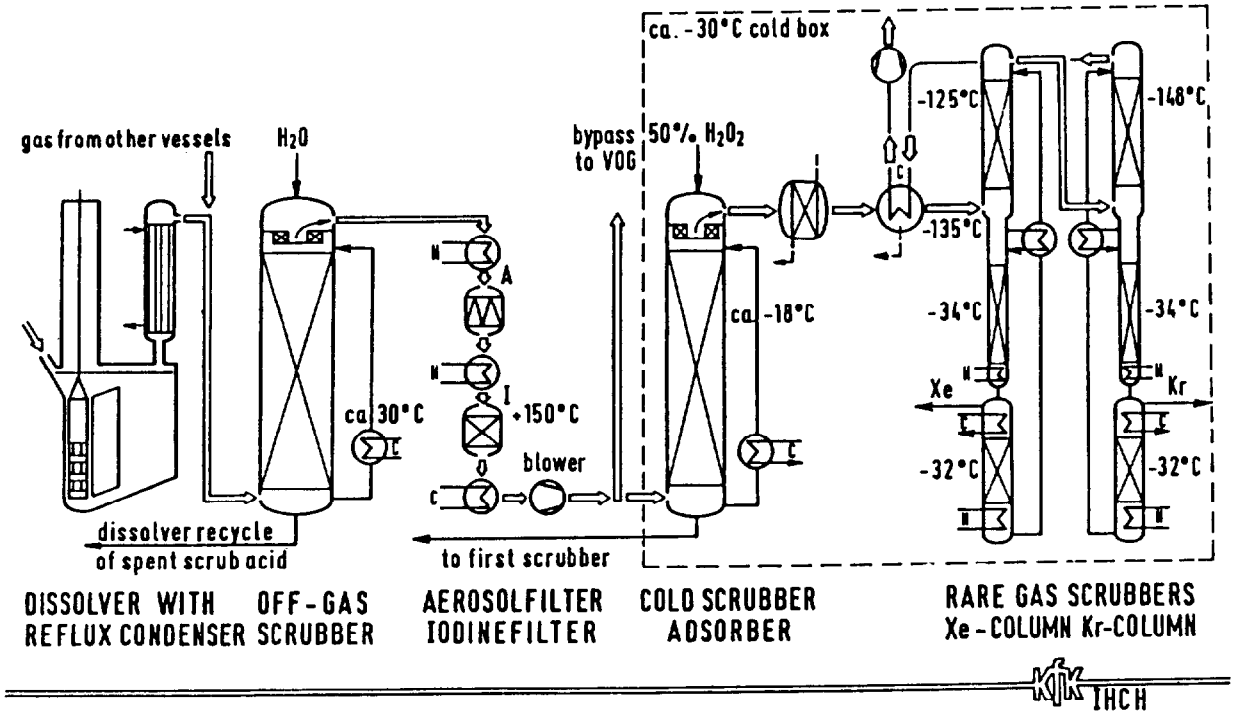

SIMPLIFIED FLOWSHEET OF A DISSOLVER OFF-GAS PURIFICATION SYSTEM

Fig.1

The first off-gas scrubber operates with dilute nitric acid at about ambient temperature (process cell 30+ °C). It removes the bulk of aerosols, oxides of nitrogen and water vapour. The remainder of aerosols and the iodine are completely removed in the following filter train. Spent HEPA and iodine filters are replaced periodically. Alternatively, several plants use caustic scrubbers for simultaneous iodine plus CO_2 removal; traces of organic iodine are then poorly retained.

Downstream from aerosol and iodine removal, the purified DOG is usually released into the atmosphere. A typical composition is several percent water vapour, corresponding to the dew point at the exit temperature of the scrubber, about 1 % oxides of nitrogen, 0.1 % rare gases plus some CO_2 and N_2O from side reactions during UO_2 dissolution. These components can be removed to the trace level in the tailend subsystem. All tailend units operate at subambient pressure and low, stepwise decreasing temperatures in an accessible cold box. At about -30° C box

temperature, many components do not need much individual insulation, which eases inspection, maintenance and repair. The cold box subsystem can be added to any conventional DOG-system downstream from iodine removal.

Prior to final rare gas absorption, two precleaning steps remove water vapour and residual oxides of nitrogen to the trace level. Efficient precleaning helps to avoid downstream freeze-out problems and solvent contamination. Preventive prepurification is simpler than dealing with an impure solvent. The first step is a continuous scrub with a somewhat more concentrated nitric acid plus hydrogen peroxide at temperatures below 0^{o} C. This reduces the content of water vapour and oxides of nitrogen by about one order of magnitude. The second step is a discontinuous adsorption on a molecular sieve. This removes the small remainder of freezing components to the trace level. Spent scrub acid and the periodic regeneration gas stream from the adsorber bed are recycled without treatment to the first scrubber upstream from iodine removal. Any traces of freezing components are further removed to extremely low levels in the downstream feed gas cooler at about -135 °C.

In the last two columns, the rare gases are absorbed at cryogenic temperatures. A suitable solvent is dichlorodifluoromethane CCl_2F_2, known as freon-12 or refrigerant-12 (R-12), the usual non-toxic and non-flammable refrigerant of refrigeration units. The first column removes the Xe together with CO_2 and N_2O at -125 °C. The second column removes the Kr at about -150 °C.

In our cold engineering scale facilities for off-gas purification the equipment is located side by side. Successful tests at about 25 m^3/h off-gas throughput have been performed for many variants of the individual steps, and also for the integrated tailend subsystem and the total DOG purification train as well. The continuing work deals especially with further details of process, process control and equipment design optimization as well as adaptation to the requirements from our reprocessing industry or licensing authorities.

3. PREPURIFICATION STEPS PRIOR TO RARE GAS ABSORPTION

Since the rare gases are absorbed at rather low temperature, it suggests itself to take advantage of lower temperatures to simplify the precleaning steps.

3.1 Low temperature scrub with nitric acid plus hydrogen peroxide

Low temperature scrubs and their variants have been described in more detail elsewhere /4,5/. The following section gives a brief summary of essential aspects for this special application.

3.1.1 Physico-chemical basis of the process:

Water and nitric acid partial pressures over the scrub acid decrease with decreasing operating temperature as shown in fig.2 for 35 and 50 % by weight HNO_3. Absorption of NO_x (NO plus NO_2) is improved at lower temperatures: (1) NO is poorly soluble in HNO_3 and only absorbed after oxidation to NO_2 or HNO_2. Oxidation of NO

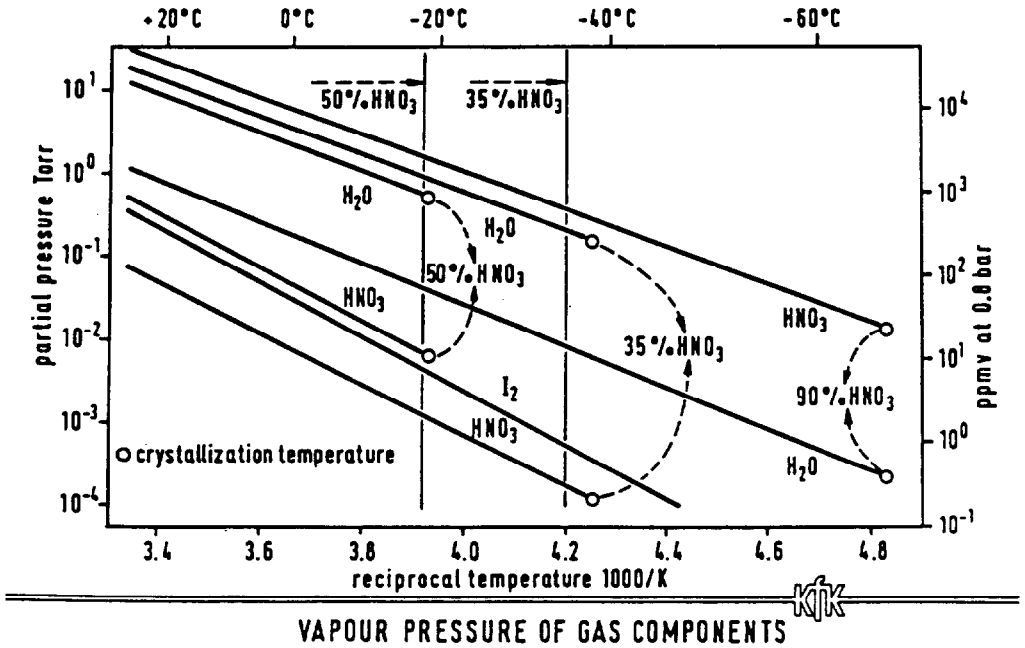

Fig.2

in the gas phase is faster at lower temperatures; this is one of the few exceptions in chemistry. At lower temperatures the NO_2 dimerizes to a larger extent to N_2O_4 and is better absorbed in the dimerized form. (2) At very low partial pressure of NO, the oxidation in the gas phase becomes extremely slow. Under such conditions, the oxidation of NO proceeds faster by equilibration with a more concentrated nitric acid according to the following reaction:

$$NO + 2\ HNO_3 \rightleftharpoons 3\ NO_2 + H_2O; \qquad (R1)$$

At low total NO_x partial pressure and higher HNO_3 concentration, the equilibrium is extremely shifted to the NO_2 side. NO oxidation with O_2 in the gas phase and oxidation with more concentrated HNO_3 in the liquid phase are therefore complementary to each other.

Absorption of N_2O_4 produces nitric and nitrous acid:

$$N_2O_4 + H_2O \longrightarrow HNO_3 + HNO_2; \qquad (R2)$$

The predominant absorption mechanism at very low NO_x partial pressure is direct absorption of HNO_2 formed in the gas phase.The nitrous acid concentration increases to a steady state value, until an equilibrium between production and decomposition rate is attained. In scrubbers with acid circulation, the HNO_2 decomposition reaction liberates NO_x into the purified off-gas:

$$3\ HNO_2 \longrightarrow HNO_3 + H_2O + 2\ NO; \qquad (R3)$$

This reaction is followed by NO-equilibration with HNO_3 according to reaction R1.

Hydrogen peroxide H_2O_2 quickly oxidizes the nitrous acid to nitric acid and prevents off-gas recontamination with NO_x:

$$HNO_2 + H_2O_2 \longrightarrow HNO_3 + H_2O; \qquad (R4)$$

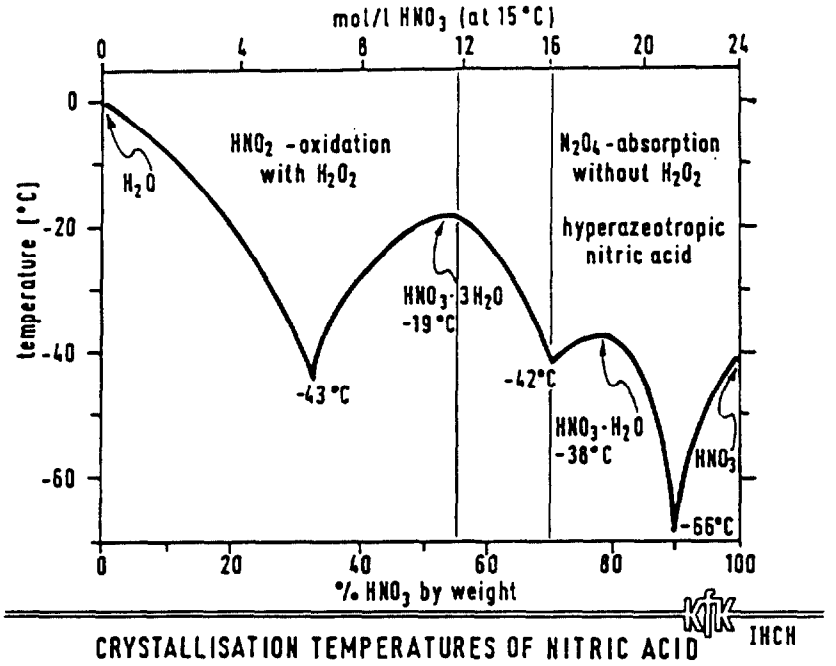

Fig.3

In practice, commercial 30 or 50 % H_2O_2 is continuously fed to the circulating acid in proportion to the NO_x in the feed gas. A H_2O_2 concentration below 0.1 mole/L is favourable and easily maintained with a sufficiently high acid circulation rate. Due to the low temperature and H_2O_2 concentration, the H_2O_2 decomposition is negligeable and only a small stochiometric excess is needed. The small amount of stabilizers in commercial peroxide, usually phosphates, does not affect the reuse of the scrub acid in the dissolver.

3.1.2 Equipment and experimental results:

Conventional plate and packed columns with scrub acid circulation via a controlled cooler have been tested in our pilot facilities over a wide range of temperatures and nitric acid concentrations /4,5/. Both, co-current or counter-current column operation is possible. Scrubbers with regular packings are prefered due to the low superficial gas velocity at gas residence times in the order of about 1 min and because of the low pressure drop of < 10 hPc. Residual NO_x concentrations between 10^2 - 10^3 ppmv have been obtained at temperatures below 0 °C and feed gas concentrations of 1 % NO_x. Much lower values have been observed at extended gas residence times and high initial NO_2/NO-ratios.

3.1.3 Suitable operating conditions and process integration:

Hydrogen peroxide addition to nitric acid is only acceptable up to about 54 % by weight HNO_3 ($HNO_3 \cdot 3H_2O$, m.p. -18.5° C); at higher concentrations, oxides of nitrogen are evolved after an induction period. Further limitations of the HNO_3-concentration are given by freezing. Fig.3 shows the crystallization temperatures of aqueous nitric acid solutions. At scrubbing temperatures below about -30° C, the HNO_3 concentration must be kept within a narrower range to prevent crystallization of either ice or $HNO_3 \cdot 3H_2O$. A much boader range, from about 20 to 54 % HNO_3

(4 - 11 M HNO_3), is acceptable down to -18° C and is a good compromise between concentration control requirements (density) and the desirable low temperature.

This acid concentration range can be obtained automatically without much adjustment from the residual NO_x and humidity in the off-gas plus 30 or 50 % weight H_2O_2. The water vapour-to-NO_x ratio is mainly affected by temperature and NO_x removal efficiency of the first off-gas scrubber. Poorer NO_x removal, a lower off-gas dew point and use of 50 % H_2O_2 result in higher acid concentration in the low temperature scrubber. Concentration fluctuations are smoothed out to a large extent, since the dynamic scrub acid hold-up required for circulation, corresponds to several tons of fuel. About 0,15 m^3 5 - 6 M HNO_3 are produced per t U from 2500 m^3 off-gas with 1 % NO_x at 30 °C dew point and 0,9 bar, using 50 % H_2O_2. Continuous dissolver recycle of the spent scrub acid via the first scrubber recycles iodine traces in case of upstream malfunction and destroys the slight excess of < 0,1 mole/L H_2O_2.

3.2 Water and NO_x removal with a H-mordenite molecular sieve

Downstream from a low temperature scrubber, the humidity and NO_x will be reduced to about 10^3 ppmv or below. A relatively small adsorber bed volume with a low pressure drop is therefore sufficient. At temperatures below 0 °C, the loading-regeneration periods can be extended to several days; this contributes to adsorber life-time and convenient operation. Liberation of adsorption heat is low due to the low loading rate and eases low temperature operation.

H-Mordenite (Norton zeolon 900 H, 1.5 mm extrudate) has been selected because of the following reasons: (1) It is highly acid and temperature resistant and (2) It catalytically oxidizes NO to NO_2 in the presence of at least few percent O_2; NO_2 is then strongly adsorbed as N_2O_4. The two diagrams in fig.4 show an example. Breakthrough of the gas components occurs in the following order: O_2, N_2, Kr, Xe, N_2O, CO_2, N_2O_4 (NO_2 plus NO) and finally H_2O. The catalytic NO oxidation is obviously not affected by the initial preloading with Kr, Xe, N_2O or CO_2. These slightly adsorbed components are gradually displaced by the strongly adsorbed H_2O and N_2O_4. Counter-current regeneration with a small stream of dry air or N_2 is indicated at the start of NO_x breakthrough at $\lesssim$ 1 ppmv. It is worth to be mentioned, that NO_2 breakthrough starts earlier than NO-breakthrough. Because of the long loading time of the second adsorber, there is sufficient time for slow regeneration of the first one at 250 - 300° C. In case of occasional upstream malfunction, the adsorber may be contaminated by e.g. iodine. Therefore, all regeneration gas streams are recycled upstream to the first scrubber. A foreward purging step prior to regeneration is not required.

Any traces of freezing components escaped from the adsorber bed are further removed to extremely low levels at about -135° C in the defrostable feed gas cooler. This adds in-line removal redundancy: Automatic correction of some upstream malfunction is inherent to gas purification trains with stepwise decreasing temperatures.

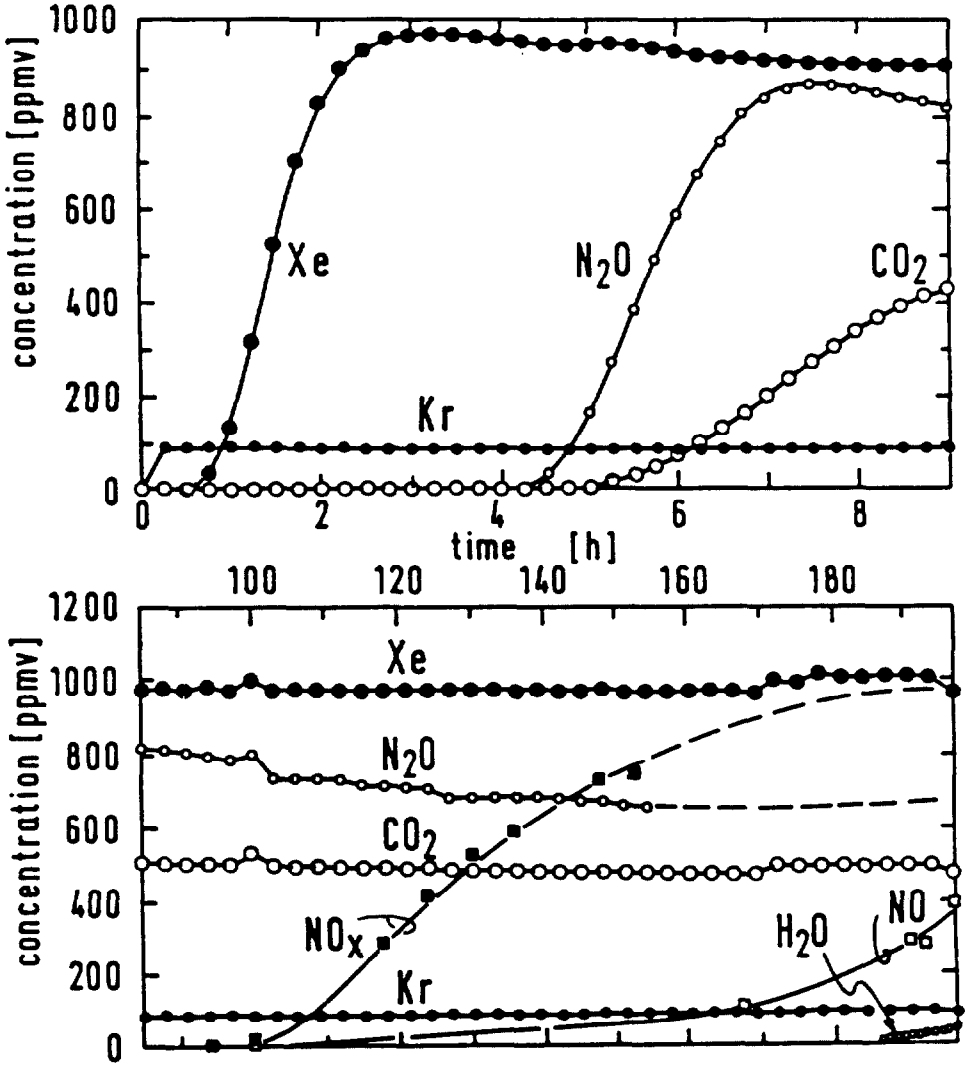

feed gas: O_2 - deficient air (10% O_2) plus

Xe	10^3 ppmv	NO	$5 \cdot 10^2$ ppmv
Kr	10^2 ppmv	NO_2	$5 \cdot 10^2$ ppmv
N_2O	$7 \cdot 10^2$ ppmv	H_2O	$5 \cdot 10^2$ ppmv
CO_2	$5 \cdot 10^2$ ppmv		

KfK IHCH

BREAKTHROUGH CURVES FOR H-MORDENITE AT -17° C

bed length 0.9 m 1.5 mm extrudate
superficial gas velocity 0.12 m/s

Fig.4

4. RARE GAS ABSORPTION AT CRYOGENIC TEMPERATURE

4.1 Solubility of gases in liquid R-12

Many organic solvents are principally suited for the selective absorption of heavy rare gases from off-gas streams /6,7/. In the presence of oxygen, only non-flammable halogenated solvents are suited for safety reasons. In practice, commercial refrigerants having very low melting points eg. R12, allow cryogenic absorption temperatures, which help to reduce the solvent flow rate and equipment size.

Individual distribution coefficients D of major DOG constituents have been determined in the temperature range from the normal boiling point of R12 at -30°C to the melting point at -158°C. Fig.5 shows the fit curves for our experimental data. The solubilities correspond to about the sequence of boiling points; this allows crude solubility estimates for other gases. Solubility and solubility differences increase at decreasing temperature. The slope of the distribution curves in the lg D versus 1/T plot is proportional to the heat of solution. Solubility differences for the key design components Xe/Kr and Kr/O_2 increase from about half an order of magnitude at boiling point temperature on the left, to about one order of magnitude at the indicated absorber temperatures. The air components N_2, O_2 and Ar are far less soluble than Xe, Kr, N_2O and CO_2. Suitable gas-to-solvent flow ratios on a volume basis for the different column sections are also shown as dashed areas. These areas are located at the operating temperature and between the distribution lines of the key design components which have to be separated from each other. During freezing of the solvent, dissolved gases are expelled, because they do not fit into the strict geometry of the R12 crystal lattice.

Solubilities of some solids have been determined by visual inspection of crystal dissolution or growth at slightly increasing or decreasing temperatures, to approach the equilibrium from both sides. The solubility data are shown in Fig.6 /8/.

4.2 Brief description of the process

More detailed process descriptions have been reported in the literature /9,10,11/. A simplified flowsheet of the process, including the preferred operating temperatures and evaporation rates in percent of the solvent circulation rate for the different column sections is shown in Fig.7. The principle of the process is a conventional gas absorption-desorption procedure.

The absorber sections are responsible for the off-gas decontamination. The chilled R12 solvent selectively absorbs the product gas from a dry counter-current off-gas stream at a suitable gas-to-solvent flow ratio. The Xe absorber operates somewhat above the temperature of the feed gas cooler, to prevent freezing of less soluble impurities carried over into the solvent. The absorber temperature for the less soluble Kr is only about 10 K above the R12 melting point (-158°C) and as low as reasonably possible, to reduce the circulating solvent flow and losses of solvent vapour into the purified off-gas (at -148°C about 40 ppmv).

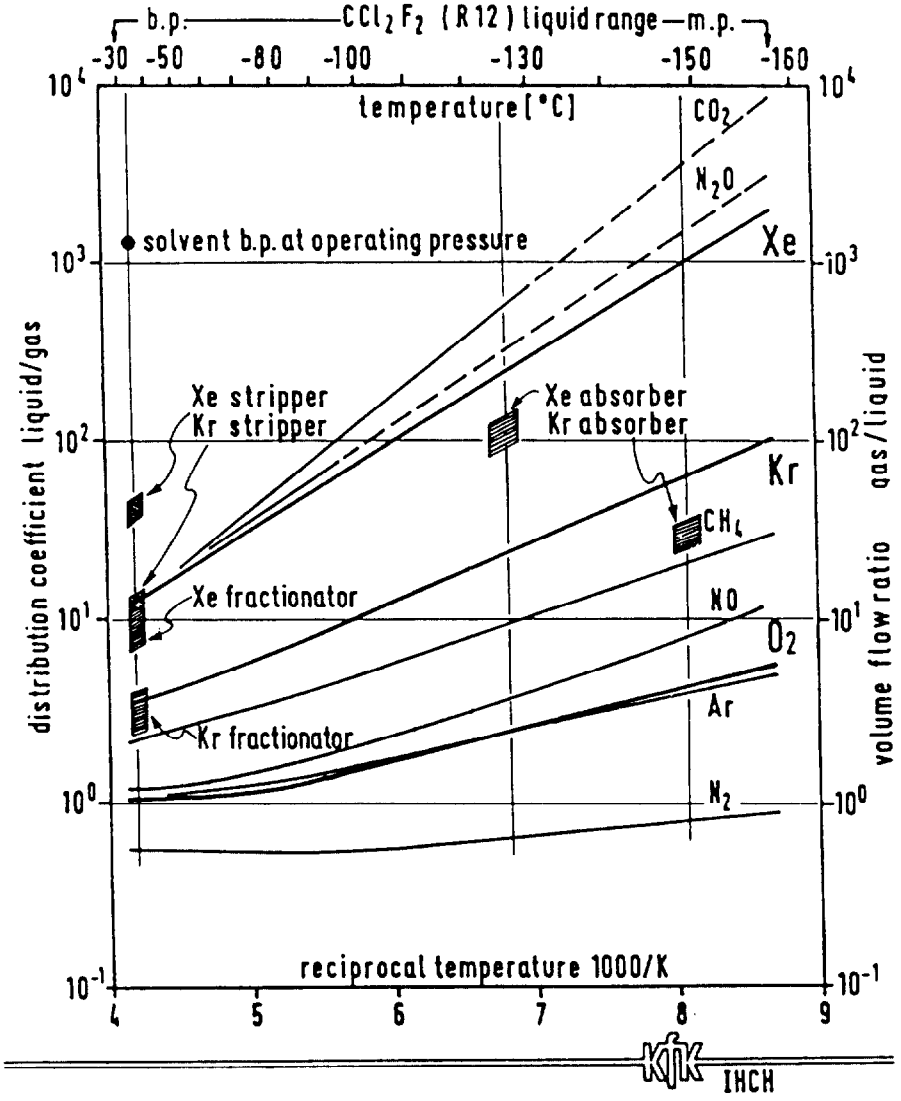

SOLUBILITY OF GASES IN LIQUID R12
OPERATING CONDITIONS IN THE PACKING SECTIONS

Fig.5

The intermediate stripper (or fractionator) sections are responsible for the final product purity. The cold loaded solvent from the absorber is first warmed up by efficient counter-current heat exchange with the warm unloaded solvent recycled from the pump. Most of the coabsorbed carrier gases as well as a minor product fraction are desorbed and recycled to the feed gas during this operation. The solvent then enters the top of the packed fractionator section at a controlled temperature about one or few centigrade below the solvent boiling point at operating pressure. A relatively small and controlled flow of solvent vapour is generated in the fractionator evaporator and counter-currently strips the remainder of coabsorbed carrier gases back into the feed gas. Part of the solvent vapour is condensed in the packing and the vapour-to-solvent ratio decreases slightly from the lower to the upper end.

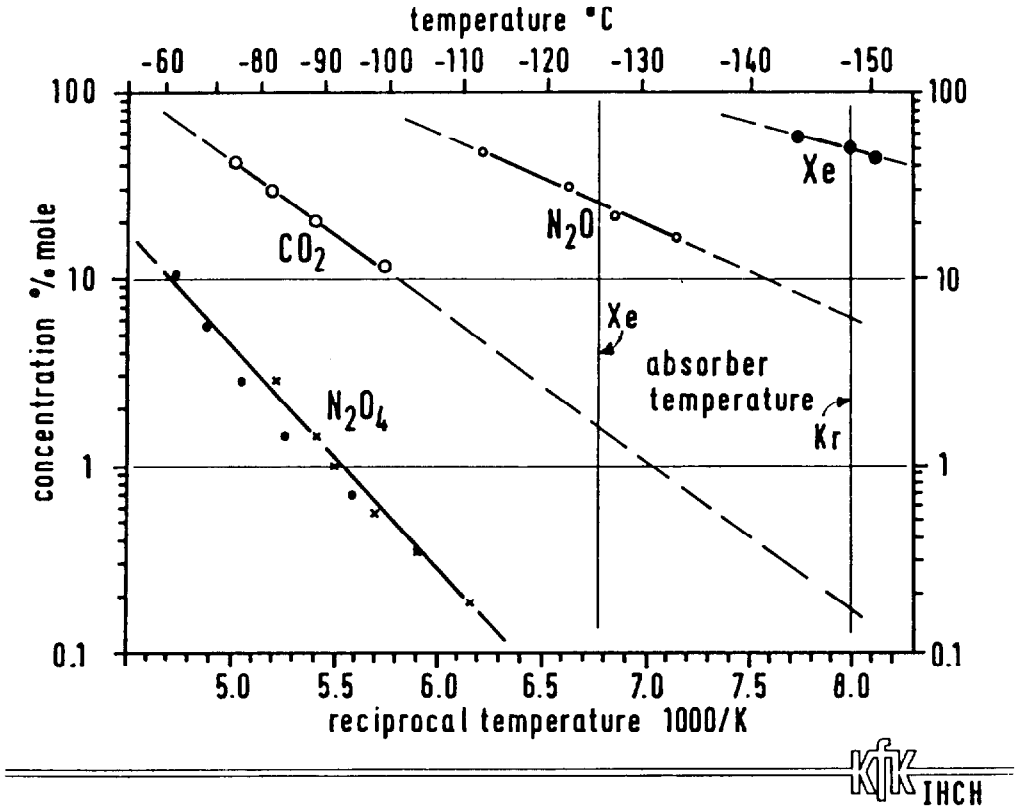

Solubility of solids in R 12

Fig.6

The heat exchanger in the Kr column is divided into a serially connected external and internal part. The internal part is located at the top of the Kr fractionator packing and acts as a small absorber section with an about linearly decreasing temperature profile. This is necessary due to the larger volume of coabsorbed carrier gas in the Kr-absorber and prevents excessive solvent vapour and product gas recycle into the feed gas.

The final stripper sections are responsible for complete product gas desorption. A large flow of solvent vapour is generated in the stripper evaporator and strips the product gases from the solvent. The bulk of solvent vapour is removed from the product gas in a two-stage reflux condenser; additional raw product refining steps remove the small remainder of solvent vapour. The Xe product contains the CO_2 (C-14) and N_2O. The stripper sections are separated from the absorber-fractionator sections via a siphon. They operate at a slightly higher pressure to allow automatic product gas recycle to the Xe absorber in case of insufficient product purity.

The solvent pump recycles a constant stream of unloaded solvent to the absorber via a heat exchanger. An efficient counter-current heat exchange between the cold absorber and the warmer stripper sections of the solvent loop is the key to energy economy. These heat exchangers are designed to recover at least 90 % of the cryogenic refrigeration energy. Small solvent coolers,

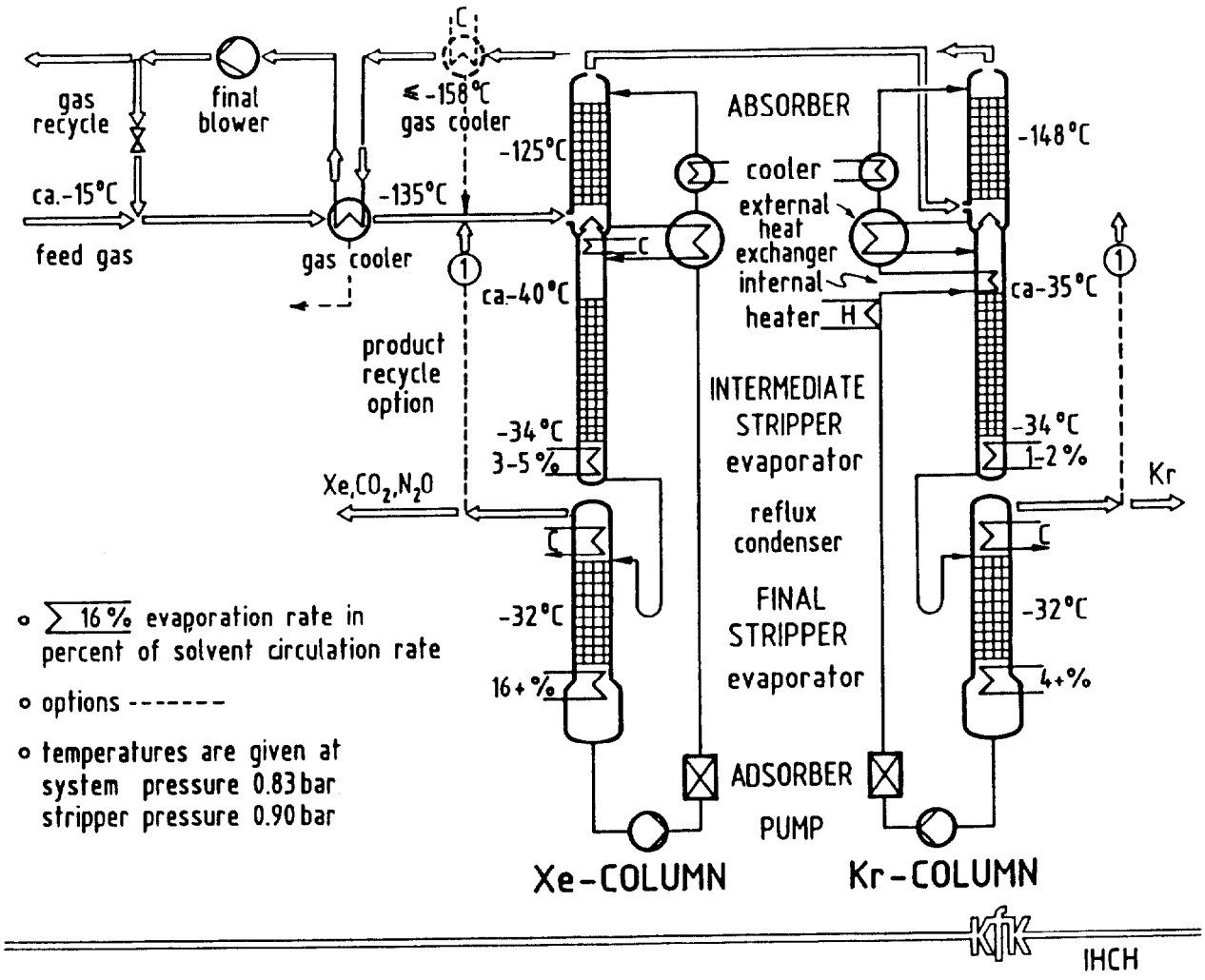

RARE GAS ABSORPTION IN REFRIGERANT-12
SIMPLIFIED FLOWSHEET

Fig.7

e.g. with evaporating liquid N_2, compensate for the incomplete heat exchange and control the absorber temperatures at -125 °C and -148 °C in the Xe and Kr absorbers.

An adsorber bed in the solvent loop maintains a dry and clean solvent even at minor malfunctions in the upstream prepurification steps.

Though the solvent vapour content in the purified off-gas is rather low and already more than an order of magnitude below maximum permissible working place concentration, present environmental concerns may dictate further reduction of R12 emission. Technically, this is easily achieved either with an additional gas cooler, preferably prior to counter-current heat exchange in the feed gas cooler to reduce the heat exchange surface, or even more efficiently by molecular sieve X13 downstream from the final blower. Such additional measures have to be justified by a realistic cost-benefit analysis.

4.3 Design and layout of the noble gas pilot facility

The construction material of the Xe and Kr columns is stainless steel 1.4541 or 4306 (304 L). The columns have a total height of 12 m and are mounted in a steel rack on 1.4 m^2 area. The column assembly can move freely in a cold box with 0.2 m thick walls of polyurethane foam, sandwiched between plastic coated steel sheets. The layout of the assembly is sketched in Fig.8. Essential design data of column components are summarized in Tab. 1.

	Xe-COLUMN		Kr-COLUMN	
packing type (SS)	Metex "Goodloe"		Sulzer "CY"	
packing dimensions	diameter	height	diameter	height
absorber	0.1 m	1.8 m	0.1 m	3.0 m
internal heat exchanger			0.18 m square	0.6 m
intermediate stripper	0.075 m	2.7 m	0.1 m	2.7 m
final stripper	0.1 m	1.8 m	0.1 m	1.9 m
total column height		12 m		12 m
max. solvent inventory	0.07 m^3		0.07 m^3	
max. solvent rate	0.5 t/h		1.0 t/h	
max. gas rate	30 m^3 (STP)/h		25 m^3 (STP)/h	
heat exchangers	type	surface	type	surface
external	plate	1.8 m^2	plate	6 m^2
internal			horizontal pipe rows	3 m^2

Table 1: DESIGN DATA OF THE NOBLE GAS PILOT FACILITY

Brief characterization of some additional components:

- Solvent pumps are magnetically coupled gear pumps with a controlled geared DC motor, to maintain a constant solvent flow rate within ± 1 %.
- The solvent evaporators in the fractionator and stripper sumps are heated electrically and operate in a once-through mode with a low solvent inventory. The surface heat load is kept below 2 Watt/cm^2 to avoid thermal solvent degradation and to achieve good heat transfer by operation in the bubble regime.
- The reflux condensers have two differently designed parts. The lower part is a vertical shell and tube type condenser with the coolant inside the tubes and removes the bulk of solvent vapour. The upper part is a coil in a narrow annular gap and acts mainly as a gas cooler. A small gas space in the upper part helps to keep a low inventory of concentrated Kr-85 product. A constant and temperature controlled R11 coolant stream passes the upper and then the lower condenser section.

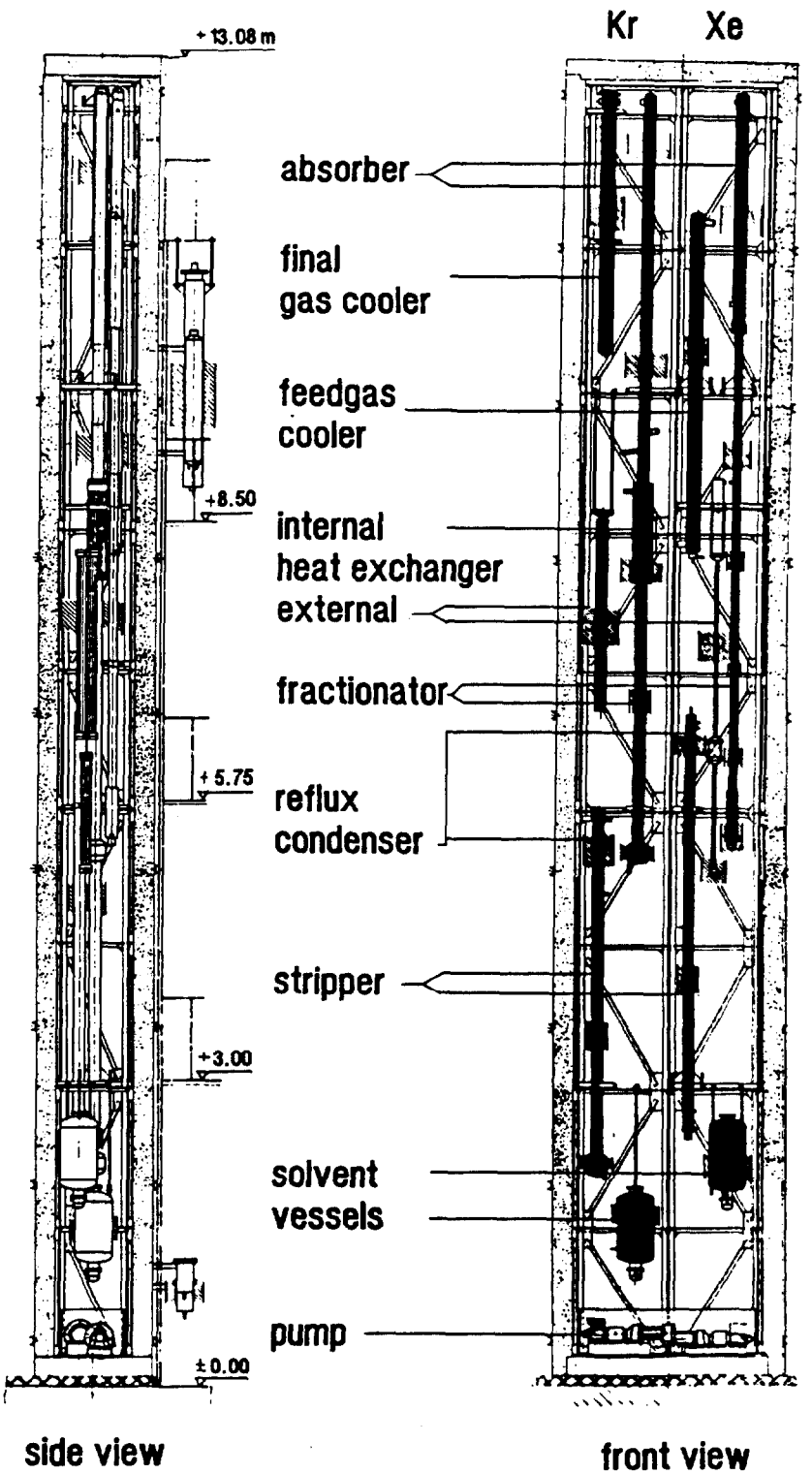

PILOT FACILITY LAY OUT

Fig.8

- The solvent coolers are vacuum insulated metal dewars, filled with liquid N_2. The unloaded solvent stream from the external heat exchanger flows through a pipe coil immersed into the evaporating liquid N_2. Temperature control of the outflowing solvent to $\pm$ 1 °C has been obtained by level control in the LN_2 bath. Recondensation of the evaporated N_2 in commercial recondensation machines does not make sense for our pilot facilities, but is desirable for a demonstration facility.
- The shell and tube type feed gas cooler has longitudial fins at the gas side and is cooled with a controlled flow of LN_2 inside the tubes. It has not been designed for counter-current heat exchange with the purified off-gas.
- The internal heat exchanger in the Kr column has been designed for simultaneous material and heat exchange. It consists of a square shell, densely packed with horizontal rows of pipes welded into the shell. The warm unloaded solvent flows inside the pipes from the bottom successively through each pipe row to the top. The cold loaded solvent trickles downwards on the shell side and then enters the fractionator packing at a temperature near the solvent boiling point.

Packing: Two different types of highly efficient wire mesh packings, made from stainless steel, have been tested. The Xe column contains "Goodloe" packing, Metex company, Ohio USA; the Kr column contains "CY" packing, Sulzer company, Winterthur Switzerland. "Goodloe" packing takes about 8 and "CY" packing only about 4 % of the free column volume.

Refrigeration equipment: Refrigeration energy at cryogenic temperatures is required for the solvent coolers and supplied from a LN_2 tank. Refrigeration energy at -60 $\pm$ 10 °C is needed for the reflux condensers in the strippers. The chilled R11 coolant (CCl_3F) is supplied by a 2-stage refrigeration compressor unit.

Analytical equipment: The composition of the Xe and Kr products are analysed by gas chromatography. Approximate detection limits for a simultaneous determination are about 10 ppmv for Kr, Xe and R12, about 20 ppmv for N_2, O_2, CO_2, N_2O and CH_4 and about 30 ppmv for Ne. A known Ne flow is routinely added, to get a more accurate internal flow calibration. The small residual amounts of Xe or Kr in the purified off-gas are determined by a sensitive quadrupole mass spectrometer; determination limits for Xe and Kr are 1 and 20 ppbv respectively, even in the presence of some solvent vapour.

Process control system: After experience by manual operation, the pilot facility has been equipped with an automatic process control and alarm system from Siemens company. This allowed automatic plant operation without personnel overnight and the weekends. Start up and shut down procedures are still carried out manually. Automatic control has been precondition for long-term tests over several weeks.

4.4 Experimental results

4.4.1 Operating experience:

The pilot plant for rare gas absorption has now been operated for more than 5000 h and more than 100 different operating conditions could be characterized, since new steady state conditions are usually attained in less than 1 h. Most of the operating time has been accumulated in long-time operation after the installation of an automatic process control system. About 1000+ h of short-time operation have been devoted to start-up and shut down procedures and tests of individual components.

During additional about 5000 h, the pilot plant was maintained under standby conditions without solvent circulation. During standby, only the reflux condensers are in operation and the total solvent slowly accumulates in the solvent vessel by condensation at the cold reflux condenser. Start-up from standby conditions is possible in few hours.

Integrated operation together with the precleaning steps or the total DOG system has been carried out without problems. The results of integrated tests can be reliably predicted from results of the more detailed investigations of individual steps. An essential operating experience is a good-natured and forgiving process behaviour.

4.4.2 Experimental decontamination and separation factors:

The essential results and operating conditions are briefly summarized in Table 2 and 3.

	Xe-column	Kr-column
operating pressure	0.8 - 1 bar	0.8 - 1 bar
gas flow rate	up to 28 m^3(STP)/h	up to 24m^3(STP)/h
solvent flow rate	0.25-0.45 m^3/h	0.65-0.85 m^3/h
absorber temperature	-90 to -140°C	-135 to -151°C
solvent evaporation rate:		
fractionator	3 - 6 %	1 - 2.5 %
final stripper	up to 18 %	up to 6 %
heat exchange:		
LN_2 solvent cooler	ΔT ca. 9-11°C	ΔT ca. 10-12°C
internal heat exchanger		ca. 45 %
external heat exchanger	———	ca. 55 %
feed gas cooler	down to -140°C	

Table 2: USUAL RANGE OF OPERATING CONDITIONS IN THE PILOT FACILITY

Feed gas components: carrier gases N_2, O_2, Ar; usually air
product gases Xe, CO_2, N_2O and Kr impurities O_3, CH_4, NO

	Xe-column	Kr-column
absorber temperature	- 125°C	- 148°C
decontamination factor	> 10^5	> 10^3
product purity (without R12)	> 99% Xe, CO_2 N_2O	> 99%; Kr
separation factor	> 10^6 Xe/Kr	> 10^7 Kr/O_2 > 10 Kr/CH_4
product residence time	< 0.2 h	< 0.5 h
absorber stages	5 per m	ca. 3 per m
fractionator stages	5+per m	5 per m
internal heat exchanger stages	-	ca.8 per m
stripper stages	5+per m	5+per m

Table 3: SUMMARY OF EXPERIMENTAL RESULTS WITHIN THE SUITABLE OPERATING RANGE

Suitable operating conditions and results for the Kr-column are shown in Fig.9. More details have been reported in /9,10 /. High decontamination and separation factors and product purities, have been attained. Above all, these values indicate only a suitable design of the pilot plant and a suitable range of operating conditions, but do not contribute much to a thorough process characterization. To a large extent, these individual values can be preselected at will, though not completely independent from each other, by proper plant design and operating conditions.

The behaviour of some impurities deserves special attention. For several hours 500 ppmv ozone was fed into the feed gas. The O_3 follows the Xe as expected from the general solubility trends mentioned in section 4.1. In the Xe product line, the O_3 has been decomposed on a small 10 ml CuO catalyst bed.

O_2 is far less soluble than Kr and a good separation with less than 20 ppmv O_2 (detection limit) in the Kr product has been achieved over a relatively broad range of operating conditions in the fractionator. CH_4 is only about 30 % less soluble than Kr. Within a somewhat narrower range of operating conditions in the fractionator-absorber section, the bulk of CH_4 could also be routed to the off-gas. The special fractionator design with an internal heat exchanger at the top helps, to simultaneously keep a low Kr inventory (residence time). In our Kr pilot column, CH_4 separation to over 95 % is possible only at the expense of an increased Kr-residence time of about 1 h. At Kr residence times > 1 h, CH_4/Kr separation factors >100 have been measured. This depends on the somewhat oversized internal heat exchanger. An optimized design will result in better separation efficiency at usual Kr-residence times of about 0.5 h or less. A good separation from normally 1-3 ppmv CH_4 in air is important for long-time operation without dissolution. The possibility of a good CH_4/Kr separation demonstrates the high separation selectivity of the process.

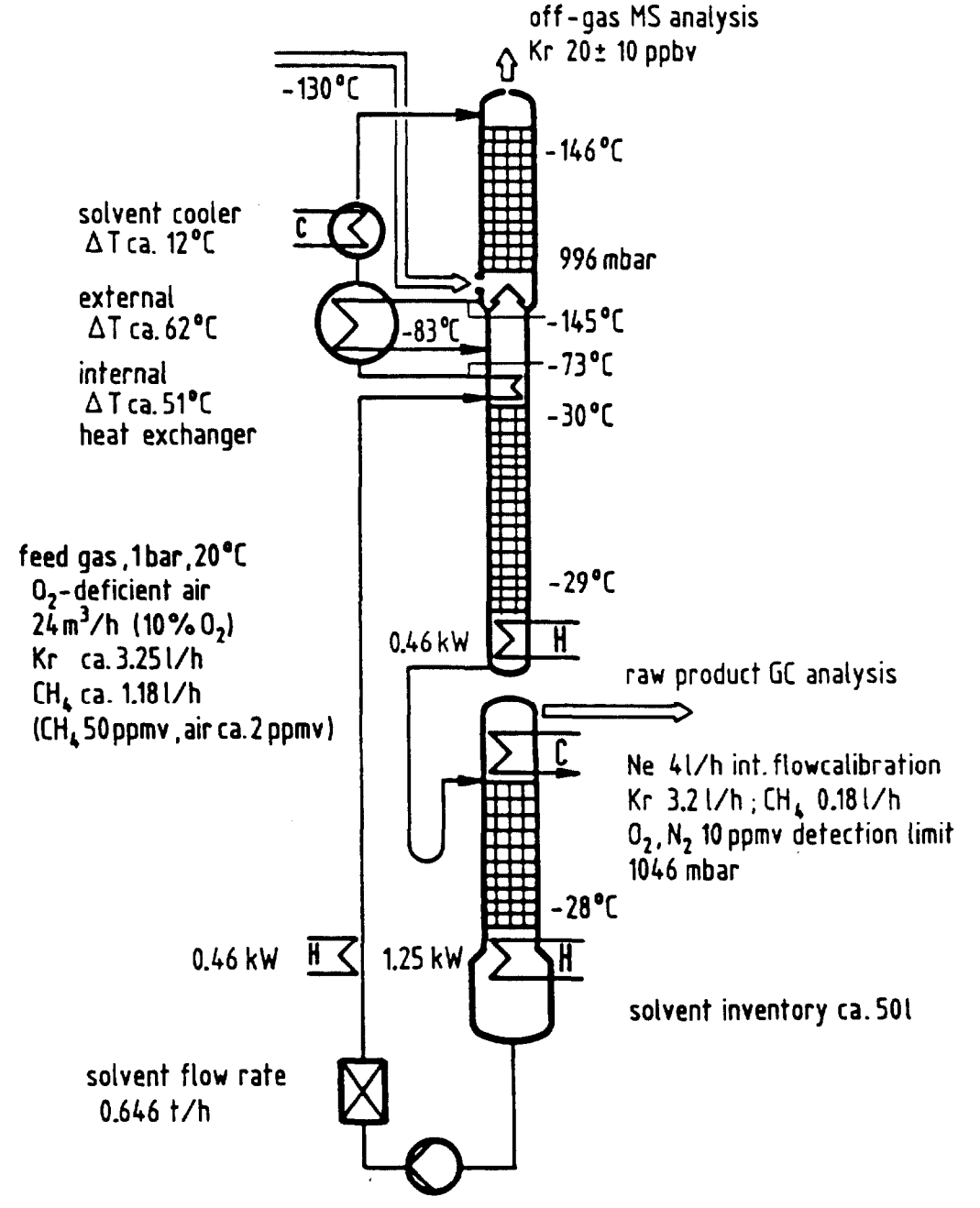

EXAMPLE OF OPERATING CONDITIONS AND RESULTS IN THE KR-PILOT COLUMN

Fig. 9

Operation with continuous product recycle and without product removal from the closed loop allowed a simple determination of the Kr residence time. After addition of a known Kr volume (known inventory), the mean residence time has been determined from the Kr flow in the loop. Improved separation efficiency has been obtained at the expense of a somewhat larger Kr inventory and vice versa. The Kr inventory is of importance for estimates of radiolytic solvent degradation.

The two different packing types which have been tested, are about equally efficient as has been mentioned in table 3. The more open structure of the Sulzer "CY" packing however, allows a somewhat higher gas and liquid load. This packing type is therefore prefered, since the necessary cross sections of the columns can be reduced.

4.4.3 Modelling of the process:

A stage model has been preferred to a continuous model due to the simpler mathematical structure, which allows fast estimates by manual calculation. A more detailed model description has been presented at this conference /12/. Basis of the model are (1) distribution coefficients for the gases as shown in fig.5; (2) column design data, especially the number of stages in the packing as shown in table 3; (3) operating conditions and the feed gas composition. From these data the decontamination factors, product compositions and residence times as well as gas concentration profiles and temperatures in the column sections can be predicted. Experimental results and model predictions are in fair agreement. A reliable model is precondition for a reliable scale-up.

4.4.4 Process control concept:

The main purpose of process control is to keep the extraction factor E in each column section within a certain range. E is the product of the gas-to-solvent flow ratio G/L on a volume basis times the reciprocal distribution coefficient D from fig. 5 at the operating temperature T:

$$E = (G/L) \cdot D^{-1}(T)$$

For the absorber and final stripper sections, the control requirements are low. The solvent circulation rate is kept at a predetermined constant value within ± 1 % by pump control. If a good Kr/CH_4 separation is desired, the gas rate should be kept constant within a ± 10 % range. Large gas rate fluctuations can be smoothed by controlled recycle of purified off-gas. Larger gas rate flow fluctuations down to about 40 % can be tolerated, if no CH_4 separation is required. The absorber temperatures can be kept within ± 1 °C, by control of the solvent cooler downstream from the heat exchanger. Short-time temperature fluctuations are smoothed out by the heat capacity of the components and usually result in a more accurate temperature.

The final strippers operate automatically at the solvent b.p. without temperature control. The solvent vapour rate for counter-current stripping is generated in the sump evaporators. At the expense of an about 10 % higher evaporation rate, the strippers digest the normal flow rate or pressure etc. fluctuations without any control.

Control requirements in the intermediate strippers (fractionators) are somewhat more complex but can be simplified to a large extent by proper design of the heat exchangers in the solvent loop. Various fractionator control concepts have been tested in our pilot plant. Such tests are still continued, using the automatic process control system. A suitable concept is as follows: Different to the absorbers and final strippers, flow ratio and temperature in the fractionator are not constant over the packed height, but decrease from the bottom to the top. Under optimum conditions a certain temperature difference must be combined with a certain evaporation rate in the fractionator sump. Less than half of the solvent vapour is usually condensed within the packing.

In the Xe fractionator, the suitable control range is relatively broad. At normal or slightly subambient pressure, evaporation rates of 3-5 % of the solvent flow may be combined, with about 3-7 K lower temperatures at the top of the packing. This temperature is not identical with the temperature of the incoming solvent. The higher the evaporation rate, the higher is the corresponding optimal temperature difference. A practical consequence is, that the solvent stream from the external Xe heat exchanger needs no further temperature adjustment, if the exchanger is designed to give a solvent stream about 10 ± 2 K below the solvent boiling point. An appropriate evaporation rate then generates the desired temperature profile.

In the Kr fractionator, the suitable control range is somewhat narrower, especially if a good Kr/CH_4 and not only a Kr/O_2 separation is desired. Evaporation rates of 1-2 % of the solvent flow may be combined with about 0.5-2,5 K lower temperatures at the top of the packing below the internal heat exchanger. With a small heater in the warm unloaded solvent stream from the pump, this temperature difference can be controlled in correlation with the evaporation rate. High Kr flow rates in the feed gas require a slightly higher solvent evaporation rate and correlated temperature difference in the fractionator, to maintain a low Kr inventory.

If the absorber cross sections are slightly oversized, sudden and large feed gas flow fluctuations do only negligeably affect the system pressure. Slow total system pressure changes of less than about 3 mbar/min are compensated for, by adjusting the evaporation rates in the fractionators in proportion to the system pressure. Sudden pressure changes cause a sudden change of the solvent b. p. in the fractionators and induce either a short-time solvent boilup or a partial vapour front breakdown in the packing. this is connected with the heat capacity of the fractionator section. In such an event, product take-off can be interrupted and during product recycle, suitable product purities and operating conditions can be rearranged after some time.

4.4.5 Radiolytic solvent degradation:

Radiolytic solvent degradation has been investigated at the technical university of Munich /13,14/. The extent of solvent degradation during hot operation can be calculated from these data and the Kr-inventory in the process. In a suitably designed Kr-

column, operated at suitable conditions, the mean residence time of Kr is about 0.4 h. In a reprocessing plant with 2 t/d U througput, this corresponds to an average Kr-85 inventory of less than 500 Ci. This low quasi-steady state inventory varies in approximate proportion to the fuel dissolution rate. About 3/4 of the Kr is found in the fractionator section (plus heat exchangers) in presence of oxygen. About 1/4 is contained in concentrated form in the upper section of a suitably designed (high specific exchange surface) reflux condenser in absence of oxygen. Less the 2 % of the Kr inventory is present in the Xe column.

Kr-85 decay generates decay electrons with a mean energy of 0.25 MeV but only 0.4 % γ-rays. The electrons are responsible for solvent degradation and produce either inert organic species or hydrolysable species (eg. COX_2, RCOX, Cl_2 etc., X=Cl, F). Hydrolysable species may produce HCl and HF and are potentially corrosive in a wet solvent. In the presence of O_2 about 10 times more of these potentially corrosive species are formed. An estimate of the annual production rate in a plant for 350 t/y U-throughput gives about 1 kg/y. Due to the small amount, the very dry off-gas and the continuously dried and purified solvent, corrosion problems are unlikely. The adsorber bed in the solvent loop is above all a preventive measure in case of defective precleaning steps. Under normal operation, the basic adsorber beds (eg. Al_2O_3) are slowly consumed by the acidic degradation products and must be replaced annually or semiannually without regeneration. Other construction materials, eg. Ni(Mo) based alloys, or the use of dissolved scavengers like C_2Cl_4, which quickly transform the reactive species to inert ones are additional measures, which have not yet been investigated in detail.

5 DESIGN DATA, OPERATING CONDITIONS AND EXPECTED RESULTS FOR A DEMONSTRATION FACILITY

The design of a larger demonstration facility is based on pilot plant experience and the process model. Conceptual design and operating data are outlined in table 4. The expected results are based on conservative model predictions. Model predictions for the gas concentration profiles in the Xe and Kr-fractionators are shown in fig. 10. Total energy requirements, including the auxiliary refrigeration equipment etc., but without the precleaning steps are expected to be about 2 kWh per m^3 (STP) of off-gas. This value depends especially from the low absorber temperature and an efficient design of the heat exchangers in the Kr-column.

6 SUMMARY AND CONCLUSION

The major advantages and disadvantages of the selective absorption of rare gases at cryogenic temperatures are connected with the use of the auxiliary R12 solvent. The advantages are obtained at the expense of additional operations for the solvent:

- Product removal from the solvent requires a desorption step
- A pump is needed for continuous solvent transfer

DESIGN DATA	Xe-column			Kr-column		
packing type (SS or other)	Sulzer "CY"			Sulzer "CY"		
packing dimensions	diameter	height	stages	diameter	height	stages
absorber	0.35 m	3.0 m	14	0.4 m	3.2 m	9
internal heat exchanger	———			0.7 m square	0.4 m	3
fractionator	0.20 m	3.1 m	15	0.3 m	2.5 m	12
final stripper	0.25 m	2.0 m	10+	0.3 m	2.0 m	10+
total column height	ca. 12 m			ca. 12 m		

OPERATING DATA				
off-gas rate	160-200 m^3(STP)/h		ditto	
solvent rate	1.2 m^3/h at b.p		5.0 m^3/h at b.p	
solvent inventory	ca. 0.3 m^3 at b.p		ca. 0.8 m^3 at b.p	
	temperature	pressure	temperature	pressure
absorber	-125°C	0.83 bar	-148°C	0.82 bar
internal heat exchanger	———		from -70°C to -35°C	
fractionator	-40±to-34°C	0.84 bar	-35±to-34°C	0.83 bar
evaporation rate	ca. 4.7± %		ca. 1.4± %	
final stripper	-32.5°C	0.90 bar	-32.5°C	0.90 bar
evaporation rate	16+ %		4+ %	

EXPECTED RESULTS		
decont factor	> 10^4 Xe	> 10^2 Kr
separation factors	> 10^7 Xe/Kr	> 10^7 Kr/O_2, >10Kr/CH_4
product purity (trace impurities)	> 99 % Xe+CO_2+N_2O (<1mCi Kr-85 per m^3Xe)	> 99 % Kr (CO_2*, CH_4)

Table 4: DATA FOR A DEMONSTRATION FACILITY
* from radiolytic solvent degradation in presence of O_2

- Large but uncontrolled heat exchangers in the solvent loop are needed for energy economy
- Small amounts of solvent vapour must be removed from the product and eventually the purified off-gas
- The non-flammable but halogenated solvent must be kept dry and clean, to prevent potential corrosion by small amounts of radiolytic solvent degradation products.

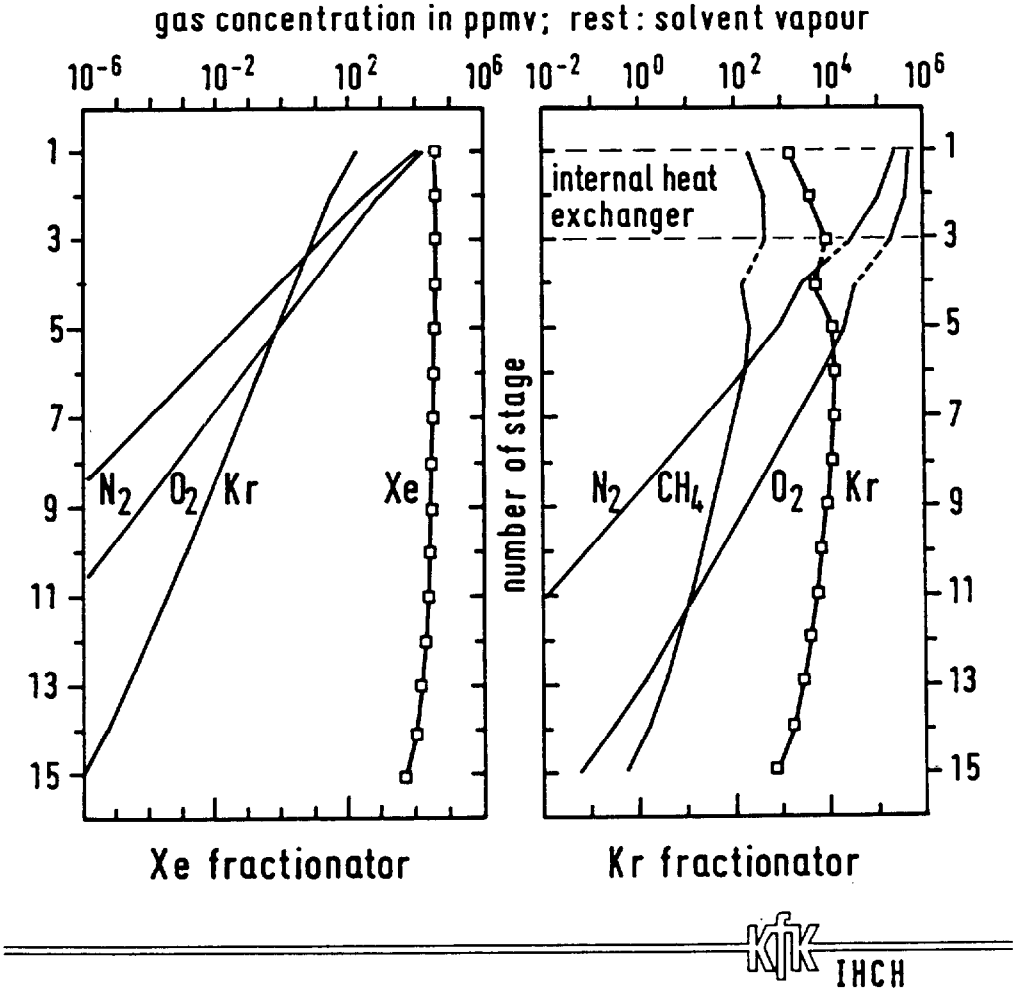

GAS CONCENTRATION PROFILES IN THE FRACTIONATORS
Model predictions for 80 ppmv Kr, 700 ppmv Xe and 5 ppmv CH_4 in the DOG

Fig.10

The disadvantages are overcompensated by favourable process characteristics which contribute to technical simplicity, economy and especially to safety:

- Decontamination factors, separation selectivity and product purity are high. Desired values can be preselected by proper equipment design and operating conditions. Kr is very efficiently separated from Xe and eases further refining for commercial use. 14-CO_2 is separated together with the Xe.
- Cryogenic absorption temperatures, though inconvenient in principle, improve separation selectivity and considerably reduce equipment size and energy consumption.
- Operation at subambient pressure reduces the risk of an accidental Kr-85 release; no compressor is needed.
- The Kr-85 inventory is very low. This reduces radiolytic solvent degradation and radiation shielding requirements. Long-term hot process demonstration is possible with few 10^3 Ci Kr-85 and without a reprocessing plant.

- The sensitivity of the process to impurities is low. Preremoval of O_2, CO_2 or N_2O is not required. The process is also compatible with some O_3 and CH_4. Prepurification steps are simple and do not require sophisticated control.
- The concept of an accessible cold box eases direct maintenance and repair.
- There is no fire risk, no hazardous chemicals are used. Secondary waste arisings are low; H_2O_2, chemicals and their reaction products are recycled as process constituents; spent solvent adsorber beds must be replaced only once or few times per year. R12-solvent is not wasted but purified and reused.

Few month ago, the cryogenic absorption process for rare gas removal from reprocessing off-gas has been selected by the German reprocessing company (DWK, Hannover) for hot demonstration in the Wackersdorf reprocessing plant.

REFERENCES

/ 1/ W. Weiss, A. Sittkus, H. Stockburger, H. Sartorius, K.O. Münnich; Journal of Geophysical Research 88, No. C 13, pp. 8574-8578; and W. Weiss private communication 1988

/ 2/ Empfehlung der Strahlenschutzkommission zur Rückhaltung radioaktiver Stoffe bei einer Wiederaufarbeitungsanlage, vom 24.02.1983, Bundesanzeiger No. 128, Bd. 35, S. 7037; 14. Juli 1983

/ 3/ W. Hebel, G. Cottone (CEC editors); "Methods of Krypton-85 Management", Radioactive Waste Management, series vol. 10, Chur 1983

/ 4/ E. Henrich, U. Bauder, H.J. Steinhardt, W. Bumiller; 18th DOE Nucl. Airborne Waste Management and Air Cleaning Conf., Baltimore, USA; August 13-16, 1984; Proceedings p. 472-484

/ 5/ E. Henrich, U. Bauder, H.J. Steinhardt; Jahrestagung Kerntechnik 85, München 21.-23. Mai 1985, S. 407-410

/ 6/ J.R. Merriman, Paducah Gaseous Diffusion Plant, KY-G-400

/ 7/ Landolt-Börnstein, "Zahlenwerte und Funktionen", Technik Bd. 4 4. Teil Wärmetechnik C, Springer Verlag 1976

/ 8/ KfK/IHCH Annual report, KfK-4226, 1986

/ 9/ E. Henrich, R. Hüfner, F. Weirich, W. Bumiller, A. Wolff; 18th DOE Nucl. Airborne Waste Management and Air Cleaning Conf., Baltimore, USA; August 13-16, 1984; Proceedings p. 959-981

/10/ E. Henrich, U. Bauder, F. Weirich; Int. Conf. Nuclear Fuel Reprocessing and Waste Management "Recod 87", Paris, August 23-27, 1987, Proceedings vol. 2 pp. 553-562

/11/ E. Henrich, R. Hüfner, F. Weirich; in /3/, p. 277

/12/ J. Roemer, E. Henrich; this conference

/13/ W. Fürst, H. Heusinger; Atomkernenergie-Kerntechnik 45(1984) 111

/14/ W. Fürst, H. Heusinger; in report KfK-PtUB9 Mai 1984, pp. 234-255

DISCUSSION

POWELL: What do you expect will be done with the noble gases once you collect them?

HENRICH: Several alternatives have been investigated such as storage in pressurized vessels for intermediate storage. Fixation in zeolite has been investigated and ion implantation. There has been no final decision but it will probably be intermediate storage in pressurized vessels. There is no decision what will be done for final storage.

THOMAS, T.: Did I hear you say at the end of the talk that your process has been chosen for demonstration at Wackersdorf reprocessing plant?

HENRICH: Yes. Our German reprocessing company, DWK-Hannover, has made a process evaluation and from the alternatives which have been investigated in Germany, the cryogenic absorption process has been selected for further technical development. It has been chosen for hot demonstration at Wackersdorf reprocessing plant.

THOMAS, T.: Full scale?

HENRICH: I think so. I do not expect a side stream. It will be about 200 cubic meters per hour, or in other words about 2,000 cubic meters per hour per ton of reprocessed fuel.

THOMAS, T.: Will any other processes be demonstrated also?

HENRICH: No, just for krypton removal.

MOELLER: In the modeling work (paper 2-1), the decontamination factor for Xe was estimated to be 10^{10} and the value observed was $>10^{8}$. In paper 2-3 the decontamination factor found for Xe was reported as $>10^{5}$, could you please explain these differences?

HENRICH: The approximate decontamination factor, DF, derived from the "Fenske"-equation, about E^{n} (for E>2). The number of stages in the Xe absorber of the pilot facility, n, is 10. The extraction factor, E (= L·D/G) depends on the operating conditions. E increases with the solvent rate L, the reciprocal gas rate 1/G, and with decreasing temperature (higher distribution coefficient D). A normal and practically reasonable E range is between 2 and 3. The corresponding DF's are 2^{10} and 3^{10} or about 10^{3} and 10^{5}. Under off-normal conditions with E>7, DF values $\geq 10^{8}$ can be reached. Thus, the DF-values can be varied over a wide range. Experiments under off-normal conditions have been made for model tests.

The value of 10^{8} in preprint 2-1 refers to the separation of Kr from Xe and has been measured under extremely off-normal conditions (simultaneous Xe plus Kr absorption) to test the model. Under normal operating conditions, the limits given by our analytical accuracy allow only a determination of Xe/Kr separation factors up to 10^{6}. All values in paper 2-3 refer to normal conditions and do not include the values obtained in special tests.

A LABORATORY APPARATUS FOR MEASURING OPERATING PARAMETERS FOR A SELECTIVE CATALYTIC REDUCTION APPLICATION TO NOx ABATEMENT*

John McCray and Dirk Gombert II
Westinghouse Idaho Nuclear Company
Idaho National Engineering Laboratory
Idaho Falls, ID

Abstract

A Selective Catalytic Reduction Process for the abatement of oxides of nitrogen is being developed for use at the Idaho Chemical Processing Plant (nuclear fuel reprocessing). To define operating ranges, and to aid in pilot plant design, a laboratory-scale single-stage reactor module was constructed. Several unique challenges were encounted and overcome in the design and fabrication of the reactor module.

Mass flowmeters were used to accurately measure gas flows, regardless of temperature and pressure fluctuations. To make data acquisition simple and accurate, a personal computer was used to automatically indicate temperatures and pressures throughout the system at 5-second intervals, and record the data at 5-minute intervals. A system was designed, using an optical pyrometer, to determine catalyst surface temperatures, during reaction, within the bed at different bed levels. A vaporizer was developed to provide a constant controlled supply of dry NO_2 gas from a liquid N_2O_4 source. Two gas sampling methods were developed to extract samples directly from a gas stream at temperatures up to 600^oC.

I. Introduction

The Idaho Chemical Processing Plant (ICPP), located at the Idaho National Engineering Laboratory (INEL) is operated by Westinghouse Idaho Nuclear Company for the Department of Energy. At the ICPP, spent nuclear fuel is reprocessed for recovery of usable uranium. Liquid waste from this process is converted to a dry granular solid for volume reduction and ease of storage. The fluidized-bed calcination process used produces an off-gas containing up to 3% oxides of nitrogen (NO_x). A program to remove NO_x from the off-gas is currently underway.

Based on previous testing (using less concentrated NO_x gas streams), selective catalytic reduction (SCR) was chosen as the preferred technology for NO_x removal. This involves the reduction of NO_x with NH_3 to form N_2O, N_2 and H_2O. A three-stage reactor pilot plant has been designed to demonstrate operability and reduction efficiency of the proposed NO_x abatement facility. Pilot plant operation will be conducted using a side stream of the actual plant off-gas.

To define operating ranges for, and to aid in the design of the pilot plant, a laboratory-scale single-stage reactor module was constructed. The data required from the module included bed pressure drop, catalyst surface temperature vs. bulk gas temperature, and reduction efficiency. Measurements were made over a wide range of operating conditions.

* Work supported by the U.S. Department of Energy under DOE Contract No. DE-AC07-84ID12435

Presented in this paper are the detailed design and fabrication of the single stage reactor system. Special emphasis is given to: 1) the unique sight-tube method used to penetrate the reacting bed to acquire catalyst surface temperature data at different bed levels, 2) the development of a vaporizer for liquid nitrogen tetroxide (N_2O_4) to obtain a constant pressure supply of nitrogen dioxide (NO_2), and 3) the development of sampling methods.

II. System Requirements

To accomplish the reactor testing program, special system attributes include the following:

1. Accurate individual gas flowrate measurement and control for air, NO_2, and NH_3. Plant off-gas was simulated by mixing air with up to 3% NO_2. Flowrates for the simulated off-gas were varied to obtain a range of gas residence times in the bed. NH_3 flowrates were varied to obtain a range of NH_3/NO_2 ratios for each residence time.

2. Accurate control of gas preheating and system heat-tracing to 1) prevent the formation of ammonium nitrate (reaction of NO_2 and NH_3 at temperatures below 210°C), 2) allow control of the gas temperature at the inlet to the reactor, and 3) maintain steady-state temperature profiles across the catalyst bed.

3. The ability to vaporize liquid nitrogen tetroxide (N_2O_4) to obtain a constant pressure NO_2 gas supply.

4. The ability to measure catalyst surface temperatures, at different bed levels, during reaction.

5. A gas sampling method to determine reaction efficiencies.

III. General Reactor System Lay-Out

A schematic of the reactor system is shown in Figure 1. The main gas line to and from the reactor was fabricated from 1/2-inch Type 304 stainless steel (SS) tubing. Ammonia and NO_2 were introduced into the main gas stream via 1/4-inch SS tubing. The reactor vessel was fabricated from a 26-inch section of 2-inch Sch. 40 Type 304 SS pipe, flanged at both ends. This allowed for a maximum catalyst bed depth of 19 inches. A stainless steel screen was positioned 2 inches above the reactor bottom to support catalyst particles in the reactor while allowing gas passage from the top, and to allow room below the bed for thermocouple and pressure ports. Thermocouple and pressure ports were also located above the bed, 24 inches from the reactor bottom. The pressure drop across the bed was measured by a magnehelic gauge. Thermocouples (1/16-inch diameter) penetrated the reactor to measure the catalyst bed centerline temperature at 2-inch intervals. A pyrometer with a reactor-penetrating sight tube was used to measure catalyst surface temperature at a single location, 2 1/2 inches above the bed supporting screen. Additional thermocouples were used throughout the system to aid in monitoring gas temperatures.

Simulated plant off-gas was made up with a mixture of filtered plant air and up to 3% nitrogen dioxide (NO_2) from a nitrogen tetroxide (N_2O_4) cylinder. Ammonia (NH_3) was also fed from a gas cylinder. All gas flows were controlled

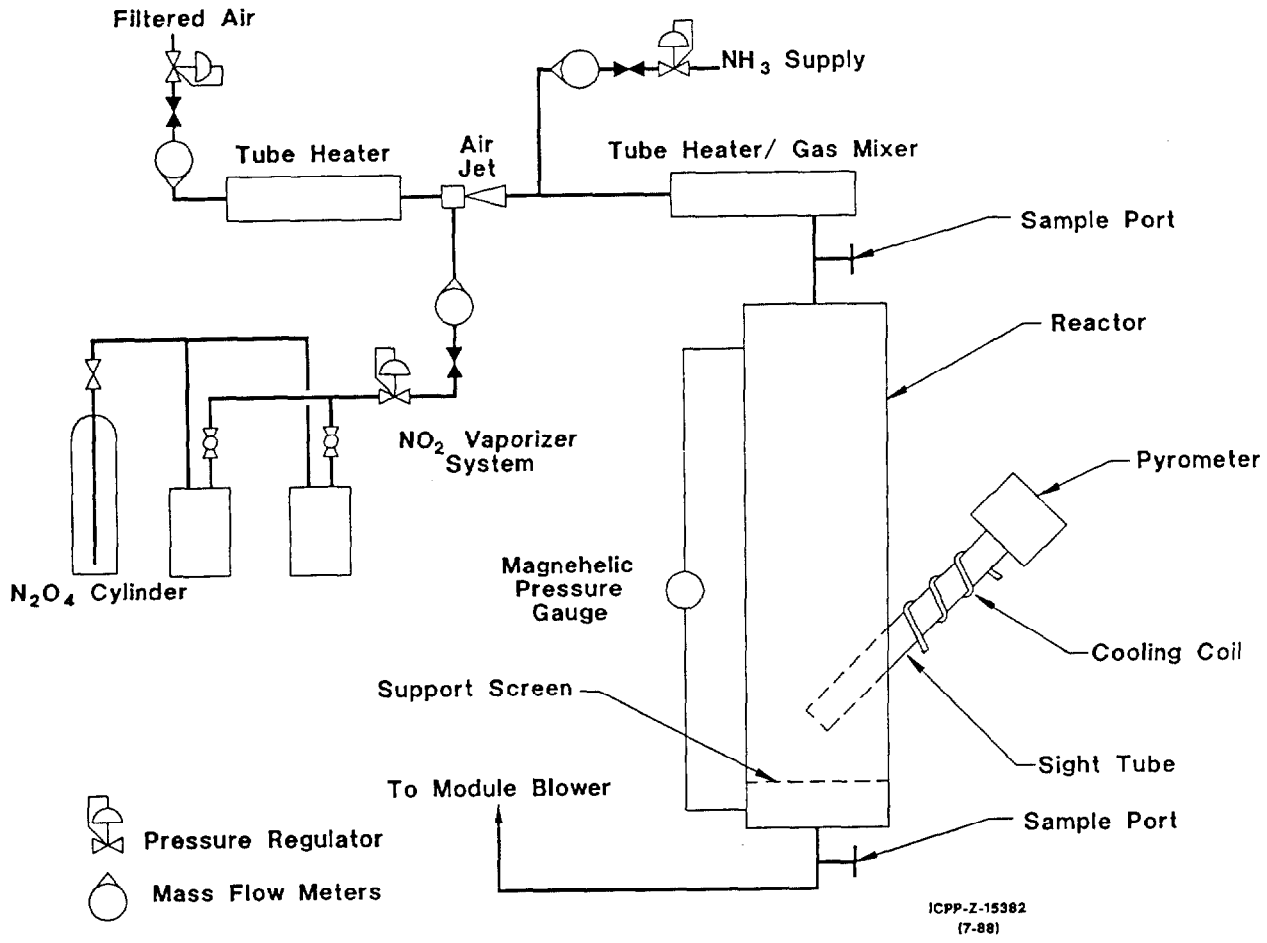

Figure 1. Simplified NO_x abatement laboratory-scale reactor system schematic.

with independent metering valves, and measured with separate mass flowmeters for each gas specie. Each mass flowmeter was sized for the range of flows required, and calibrated for the specific gas used. A personal computer was set up to concurrently indicate at 5-second intervals, and record at 5-minute intervals, all gas flowrates and thermocouple temperatures.

NO_2 reacts with NH_3 to form potentially explosive ammonium nitrate solid at temperatures below 210°C. To prevent this from happening, gas line temperatures had to be maintained above 210°C from the point NH_3 is introduced, to the exhaust point at the module blower.

To provide desired temperatures throughout the system, two tube heaters and 6 heat tape sections, each with its own power rheostat, were used. Tubing running through the tube heaters was filled with stainless steel pall rings to increase heat transfer area. All gas line sections and the reactor were wrapped with heat tape and insulated. Thermocouple readings from various system locations provided adequate input for tube heater and heat tape power adjustments.

Filtered plant air passed through a pressure regulator, a metering valve, and a mass flowmeter. The air was then preheated and passed through an air jet where NO_2 gas was injected to form the intimately mixed simulated plant off-gas.

Following additional heating, ammonia gas was injected and the gas stream passed through a gas mixer (a tube section filled with 1/8" Type 316 SS pall rings). The preheated gas mixture could then be sampled before introduction to the reactor. After passing through the reactor, the gas could again be sampled before exhausting through the module roof blower.

IV. Catalyst Surface Temperature Measurement Apparatus

Catalyst surface temperature was measured at a single location, at the bed center line one inch above the bed retaining screen. By varying bed depth, the surface temperature at any bed level could be determined. Temperature measurement was done with an optical pyrometer located outside the bed, through a 3/4-inch ID sight tube. The catalyst surface temperature measurement apparatus is shown in Figure 2. The sight tube was fabricated from stainless steel tubing on the outside of the reactor vessel, and from stainless steel screen on the inside of the reactor, to allow gas passage through it. The sight tube outside the reactor was water cooled using a copper coil to prevent overheating of the pyrometer. The sight tube was positioned at an angle to the vertical reactor to provide a catalyst "surface" perpendicular to the inside tube. Purge air (5 scfh) flowed from the pyrometer, through the sight tube, and into the reactor bed, to keep the pyrometer lens free of debris and reactive gases.

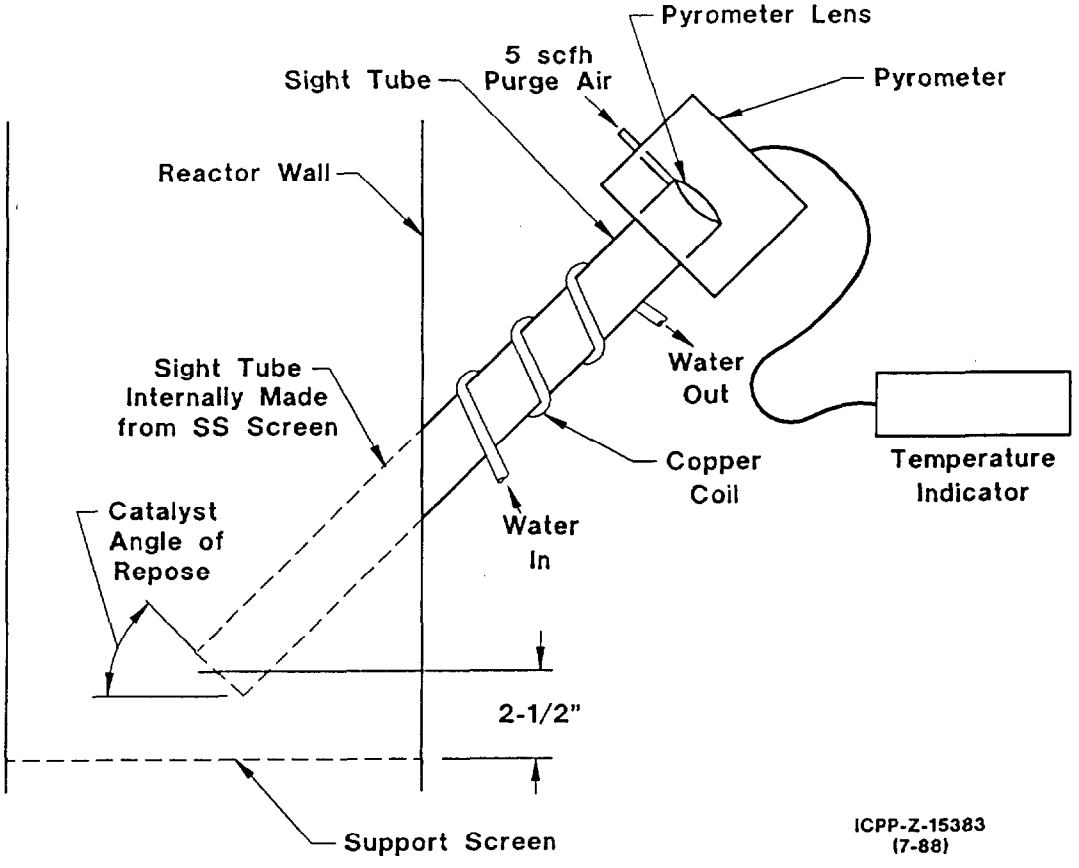

Figure 2. Schematic of catalyst surface temperature measurement apparatus.

V. NO_2 Vaporizer

The NO_2 source was a cylinder of liquid nitrogen tetroxide (N_2O_4), which has a vapor pressure of 14.7 psia at 70°F. Since a vaporizer for small amounts of this toxic gas is not commercially available, one was designed and built for this system. The NO_2 vaporizer used for the system is shown in Figure 3.

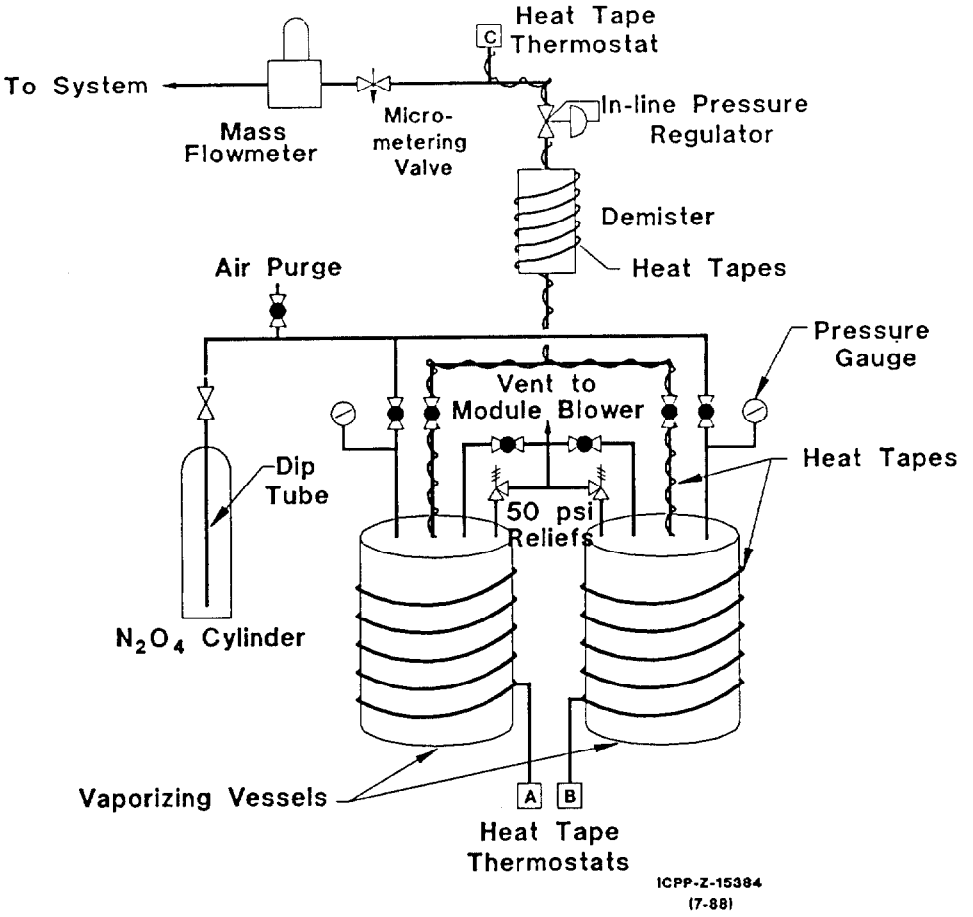

Figure 3. Schematic of NO_2 vaporizer system.

Features of the NO_2 vaporizer design included:

1. Two vaporizing vessels were used to allow for constant operation: allowed filling one while feeding from the other.

2. Separate thermostatically controlled heat tapes for each of the two vaporizer vessels and for the NO_2 gas line from the vaporizers to the mass flowmeter.

3. A pressure relief valve (set at 50 psig) for each vaporizer vessel. These exhausted to the outside via the blower on the module roof.

4. A valved vent line from each vaporizer vessel, also piped to the module roof blower. This allowed for volume displacement when filling the vessels with N_2O_4.

5. A thermocouple penetrating each vaporizer vessel to monitor liquid level when filling.

6. An in-line pressure regulator to regulate and maintain a constant gas pressure to the metering valve.

7. An air line (normally closed) connected to the N_2O_4 supply line just downstream of the N_2O_4 cylinder, to allow complete flushing of the system prior to maintenance work or dismantling.

Heat tape thermostats for the vaporizer vessel being used, and for the NO_2 gas line, were set for the desired temperature. When the vessel pressure gauge exceeded the desired NO_2 supply pressure, the in-line pressure regulator was opened and set at that pressure to provide a constant pressure supply of NO_2 gas to the system. NO_2 flowrates were controlled using the metering valve and the mass flowmeter. The air jet on the main process gas line created a vacuum in the NO_2 line, preventing NO_2 condensation from the metering valve to the process gas line. Switching and/or refilling vaporizer vessels during operation was possible by appropriate use of heat tape thermostats and valves.

VI. Gas Sampling

Sampling of the reactor inlet and outlet gas streams, at known conditions to allow direct analysis of the gas, was one of the primary goals of the system design. Cooling of the sample below the dissociation temperature of ammonium nitrate resulted in a two-phase sample. Cooling to room temperature resulted in a three-phase sample (condensate). Obtaining a sample at system temperature and pressure, and verifying those conditions, was attempted in several ways.

Originally, gas sampling was done using in-line stainless steel sample bombs, allowing steady-state conditions to be established in the bomb before isolating the sample. This method was discontinued because of chemical adsorption of the nitrate on the stainless steel walls of the sample bombs. Two other gas sampling methods, syringe extraction and vacuum extraction into a glass sample bomb were also used. Sampling locations for both methods were upstream and downstream of the reactor.

Syringe Sampler

The syringe extraction gas sampling apparatus is shown in Figure 4. A short length of tubing, plugged with a rubber septum, was fitted to a tee in the main gas line. An aluminum cylinder (~1 inch long and 3 inches in diameter) was drilled through the center and machined to tightly fit over the tubing section. Several deep grooves were cut into the aluminum piece to form cooling fins. This aluminum piece dissipated the heat conducted through the tubing section from the hot gas stream. Use of the aluminum "radiator" prevented deterioration of the rubber septum exposed to gas temperatures of up to 600°C. By pushing the needle of the syringe through the septum, samples were taken directly from the gas stream. The syringe was equipped with a stopcock to block sample escape.

Sample gas temperature quickly approached that of the syringe (room temperature). Sample gas pressure was believed to be close to that of the system during sampling. Ambient pressure was obtained in the sample by extracting the syringe plunger after the sample was trapped.

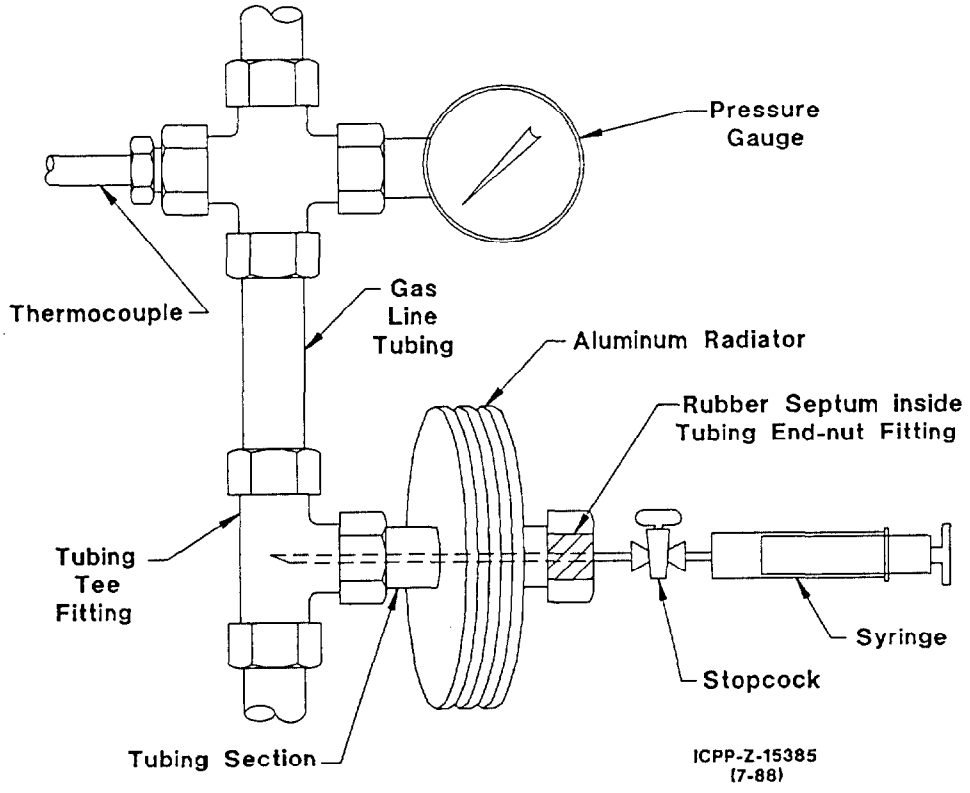

Figure 4. Schematic of syringe extraction sampling system.

Vacuum Extraction Sampler

The vacuum extraction gas sampling apparatus is shown in Figure 5. A glass sample bomb was positioned between a vacuum pump and a tee on the gas line. Pressure gauges and thermocouples were positioned to indicate pressures and temperatures of the gas stream and the sample bottle line.

With all sampler valves and stopcocks open except the ball valve between the sample bottle and the process gas line, the bottle was evacuated with the vacuum pump. The ball valve between the bottle and the vacuum pump was then closed. A sample was taken by slowly opening the ball valve between the bottle and the process gas line, while watching the vacuum/pressure gauge downstream of the bottle. The ball valve was again closed when the bottle reached ambient pressure. Stopcocks were closed to isolate the sample in the bottle.

Sample gas temperature quickly approached the ambient bomb temperature. Sample pressure was controlled with the valve on the inlet from the main gas line. This method was more sensitive to analytical method due to the larger surface area of the sample bomb versus the syringe.

VII. Conclusions and Recommendations

The single-stage reactor system, over all, worked very well. Required test program goals were met.

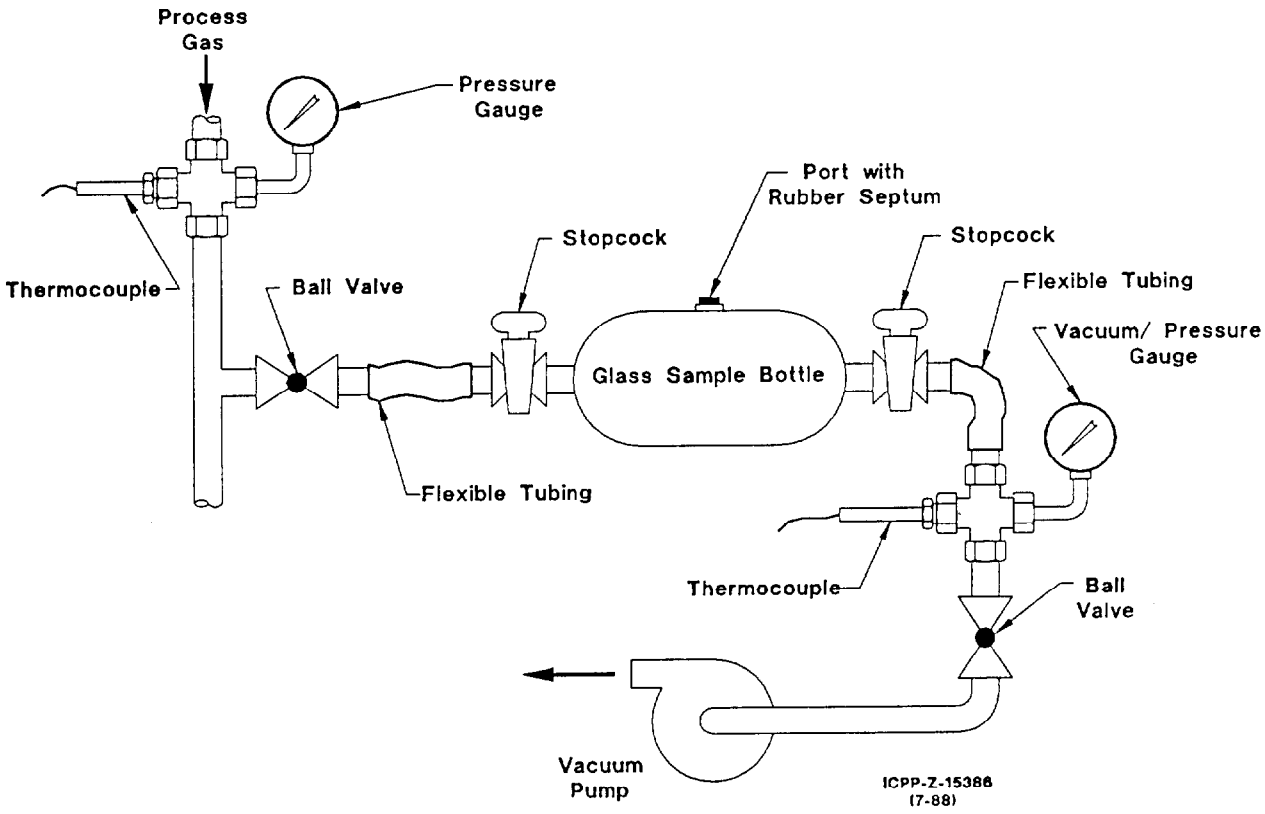

Figure 5. Schematic of vacuum extraction sampling system.

Use of mass flowmeters for gas flowrate measurements worked extremely well in enabling accurate simulations of plant off-gas containing up to 3% NO_x, and precise NH_3 flows for desired extents of reaction. Use of the personal computer for data collection provided frequent and concurrent data recording of all temperature points and gas flowrates.

The NO_2 vaporizer provided a constant supply of dry gas, at constant pressure, to the reactor. One facet of the vaporizer system that could be improved is the method used to determine vessel liquid level. A thermocouple penetrates the vessel from the top to a level approximately half-way to the bottom. The thermocouple is used to indicate the temperature change when contacted by liquid during filling. This leaves sufficient vapor space to provide a constant supply of NO_2 gas. However, the ΔT between the two phases is too small to positively identify phase change at the thermocouple level. A conductivity probe could possibly be better suited to this purpose.

Using the pyrometer and vessel-penetrating sight tube to measure catalyst surface temperatures at different bed levels was also successful. Surface temperature measurements were determined for four different bed levels. The combined cooling effect of the pyrometer lens purge air and the cooling coil around the sight tube exterior did, however, interfere with accurate thermocouple temperature measurements downstream of the pyrometer (including off-gas temperature measurements). The pyrometer system was removed after surface temperature testing was completed, allowing for more accurate results from remaining reaction efficiency tests. A pyrometer with better heat tolerance and/or not requiring a lens purge could possibly have provided improved overall test results.

Both the syringe and vacuum extraction methods worked very well in obtaining samples from a very hot gas stream. A reliable off-line analytical method must still be perfected to make better use of these samples. More sophisticated analytical instrumentation in the pilot-plant is anticipated to allow on-line species determination throughout the system.

DISCUSSION

SCHEELE: What is the composition of the NO_x catalyst that you were using?

McCRAY: A lot of that information I can not release and a lot of it I do not know. It is Norton Company's synthetic zeolite. It could be close to a synthetic mordenite.

SCHEELE: Is it the hydrogen mordenite which has been used in past experiments?

McCRAY: It has been used in the past, so that is correct. I really do not know what the active metal is in this case.

CATALYST TEMPERATURE AND REACTION EFFICIENCY IN SELECTIVE CATALYTIC REDUCTION - NO_x ABATEMENT

V. C. Maio and D. Gombert II*
Westinghouse Idaho Nuclear Company
Idaho National Engineering Laboratory
Idaho Falls, ID

Abstract

A laboratory test program was conducted to evaluate the selective catalytic reduction (SCR) process for abatement of nitrous oxides (NO_x) present in off-gases released from a nuclear fuel reprocessing facility. The purpose of the lab-scale tests was to identify optimum values for key SCR operating parameters and determine the effects of these parameters on catalyst temperature and NO_x reduction efficiency. Test conditions and data are presented and discussed. Based on the results, recommendations for future SCR pilot-scale development are provided.

I. Introduction

At the Department of Energy's (DOE) Idaho Chemical Processing Plant (ICPP) near Idaho Falls, Idaho, scheduled upgrades in nuclear fuel reprocessing capacity will also increase the production rate of high level radioactive liquid waste (HLLW). The HLLW contains appreciable amounts of nitric acid from the dissolution process. Therefore, NO_x is generated when the HLLW is converted to solid granular particles by calcining in a fluidized bed at 500°C.

The off-gas emitted from the calciner contains up to 30,000 ppm (3%) NO_x and the scheduled plant upgrades will significantly increase the NO_x production rate.[1] To address this increase, a development program is in progress by Westinghouse Idaho Nuclear Company Inc. (WINCO) to develop an NO_x abatement system to treat the calcination effluent.

An earlier technical and economic evaluation[2] of possible NO_x abatement technologies, resulted in choosing the selective catalytic reduction (SCR) method for the calciner off-gas. In the SCR process, the NO_x in an off-gas stream is reduced with ammonia (NH_3) at 220°C to 550°C in the presence of a zeolite catalyst. The process is typically applied for fossil fuel fired boilers to treat off-gases containing less than 1000 ppm NO_x, and little experimental data are available for NO_x levels of over 10,000 ppm (1%). The development program will extend the proven range of the SCR process to the 30,000 ppm NO_x concentration existing in the calciner off-gas. Additional objectives of the development program include:

1. Assessment of the process effects of the high water vapor content (up to 30%) of the calciner off-gas.

2. Determination of the maximum catalyst surface and bulk gas temperatures due to the high NO_x concentration.

* Work supported by the U.S. Department of Energy under DOE Contract No. DE-AC07-84ID12435.

3. Verification of catalyst life in the presence of minor chemical contaminants such as fluoride, chloride, and mercury, and radionuclides such as cesium and ruthenium.

The WINCO development effort includes testing at both the laboratory and pilot-plant scale levels. The NO_x Abatement Pilot-Plant Facility[3] has been designed at ~1/50 scale of the proposed plant-scale facility. It will treat a slip-stream of the actual calciner off-gas in a system using up to three catalytic reactors. The laboratory-scale unit (~1/200 of proposed plant-scale capacity) consists of one reactor and was operated with simulated calciner off-gas. The purpose of the lab-scale tests was to define an operating range for the pilot-plant test program. This paper presents the results of the laboratory-scale tests. Emphasis is given to test results relating to catalyst temperatures and reaction efficiencies, though sections are included on the test program, the test apparatus, data analysis, and process theory. Recommendations for the scheduled pilot-plant tests are also provided.

II. Laboratory Scale Test Program

The test program was designed to evaluate the effects of varying: 1) catalyst bed depth, 2) NH_3 to NO_x ratio in the feed gas, 3) feed gas face velocity (as measured at reactor inlet conditions), 4) initial reactor and feed gas temperature and 5) the concentration of NO_x in the feed gas. SCR performance would then be measured in terms of 1) magnitude and location of the maximum catalyst surface temperature, 2) temperature rise across the reactor and 3) NO_x reduction efficiency.

Earlier development work completed with a similar catalyst[4] provided a basis for the evaluation. Table 1 summarizes the conditions tested. All the tests listed in Table 1 were performed with simulated calciner off-gases (prepared from pure sources of air, NH_3 and NO_2) and with Norton Company's NC-300 synthetic zeolite catalyst pellets in the shape of 1/4" Raschig Rings. Water and nitric oxide (NO) were not included in these tests for simplicity and to attain "worst-case" conditions (i.e., maximum temperatures in the catalytic reactor).

The selection of the 1/4" Raschig Ring catalyst pellet was based on results of earlier pressure drop measurements. The low pressure drop produced by the Raschig Rings more that compensated for their relatively lower surface-to-volume ratio.

III. Lab-Scale Test Apparatus and Operation

A detailed description of the design and fabrication of the test equipment is presented in Reference 5. The lab-scale reactor was a 2" diameter, 24" long stainless steel pipe equipped with pressure probes and axial thermocouples. Simulated calciner off-gases were fed to the reactor by mixing pure sources of NO_2, NH_3 and air. Test gas compositions and flowrates were obtained with precision mass flowmeters. A jet in the main air line, employed to provide the pressure drop required for NO_2 injection, also yielded intimate mixing for the reactor feed gas. Heat was provided with tube heaters and heat tapes. Catalyst surface temperature measurements were made with an optical pyrometer. Thermocouple and mass flow meter readings were displayed and recorded on a personal computer. A simplified schematic is shown in Figure 1.

TABLE 1

NO_X ABATEMENT LABORATORY-SCALE TEST CONDITIONS

Test No.	Inlet NO_2 (ppm)	NH_3/NO_2 Ratio	Bed Depth (in.)	Face Velocity (fps)	Gas Feed Temp. (°C)	Test Duration (min.)	Sample (in)	Sample (out)	Pyrometer
1	30,000	1.2:1	2 1/2	3.0	260	15	X	X	X
2	18,500	1.2:1	2 1/2	5.0	264	38	X	X	X
3	30,000	1.2:1	2 1/2	5.0	240	45	X	X	X
4	30,000	1.2:1	2 1/2	7.0	233	53	X	X	X
5	30,000	1.2:1	6.0	3.0	296	16	X	X	X
6	30,000	1.2:1	6.0	5.0	284	69	X	X	X
7	30,000	1.2:1	6.0	7.0	276	35			X
8	30,000	.6:1	12	7.0	281	66			X
9	30,000	.8:1	12	7.0	285	55			X
10	30,000	1:1	12	7.0	286	69			X
11	30,000	1.2:1	12	7.0	288	40			X
12	30,000	.6:1	12	5.0	279	72			X
13	30,000	.8:1	12	5.0	288	36			X
14	30,000	1:1	12	5.0	288	37	X	X	X
15	30,000	1.2:1	12	5.0	*				
16	30,000	.6:1	12	3.0	282	83			X
17	30,000	1.2:1	12	3.0	294	62	X	X	X
18	30,000	.6:1	18	7.0	269	65	X	X	X
19	30,000	.8:1	18	7.0	270	95			X
20	30,000	1:1	18	7.0	291	65	X	X	X
21	30,000	.6:1	18	5.0	268	76			X
22	30,000	.8:1	18	5.0	323	137		X	X
23	30,000	.6:1	18	3.0	265	100		X	X
24	30,000	.8:1	18	3.0	259	114			X
25	30,000	1:1	18	3.0	259	53			X
26	30,000	1.2:1	18	3.0	259	79			X
27	30,000	.6:1	18	7.0	249	98			X
28	30,000	.8:1	18	7.0	248	62			X
29	30,000	1.8:1	18	7.0	246	60			X
30	30,000	1.2:1	18	7.0	248	30			X
31	30,000	1.8:1	18	7.0	248	49		X	
32	30,000	.6:1	18	7.0	228	79			
33	30,000	.6:1	18	7.0	238	79			
34	30,000	.8:1	18	7.0	239	73			
35	30,000	1:1	18	7.0	238	57			
36	30,000	1.2:1	18	7.0	239	60	X	X	
37	30,000	.6:1	18	5.0	230	89			
38	30,000	.8:1	18	5.0	226	70			
39	30,000	1:1	18	5.0	229	71			
40	30,000	1.2:1	18	5.0	229	72			
41	30,000	.6:1	18	3.0	227	85			
42	30,000	.8:1	18	3.0	229	129			
43	30,000	1:1	18	3.0	224	96			
44	30,000	1.2:1	18	3.0	231	74			
45	5,000	1.3:1	18	3.0	337	59	X	X	
46	10,000	1.3:1	18	7.0	230	74	X	X	
47	15,000	1.3:1	18	7.0	229	75	X	X	
48	20,000	1.3:1	18	7.0	227	54			
49	25,000	1.3:1	18	7.0	230	75			
50	30,000	1.3:1	18	7.0	224	45			
51	5,000	1.3:1	18	5.0	230	60			
52	10,000	1.3:1	18	5.0	231	130			
53	15,000	1.3:1	18	5.0	230	95			
54	20,000	1.3:1	18	5.0	224	85			
55	25,000	1.3:1	18	5.0	229	105			
56	5,000	1.3:1	18	9.0	233	55	X	X	
57	10,000	1.3:1	18	9.0	230	65			
58	15,000	1.3:1	18	9.0	231	70	X	X	
59	20,000	1.3:1	18	9.0	231	60			
60	25,000	1.3:1	18	9.0	231	71	X	X	
61	25,000	1.3:1	18	9.0	230	115			
62	30,000	1.3:1	18	9.0	230	45	X	X	
63	5,000	1.3:1	18	7.0	320	45	X	X	
64	10,000	1.3:1	18	7.0	320	55			
65	15,000	1.3:1	18	7.0	320	69			
66	20,000	1.3:1	18	7.0	321	80	X	X	
67	25,000	1.3:1	18	7.0	321	55	X	X	
68	5,000	1.3:1	18	7.0	422	44			
69	5,000	1.3:1	18	7.0	448	27			
70	10,000	1.3:1	18	7.0	421	80	X	X	
71	15,000	1.3:1	18	7.0	421	60	X	X	

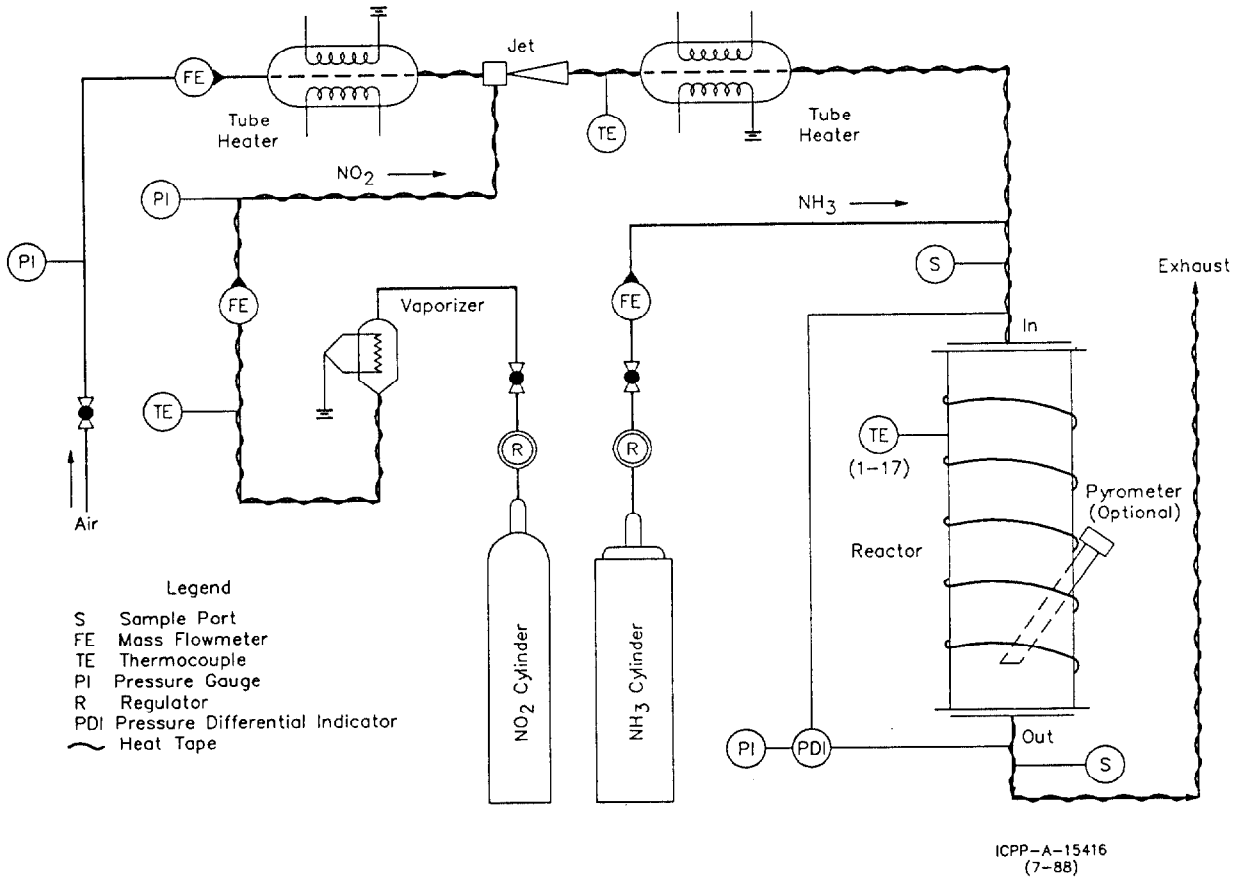

NO_x Abatement Lab-Scale Facility Process Flowsheet.
Figure 1.

Prior to testing, the reactor was preheated with air to the desired temperature. Air, NO_2 and ammonia flowrates were then established and the temperature profile allowed to reach steady state. Ammonium nitrate formation was precluded by maintaining all surfaces at greater than 210°C. Ambient air monitors for NO_2 and NH_3 gas were also employed.

IV. PROCESS THEORY AND DATA ANALYSIS

In the SCR process of employing a specially prepared zeolite catalyst, ammonia selectively and spontaneously reacts with NO_2 and NO to form N_2O, N_2 and H_2O. The primary catalytic reactions[4] are:

	Heat of Reaction	
$8\ NO_2 + 6\ NH_3 \longrightarrow 7\ N_2O + 9\ H_2O$	-53 Kcal/mole NO_2	(1)
$6\ NO_2 + 8\ NH_3 \longrightarrow 7\ N_2 + 12\ H_2O$	-108 Kcal/mole NO_2	(2)
$6\ NO + 4\ NH_3 \longrightarrow 5\ N_2 + 6\ H_2O$	-71.9 Kcal/mole NO	(3)
$8\ NO + 2\ NH_3 \longrightarrow 5\ N_2O + 3\ H_2O$	-28.2 Kcal/mole NO	(4)

Only NO_2 was used in the testing reported here, eliminating reactions 3 and 4. The following side reactions are also possible:

$$4\ NH_3 + 3\ O_2 \longrightarrow 2\ N_2 + 6\ H_2O \quad (5)$$
$$2\ NO_2 \longrightarrow N_2 + 2\ O_2 \quad (6)$$
$$3\ N_2O + 2\ NH_3 \longrightarrow 4\ N_2 + 3\ NH_2O \quad (7)$$
$$2\ N_2O \longrightarrow 2\ N_2 + O_2 \quad (8)$$

However, at the conditions tested with the zeolite catalyst reactions 1 and 2 are kinetically favored.

Assuming the well insulated catalytic reactor is virtually adiabatic and side reactions are negligible (i.e., the process is truly selective) the temperature rise across the catalytic reactor is a function of the NO_2 reacted and the heat of reaction. Based on the heats of reaction for reactions 1 and 2, the temperature rise across the reactor for every 5,000 ppm of NO_2 reduced is calculated to be 20-40°C for reduction to N_2O (reaction #1) and 50-70°C for complete reduction to N_2 (reaction #2).

Reactor temperature rise data were corrected for deviations from adiabatic operation. These deviations were the result of:

1. The cooling of the reactor by the air purge and water coils necessary for the pyrometer.

2. Initiating testing with a steady-state but nonuniform temperature profile across the reactor (heat loss across the reactor length).

A comparison of tests done with and without the use of the pyrometer defined the temperature correction factors due to the first effect. Table 2 lists the factors for tests done at face velocities of 3, 5 and 7 feet per second (fps). (Tests done at 9 ft/sec were completed without the pyrometer. Refer to Table 1.)

The heat losses along the bed length were accounted for by comparing the exhaust temperatures with and without reaction while maintaining the inlet temperature constant, rather than using the actual temperature rise from inlet to outlet.

TABLE 2

Reactor Effluent Gas Temperature Corrections for Pyrometer Use

Face Velocity (fps)	Temperature Correction (+) (C^0)
3	25 - 35
5	15 - 25
7	5 - 15

The maximum catalyst surface temperature was estimated by equating the heat generation rate at the catalyst surface to the heat transfer from the surface to the bulk gas. The resultant temperature difference between the surface and the bulk gas (delta T) is the driving force required to maintain the equality, that is the steady-state temperature at which the heat loss to the bulk gas balances the heat generation rate. The semi-empirical correlations[6] combine to form the following equation.

$$\Delta t = \frac{r_{mA}\ \Delta H_A}{a_m\ \phi\ C_p\ G_m} \left[j_H\right]^{-1} (Pr)_f^{\ 2/3} \qquad (9)$$

Where $j_H = 1.076\ (.57\ Re)^{-0.41}$. All other terms in the equation are defined as follows:

Term	Definition
r_{ma}	molar rxn rate of NO_2 per mass of catalyst
ΔH_A	molar heat of rxn
a_m	area of catalyst particle per unit mass
ϕ	shape factor (sphericity) of catalyst particle
C_p	molal heat capacity
G_m	molal mass velocity based on cross section
Re	Reynolds Number ($G/a_v\ \phi\ \mu$)
Pr_f	Prandtl number $C_p\ \mu/k$
a_v	area of particle per unit volume of bed
G	mass velocity of gas based on cross section
μ	gas velocity
k	gas thermal conductivity

Gas properties at the catalyst surface must be estimated and can easily vary by 10-25% depending on the correlation or reference used. Reaction at the surface was assumed to be instantaneous with the rate equal to the mass transfer rate of the reactants to the surface. Estimation of the mass transfer rate is also subject to wide ranges of gas property values. Finally, the actual catalyst surface area to volume ratio is a proprietary number which can only be assumed to fall somewhere within the published range for a "zeolite structure". With these limitations in mind, the calculated surface temperature ranged from 100^0 to 400^0C above the bulk gas temperature.

For a gas inlet temperature of 250^0C, and a catalyst high temperature limit of 520^0C, the calculation therefore predicted, at best, a marginal operating range, and, at worst, a need for significant dilution of the reactants to prevent irreversible catalyst sintering. Actual measurements of the true surface

temperature over a range of NO_2 concentrations, at varying depths in the catalyst bed, were essential to defining an operating envelope for an integrated process.

V. Test Results

The following test results are reported in four separate sections to highlight the effects of each of the SCR operating parameters studied. Prior to the presentation of these sections, a short explanation of the catalyst surface temperature measurement technique used is provided.

Catalyst Surface Temperature Measurements

Catalyst surface temperature tests were conducted with a constant NO_2 concentration of 30,000 ppm. Tests were run at three different gas face velocities (3, 5 and 7 fps) for each of four catalyst bed levels (2.5, 6, 12 and 18 inches of bed).

A pyrometer was mounted at the end of a sight-tube which penetrated the reactor so that the catalyst surface temperature could be measured at the reactor center, fixed at 2.5 inches above the catalyst support screen. Thus, surface temperatures determined with bed levels of 2.5, 6, 12 and 18 inches provided catalyst temperatures at the inlet surface and at bed depths of 3.5, 9.5 and 15.5 inches below the top of the bed, respectively.

Test results showed that pyrometer temperature readings were consistently less than the temperatures indicated by the thermocouple located in the bed, (1.5 inches above where the pyrometer was measuring surface temperature). The average temperature differences between these two points in the bed, whether reaction was taking place or not (preheated air only), were approximately 30^oC, 20^oC and 10^oC for gas face velocities of 3, 5 and 7 fps respectively.

This temperature difference may be attributed largely, if not entirely, to a 5 scfh air purge in the sight tube, flowing from the pyrometer and into the bed to keep the pyrometer lens free of ammonium nitrate. In addition, the pyrometer was kept from overheating by a water cooled coil wrapped around the penetrating tube on the exterior of the reactor which may have affected the reading.

In most test cases, the pyrometer temperature consistently equated to a temperature between those recorded by adjacent thermocouples (just above and below the pyrometer). Therefore, the in-bed thermocouples were accepted as a close approximation of actual catalyst surface temperature.

Figure 2 is a graph of the catalyst surface bulk/gas temperature difference versus the inlet NH_3:NO_2 for selected test cases. Neglecting heat losses, the data from Figure 2 suggest an average catalyst surface to bulk gas temperature difference of only 20^oC. The much lower than predicted temperature difference may best be explained by data presented later. First, as will be explained, reaction is very dependent on flow velocity and, therefore, mass transfer rate. The simplified estimates for mass transfer made for the heat calculation were much too conservative. Second, the heat generation rate was based on the heat released in the complete reduction of NO_2 to N_2. The data presented later suggest the presence of a low temperature regime where the NO_2 is believed to be only partially reduced to N_2O, which only releases about half

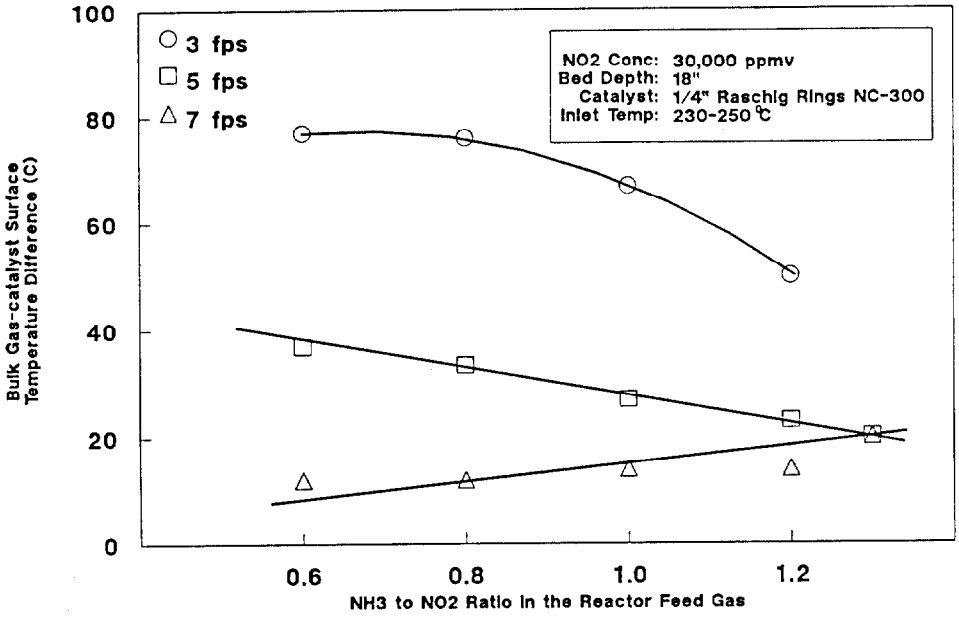

Face Velocity and NH_3 /NO_2 Effects on the Bulk Gas to Catalyst Surface Temperature Difference

Fig. 2

ICPP-Z-15419 (7-88)

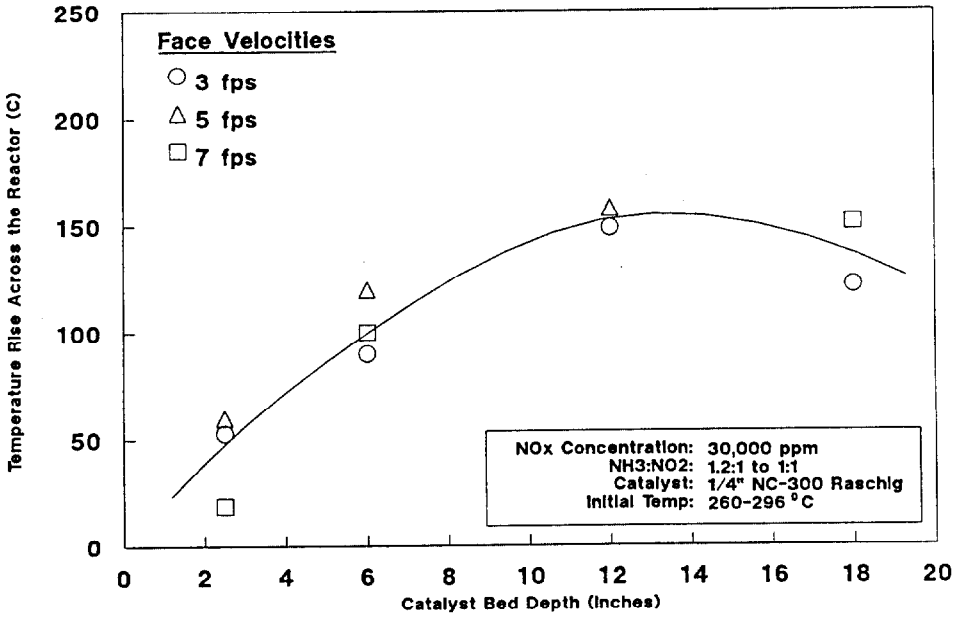

Effect of Catalyst Bed Depth on Reactor Temperature Rises

Fig. 3

ICPP-Z-15418 (7-88)

as much heat. Because the pyrometer provided no further insight into the actual surface temperature due to the reasons discussed previously the pyrometer and the penetrating tube were removed from the reactor for all remaining tests. All in-bed thermocouple readings were then taken to be catalyst surface temperatures ± 15%.

Bed Depth Tests. The first series of tests determined the reactor temperature profile for various catalyst bed depths. Tests were conducted with bed depths ranging from 2 1/2 to 18 inches and at face velocities of 3, 5 and 7 fps. The NH_3/NO_2 ratio and NO_2 concentration were held constant at 1.2 and 30,000 ppm, respectively. As shown in Figure 3, increased bed depth (up to 12" depth) increases maximum bed temperature as a direct result of greater residence time yielding increased reaction and therefore greater heat generation. A bed depth of 2.5" (with the 1/4" Raschig ring catalyst) does not provide enough residence time to yield appreciable NO_x reduction even at 3 fps. Bed depths of 12" or more yield a fairly constant NO_x reduction based on the reactor temperature rises observed. Figure 3 shows that a bed depth of 8-10" is required regardless of face velocity over the range tested. This suggests that the decrease in residence time with greater velocity is directly offset by the more intimate mixing due to greater flow turbulence.

Face Velocity and NH_3/NO_2 Ratio Tests. This series of tests, performed without the optical pyrometer, were to estimate the NO_x reduction efficiency from temperature rise data across the reactor. Figures 4, 5 and 6 represent reactor temperature profiles for tests at face velocities of 3, 5 and 7 fps. These graphs illustrate the effects of increasing the NH_3 to NO_2 feed ratio on 1) the magnitude and location of the maximum surface temperature and 2) the overall temperature rise between inlet and outlet gas streams. During these experiments, the NO_2 concentration was kept constant at 30,000 ppm, the bed depth at 18", and the inlet gas temperature between 225 and 240°C.

At a face velocity of 3 fps, the temperature profile is somewhat parabolic, with a relatively rapid temperature rise and maximum temperatures achieved before the halfway point in the catalyst bed. As the face velocity is increased the heat is more evenly distributed; the profile begins to level out and the maximum catalyst temperature is less and closer to the end of the bed. In addition, the outlet gas temperature increases slightly as the face velocity is increased. Because total heat generation is reflected only in the inlet to outlet temperature rise, this last result indicates that the NO_2 abatement efficiency increase with face velocity. Therefore, the enhanced gas-to-catalyst mass transfer rates at the increased face velocities must more than offset the loss in residence time in the reactor. In all test cases, regardless of the face velocity, the majority of the reaction occurs within the first 7" of bed, where 90% of the total reactor bed temperature rise is achieved.

Tests performed with an NH_3/NO_2 ratio of 0.6:1 gave reactor temperature rises of 110°, 150° and 160° at face velocities of 3, 5 and 7 fps, respectively. Assuming that the predominant NO_2 reaction is the low-temperature, N_2O reaction, (stoichiometric NH_3/NO_2=0.75) the above listed temperature rises correspond to NO_2 reduction efficiencies of 65, 75 and 80%. When the NH_3 to NO_2 feed ratio is doubled to 1.2:1 NO_2 reduction efficiencies for all three face velocities approach 100%. However, as the NH_3/NO_2 ratio is increased to achieve greater NO_2 reduction, colorimeter results (non-quantitative) indicate that a larger percentage of the ammonia passes unreacted through the catalyst.

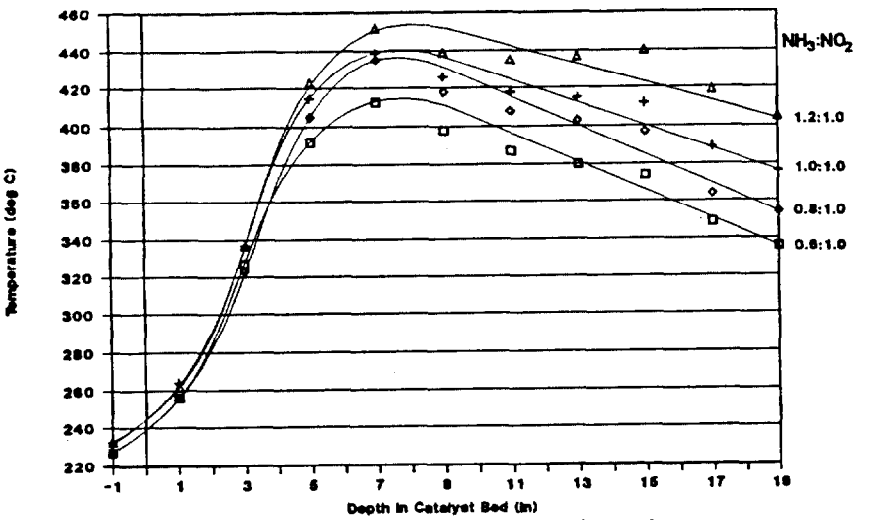

Steady State Temp. Profile at
3fps, 30,000 ppm NOx and 18" Bed Depth

Fig. 4

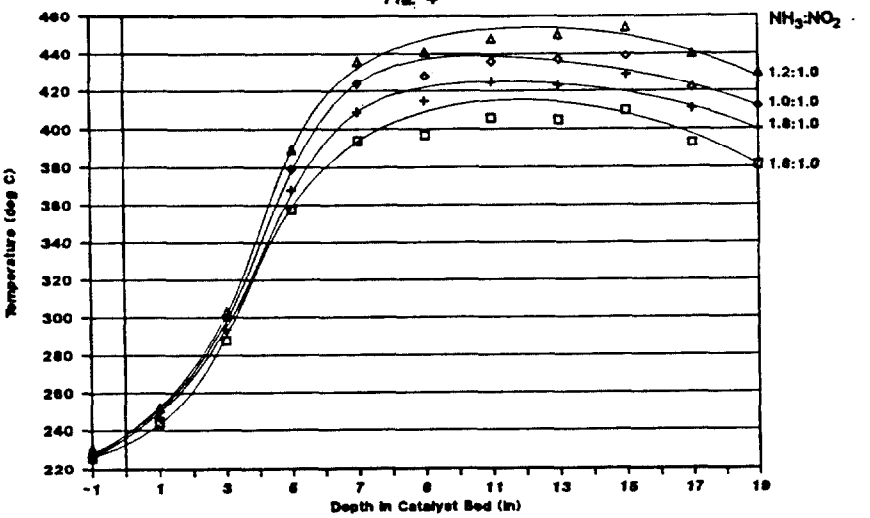

Steady State Temp. Profile at
5fps, 30,000 ppm NOx and 18" Bed Depth

Fig. 5

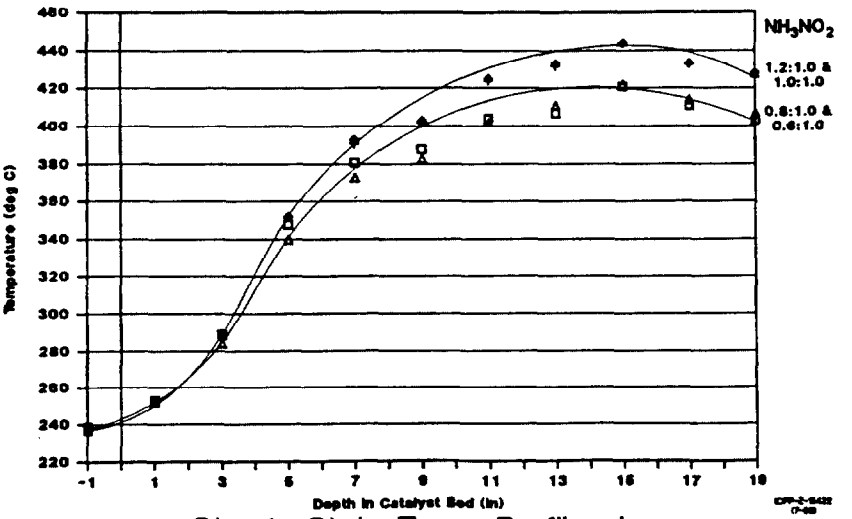

Steady State Temp. Profile at
7fps, 30,000 ppm NOx and 18" Bed Depth

Fig. 6

Initial Gas/Reactor Temperature Tests. Tests performed with an inlet gas temperature of 320°C resulted in higher catalyst surface temperatures (550+°C) and larger temperature rises across the reactor (Figures 7 and 8) than with a 230°C inlet temperature. The temperature rise across the reactor per 5,000 ppm increase in the NO_x concentration increases when bed temperatures approach 410-425°C. This result suggests a shift in the predominant NO_x reduction reaction around 410 to 425°C. In this temperature range, increases in the temperature rise across the reactor approach 50-65°C per 5,000 ppm increase in the inlet NO_x concentration. This is evidence that the NO_x reduction at the higher temperatures is due largely to the N_2-forming reaction of:

$$6\ NO_2 + 8\ NH_3 \longrightarrow 7\ N_2 + 12\ H_2O$$

The increased temperature rise for increasing NO_2 concentrations, with a 320°C inlet temperature is shown in Figure 7. The top curve in Figure 8 illustrates the increasing slope of the temperature rise across the bed as the predominant reaction shifts to the N_2 reaction. With an inlet temperature of 230°C (lower three curves) the maximum reactor temperature only approaches the transition point.

NO_x Concentration Tests. Figures 9, 10 and 11 are temperature profiles for experiments performed at changing inlet NO_x concentrations starting at 5,000 ppm NO_2 and increasing, in 5,000 ppm increments to 30,000 ppm. Bed depth (18"), NH_3/NO_2 ratio (1.3), and inlet gas temperature 220°C to 230°C were held constant. For tests performed at 7 and 9 fps, the incremental change in the temperature rise across the reactor for every 5,000 ppm change in the inlet NO_x concentration was consistently between 20 and 30°C. However, for the tests performed with a 5 fps face velocity, the temperature rise across the reactor increased as much as 60°C per 5,000 ppm NO_x change in the inlet concentration. These results provide additional evidence of the shift in the predominant NO_2 reaction as the bed temperatures exceed 420°C (see Figure 9). Because a face velocity of 5 fps does not dissipate the reaction heat rapidly enough, catalyst temperatures (at conditions of high inlet NO_x concentration) exceed 420°C, and the predominant reaction apparently shifts to the high temperature, high heat generation, N_2 reaction.

Information about the effects that 1) residence time (face velocity and bed depth) and 2) bulk gas-to-catalyst surface mass transfer (face velocity only) have on the SCR process in terms of temperature rise across the catalytic reactor (NO_x reduction) is also provided in Figure 8. For NO_2 concentrations less than 24,000 ppm, the optimum face velocity is about 7 fps. At 5 fps, the increase in the residence time does not compensate for the increased resistance to the transfer of NH_3 and NO_2 from the gas phase to the catalyst surface. At 9 fps the residence time in an 18" bed is not long enough to achieve the amount of reaction obtained at 7 fps. However at NO_2 concentrations above 24,000 ppm, the concentration gradient provides adequate mass transfer, and 5 fps becomes the optimum face velocity. Therefore, NO_2 concentration, residence time and face velocity are all interrelated variables, and no one value of any parameter is sufficient to maximize reactor performance. Rather, operating conditions will be a compromise between the effects described in this report.

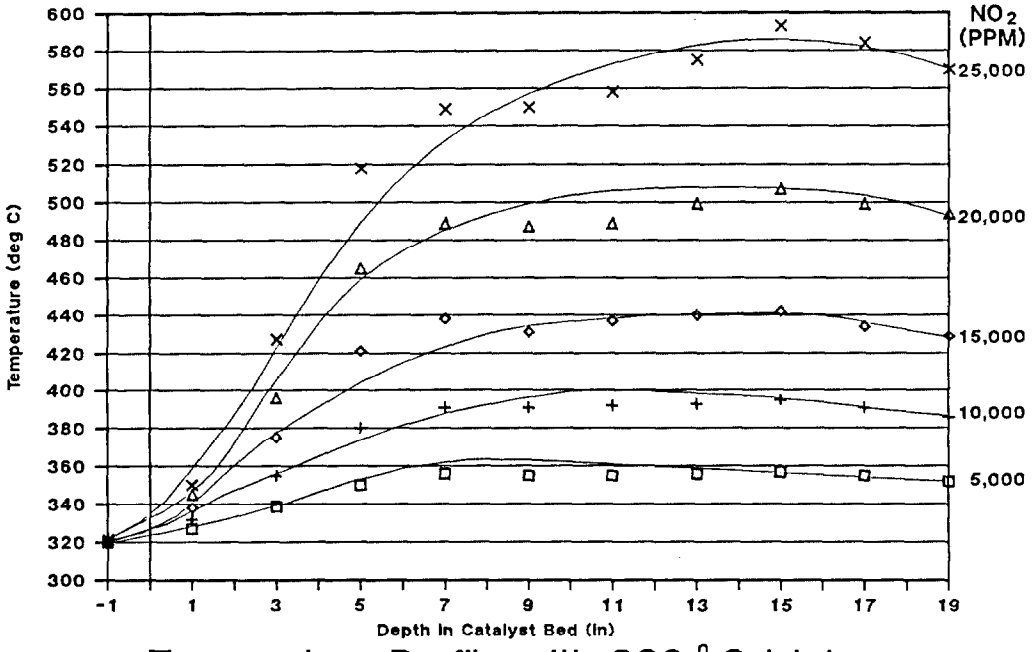

Temperature Profile with 320 ° C Inlet;
7fps, 5-30,000ppm NOx and NH3/NO2=1.3

ICPP-Z-15423 (7-88)

Fig. 7

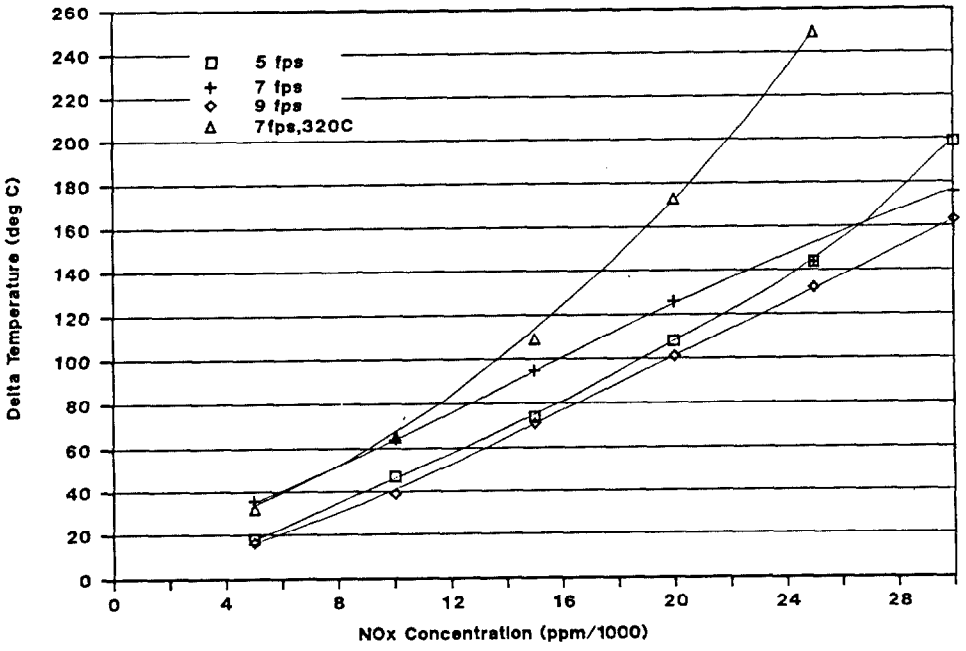

Bulk Gas Temperature Change at
5, 7, 9fps, 230 ° C inlet and NH3/NO2=1.3

ICPP-Z-15424 (7-88)

Fig. 8

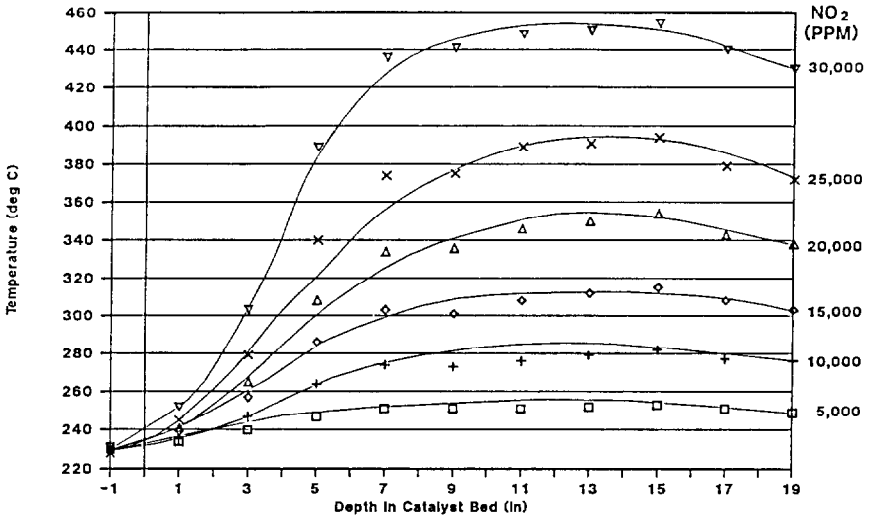

Steady State Temp. Profile at
5fps, 5-30,000ppm NOx and NH3/NO2=1.3

Fig. 9

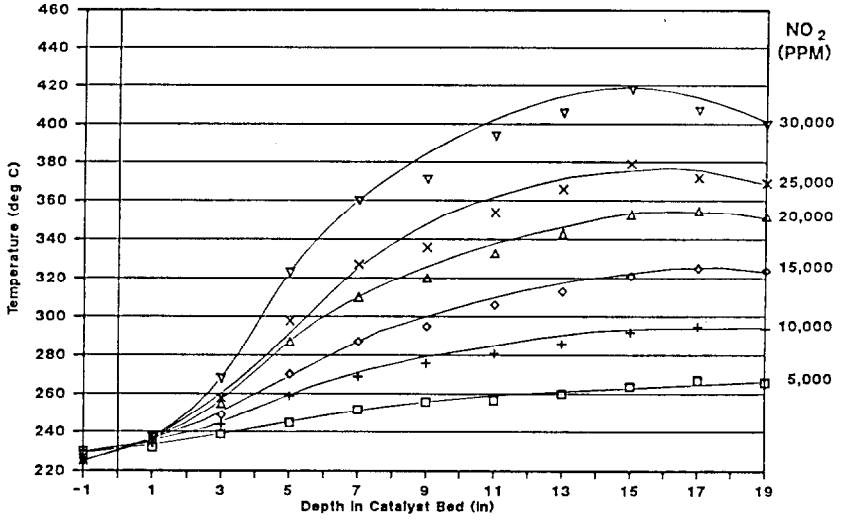

Steady State Temp. Profile at
7fps, 5-30,000ppm NOx and NH3/NO2=1.3

Fig. 10

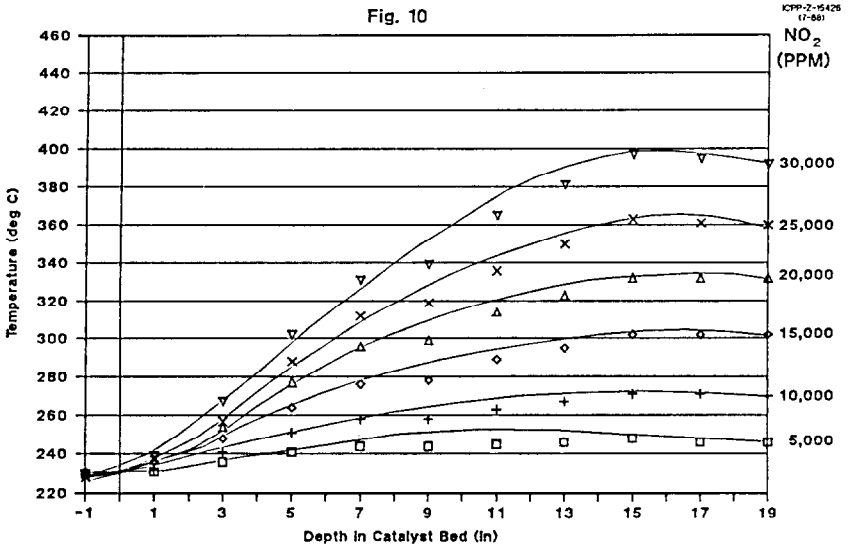

Steady State Temp. Profile at
9fps, 5-30,000ppm NOx and NH3/NO2=1.3

Fig. 11

VI. ANALYTICAL RESULTS

To verify the extent of the NO_2 and NH_3 reactions, off-line sampling and analysis were performed for selected test cases. Due to the complexity of $NO/NO_2/NO_3$ chemistry, and the extreme temperature range covered by the process, analytical method development was much more difficult than projected. The three types of sampling/analysis methods employed were:

1. Sampling the reactor inlet and effluent streams by directing the flow through stainless steel sample bombs followed by analysis via ion chromatography for total nitrates.

2. Same analysis as above, but sampling by drawing gas into evacuated glass bombs.

3. Sampling of the reactor inlet and effluent gas streams with a syringe and an in-line septum followed by immediate analysis for NH_3 by photometry.

Twenty gas samples were collected in stainless steel bombs. Only a fraction of the nitrates known to be present in the inlet stream were detected and repeated bomb rinses continued to test positive for nitrates. It was concluded that nitrates adsorbed on the stainless steel bombs, so this method was discontinued. However, a relative comparison of inlet and outlet gas samples did show a large amount of nitrates in the outlet for a bed depth of 2.5" compared to a relatively small amount of nitrates in the outlet stream of a 6" bed. This result further indicated that gas residence times were insufficient using a 2.5" bed.

In an effort to eliminate the surface and adsorbtion phenomena, forty glass bomb samples of both reactor inlet and outlet gas streams were also analyzed for nitrates. Analytical results of nitrates compared better with expected inlet concentrations than those from stainless steel sample bombs, but still did not account for all of the known nitrates.

Later study into the chemistry of the NO_2/NH_3 reaction indicated that the above methods may have been more accurate than initially believed. At room temperature (i.e., sample bomb conditions), the remaining NO_2 would have reacted with the remaining NH_3 to form ammonium nitrate by the following reaction.

$$4\ NO_2 + 2\ NH_3 \longrightarrow N_2 + 2\ NH_3NO_2 + O_2$$

Thus, a nitrate analysis could only account for about half of the nitrate actually collected in the presence of surplus ammonia.

Ammonium analysis was performed on selected syringe samples using Nessler's reagent and a photometer. Though analysis indicated, in some cases, NH_3 efficiencies of 80+%, and accounted for 95% of the inlet NH_3 concentrations, the lack of reproducibility made the method unacceptable.

Table 3 lists analytical test results for inlet and outlet samples taken for selected test cases indicated in Table 1.

Table 3
Selected Analytical Results

Test # & Conditions (Table 1)	Desired NO_2 Inlet (ppm) (flowmeter)	Analytical NO_2 Inlet (ppm)	% NO_2 Accounted for	Analytical NO_2 (ppm) Outlet	% NO_2 Abate-ment
45	5,000	3355	67	301	91
46	10,000	9201	92	550	94
47	15,000	9327	62	505	94
56	5,000	5066	101	702	86
58	15,000	18,094	120	1458	92
63	5,000	4612	92	0	100
67	25,000	19,782	79	0	100
70	10,000	9218	92	0	100
71	15,000	16,153	108	0	100
Test # & Conditions (Table 1)	Desired NH_3 Inlet (ppm) (flowmeter)	Analytical NH_3 Inlet	% NH_3 Accounted for	Analytical NH_3 (ppm) Output	% NH_3 Used
60	32,500	33,180	102	9913	70
62	39,000	39,165	101	9745	75

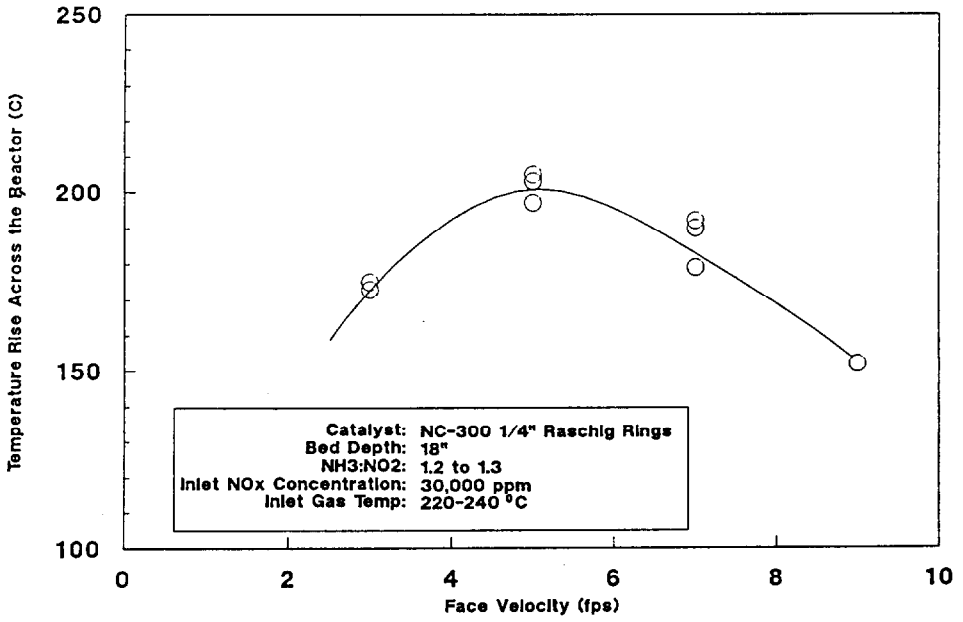

Face Velocity vs. Reactor Temperature Rises

ICPP-Z-15417 (7-88)

Fig. 12

VII. Conclusions and Hypothesis

1. A minimum of 9" of bed depth using the 1/4" Raschig ring catalyst is required for treatment of the NWCF off-gas. Probably more will be needed with the moisture-bearing gas.

2. Thermocouple and pyrometer data indicate that the exit bulk gas to catalyst surface temperature difference is less than $30^{o}C$.

3. Increases in the NH_3/NO_2 ratio fed to the reactor (.6 to 1.2) increase the NO_x reduction efficiency, the amount of NH_3 passed through the catalyst unreacted, and the catalyst surface temperature.

4. For SCR operations with gas face velocities at or below about 6 fps, the resistance to bulk gas-to-catalyst surface mass transfer controls the extent of the NO_2 reduction reaction. However, at face velocities above 6 fps the controlling resistance appears to be at or in the catalyst surface, because further increases in velocity lessen the extent of reacation. Refer to Figure 12.

5. For SCR reactions occurring below 410-425^{o}C, the predominant NO_2 reducing reaction probably requires an NH_3/NO_2 ratio of only 0.75, produces primarily N_2O in the effluent stream, and generates a temperature rise across the reactor equal to 20-30^{o}C for every 5,000 ppm NO_2 reacted.

6. For SCR reactions occurring above 410-425^{o}C, the predominant NO_2 reducing reaction is probably the complete reduction of NO_2 requiring an NH_3/NO_2 ratio of 1.3, producing N_2 in the effluent stream, and generating a 60-70^{o}C temperature rise across the reactor for every 5,000 ppm NO_2 reacted.

VIII. Recommendations for Pilot Plant Operations

The following recommendations provide guidelines for SCR operating parameters for NO_x reduction in the calciner off-gas. Pilot-scale data, particularly product distribution analyses, must be obtained to verify the lab-scale conclusions and hypotheses, and to provide the bases for design of a full-scale abatement system.

1. Use Norton Company's synthetic zeolite NC-300 as a 1/4" Raschig ring catalyst pellet. This catalyst shape provides an adequate surface-to-volume ratio, and low pressure drop per catalyst depth (<.75" H_2O per inch or bed depth). Because catalyst pressure drop will not be an operating concern in the pilot plant, load the catalyst beds to the full 18" depth.

2. Operate at a face velocity between 5 and 7 fps to achieve maximum NO_x reduction. Lower face velocities will result in greater resistance to mass transfer between the gas and catalyst surface, thus decreasing the amount of NO_x reduced. Higher face velocities will not yield adequate residence time for sufficient NO_x abatement with an 18" bed.

3. Operate the pilot plant with an inlet gas temperature into the first reactor in the range of 230^{o} to 240^{o}C to 1) avoid high in-bed temperatures

(greater than 520°C), 2) maintain the N_2O producing reaction as the predominant NO_x reducing reaction thereby minimizing reaction heat, and 3) avoid NH_4NO_3 formation.

4. For initial tests, operate only 2 reactors in series with enough inter-stage mixing to achieve 300°C at the inlet to the second reactor. Based on lab-scale data, operation in this mode should maximize NO_x reduction and minimize NH_3 slip.

5. Operate with an NH_3/NO_2 ratio between 0.6 and 1.0 to achieve maximum NO_x reduction with the least NH_3 slip.

Pilot-plant testing will provide the scale-up link between laboratory-scale and plant-scale. In addition, operation with actual NWCF off-gas will determine the effects caused by water content.[7] Finally, the more sophisticated on-line analytical instrumentation in the pilot plant will determine the actual reactions occurring and more accurate abatement efficiencies.

IX. References

1. Permit Applications - EPA-PSD Permit - State of Idaho Permit to Construct, for Fuel Processing Restoration Project, Engineering Science, Arcadia CA and WINCO, Idaho Falls, Idaho to U. S. Department of Energy, February 1986.

2. G. G. Simpson, Allied Chemical Corp., "Abatement of Nitrogen Oxides Effluent from a Commercial Waste Calcining Facility", ACI-352, June 1978.

3. D. L. Evans, S. M. Allen, V. J. Trube, J. L. Clapp, "Installation Specifications for the ICPP NO_x Abatement Pilot Plant Process Modules Specification No. AeCS-40268", EG&G, Idaho Inc. for U. S. Dept. of Energy, March 16, 1988.

4. T. R. Thomas, D. H. Munger, Allied Chemical Corp., Idaho Chemical Programs, "An Evaluation for NO_x Abatement by NH_3 over Hydrogen Mordenite for Nuclear Fuel Reprocessing Plants", Report ICP-1133, Prepared for DOE Idaho Operations Office, January 1978.

5. J. A. McCray, D. Gombert II, Idaho National Engineering Laboratory "A Laboratory Apparatus for Measuring Operating parameters for a Selective Catalytic Reduction Application to NO_x Abatement", 20th DOE/NRC Nuclear Air Cleaning Conference, Boston, MA, August 1988.

6. F. Yoshida, D. Ramaswani, D. A. Haugen, University of Wisconsin, "Temperatures and Partial Pressures at the Surfaces of Catalyst Particles", AICHE Journal; Vol. 8, No.1, 5-11, (1962).

7. J. R. Kiovsky, D. B. Koradia, C. T. Lim, Norton Company, Akron, Ohio, "Evaluation of a New Zeolite Catalyst for NO_x Reduction with NH_3", I&EC Product Research and Development; Vol. 19, pg. 218, 215-225, (1980).

RESEARCH AND DEVELOPMENT OF HYDROPHOBIC ADSORBENT FOR IODINE REMOVAL

K. Takeshita*, S. Matsumoto**
M. Kumagai*, J. Koga**
M. Sazarashi*, Y. Takashima* and T. Tamura*

* Industrial Research Institute Japan,
1201 Takada, Kashiwa,
Chiba 277 Japan

** Department of Environmental Chemistry,
Faculty of Engineering, Saitama University,
255 Shimo-okubo, Urawa,
Saitama 388 Japan

Abstract

For removal of radioactive iodine and nitrogen oxides from dissolver off-gas (DOG), we have developed a new treatment system characterized by the effective reduction of its waste volume, the high decontamination factor for iodine and NO_x, and easy operation.

The system essentially consists of two adsorption processes for iodine and NO_x removal. Iodine is removed by a bed of hydrophobic adsorbent which is impregnated with silver or silver salt. Three silver impregnation methods were tried by using different solvents, ethanol, dioxan and amine. The amine-complex method was the highest in silver content.

Adsorption experiments for a simulated DOG which was consisted of 200 -250ppm of iodine, 2000 ppm of NO_x and 5000 ppm of water vapor, showed that iodine was selectively adsorbed while no water was adsorbed and NO_x was adsorbed very little. The breakthrough of iodine was not influenced by the presence of water vapor and NO_x. Silver was utilized more than 90% for iodine adsorption.

NO_x was recovered as nitric acid by a thermal swing adsorption process with a hydrogenated natural zeolite. The recovery of NOx attained up to 95-100% by recycling the desorbed gas to the inlet, though it was only 45% without recycling. No deterioration of the zeolite was appreciated after 1000 hours.

Introduction

Commercial, large scale nuclear fuel reprocessing plants are now or will be in construction in U.K., France, F.R.G. and Japan. The technology for nuclear fuel reprocessing is now in practical stage. As a target for the R/D of the technology, the economical efficiency is becoming more and more important.

We had considered the treatment system of iodine and nitrogen oxides (NO_x) in dissolver off-gas (DOG) from this conception. The iodine has been removed by NaOH scrubber process.[1,3,4] This process has some disadvantages such as increasing the radioactive waste volume, the low decontamination factor (D.F.<10) especially for organic iodine. The various adsorbents in which silver or silver salt is impregnated on inorganic supports such as zeolite, silica and alumina have been developed. Those adsorbents, however, should be reduced in adsorption capacity of iodine in the presence of water vapor.[3]

With respect to NO_x, the selective reduction process by ammonia could be applied for its removal. However, this process has some problems such that the operation becomes more complicated and unreacted ammonia have remained in off-gas.[3]

Therefore, we have developed a new treatment system of radioactive iodine and NO_x in DOG, which should be more economical and simpler than the above mentioned systems, and could be much smaller in the volume of iodine waste.

This treatment system consists of two basic processes. The first step is an iodine removal process which uses the iodine adsorbent impregnated with silver or silver salt on a hydrophobic organic support. The second step is NO_x removal process using hydrogenated zeolites which can recover NO_x as HNO_3. As a result of the use of hydrophobic organic support in the first step, iodine was effectively and selectively adsorbed, and other gases such as water vapor and NO_x passed through. And in the second step, NO_x gases could be recovered as HNO_3 by applying the thermal swing operation.

1. Development of Iodine Removal Process by Hydrophobic Adsorbent

1.1 Preparation of hydrophobic adsorbent

The hydrophobic adsorbents impregnated with silver or silver salt, were developed for applying to the removal of iodine from dissolver off-gas (DOG). The adsorbent particles were made in a mono-sized sphere of porous stylene-divinylbenzene copolymer (SDB) by the capsule polymerization method through such numerous processes as preparation of monomer solution, drop formation, encapsulation, polymerization, decapsulation, washing and drying.[2] The SDB particles used in the experiments have the BET surface area of 220 m^2/g and the average pore diameter of 800 Å.

Silver impregnation on the hydrophobic adsorbents cannot be carried out by the usual aqueous solution method, and we have examined three methods using different organic solvents.

(1) Ethanol method —— Silver salt is impregnated on the support in the mixture of the aqueous $AgNO_3$ solution and ethanol at the room temperature. Impregnated silver salt may be reduced to metallic silver in the hydrogen stream at 150°C for 10 hours.

(2) Dioxan method —— Dioxan is used instead of ethanol. Silver impregnation is similarly carried out as in the ethanol method. Since dioxan swells the SDB easily, it allows much silver salt to penetrate deep into the particles.

(3) Amine-complex method —— Amine solution containing silver-amine complex, $[Ag(R_2NH)_2]^+$, is used as impregnation solution. The amine allows the silver salt to dissolve as an amine-complex in a high concentration and to penetrate in the support. The silver-amine complex impregnated on the SDB support is decomposed to silver completely by drying at temperatures more than 130°C.

Table 1 Silver impregnation methods and silver contents

Impregnation method	Composition of silver solution (mol.ratio)	Silver content(wt%)
ethanol method	$AgNO_3$:(H_2O+ethanol)=1:12	8.6
dioxan method	$AgNO_3$:(H_2O+dioxan) =1:8	17.2
amine-complex method	$AgNO_3$: butylamine =1:8	29.3

Table 1 shows silver content by each impregnation method. Silver content was the highest for the adsorbent prepared by the amine-complex method.

The silver distribution in an adsorbent particle prepared by each method was measured by the electron probe microanalyzer (EPMA), as shown in Figure 1. Silver was uniformly distributed in the adsorbent particles by the dioxan method and the amine-complex method. This would be the result of the property of amine and dioxan which allow the support polymer to swell sufficiently. Thus the amine-complex method gave the highest silver content and uniform silver distribution.

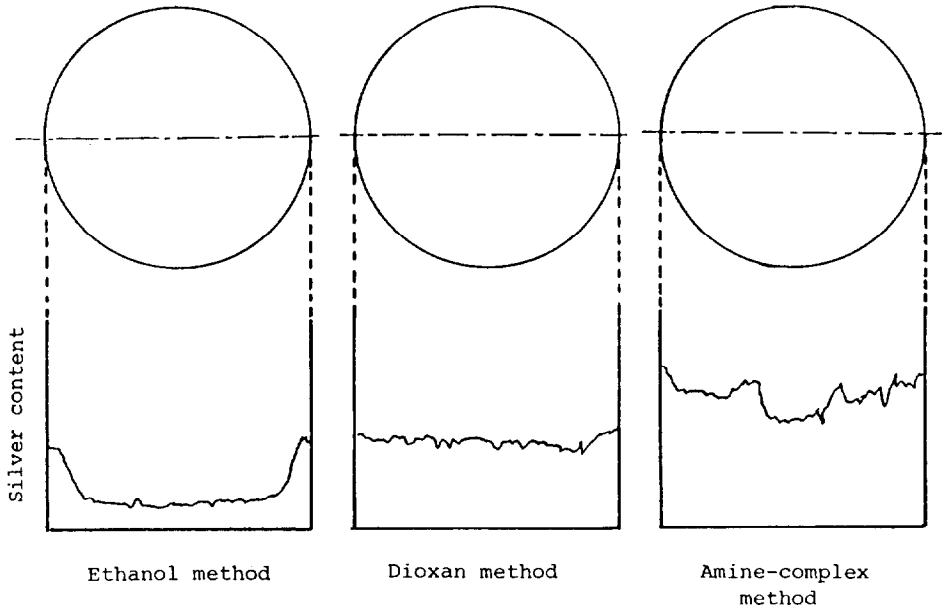

Fig.1 Silver distributions in the adsorbents prepared by ethanol, dioxan and amine-complex methods.

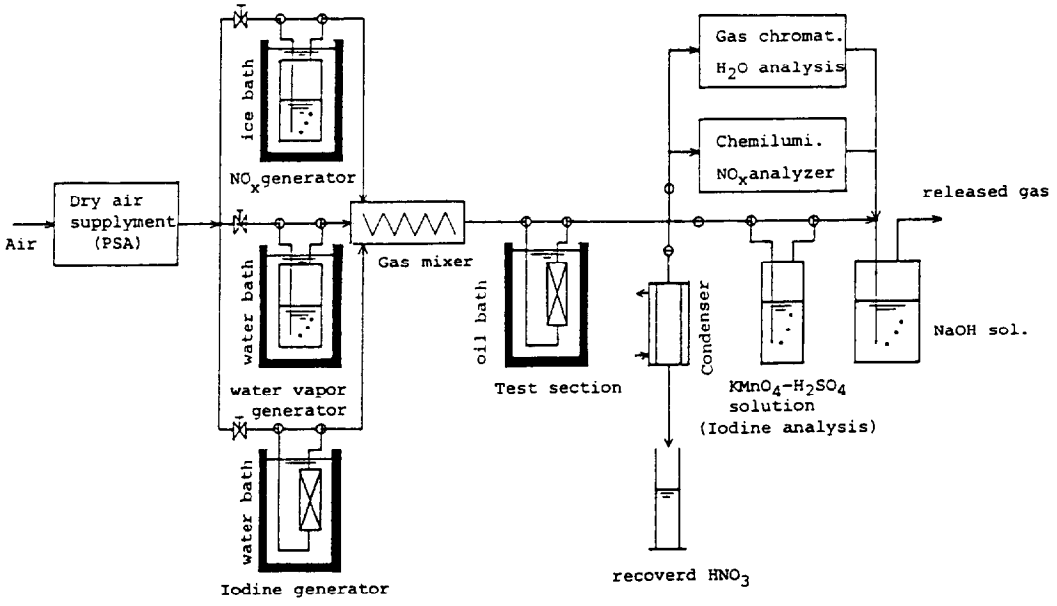

Fig.2 Schematic diagram of experimental set-up.

1.2 Removal of iodine from simulated DOG

We have tested these three adsorbents to compare the adsorption of iodine from simulated dissolver off-gas using an adsorption column of 20mm x50mmH, as shown in Figure 2. The simulated DOG consists of 200-250ppm of I_2, 2000ppm of NO_x and 5000ppm of water vapor with the balance of dry air. The bed temperature and gas flow rate were kept constant at 130°C and 4.8cm/s, respectively. The concentrations of iodine, NO_x and water vapor in the effluent gas from the test column were measured.

The iodine in the effluent gas was absorbed into $KMnO_4$-H_2SO_4 solution and reduced to iodide ion by ascorbic acid, and the concentration of I^- was measured by an ionmeter. The concentrations of NO_x and water vapor were measured by a chemiluminescence type NO_x analyzer and a gas chromatography packed with porapak-Q, respectively.

Figure 3 shows the breakthrough curves of iodine, NO_x and water vapor for the adsorbent prepared by the amine-complex method. The results show that the iodine was selectively trapped into the bed while no water was adsorbed and NO_x was adsorbed very little.

Figure 4 shows the comparison of breakthrough curves of iodine for the above mentioned three adsorbents and the commercial one (AC6120: amorphous silicic based material impregnated with silver nitrate). Note that the breakthrough of the adsorbent prepared by the amine-complex method occurred after that of AC6120. This adsorbent has the highest iodine adsorption capacity. The silver utilization of this adsorbent calculated from the breakthrough curve was more than 90%.

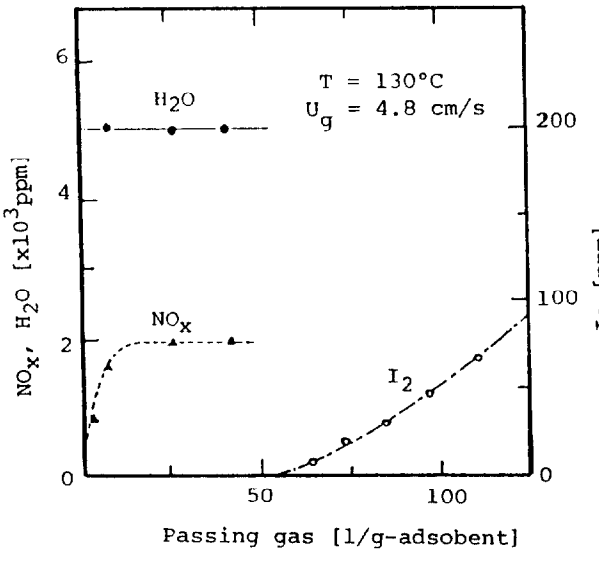

Fig.3 Breakthrough curves of the simulated DOG for the adsorbent prepared by amine-complex method.

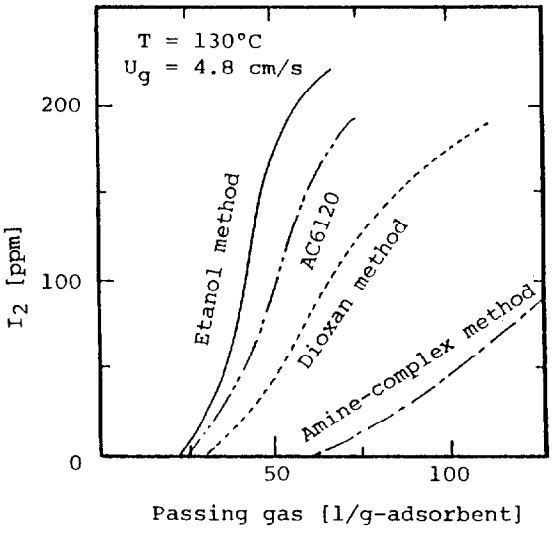

Fig.4 Breakthrough curves of iodine for three developed adsorbents and commercial one (AC6120).

1.3 Effect of water vapor and NO_x on adsorption of iodine

The iodine concentrations in effluent for two cases where water vapor is contained in the simulated gas or not, are plotted against the volume of the passing gas in Figure 5. Apparently all points lie on the same breakthrough curve. This result suggests that due to the use of hydrophobic support, the breakthrough of iodine was not influenced by the presence of water vapor.

Figure 6 shows a similar plot to Fig.5 to examine the effect of the presence of 1 vol%-NO_x in the simulated gas. Again, all points are on the same breakthrough curve. Thus the breakthrough of iodine was not influenced by the presence of NO_x.

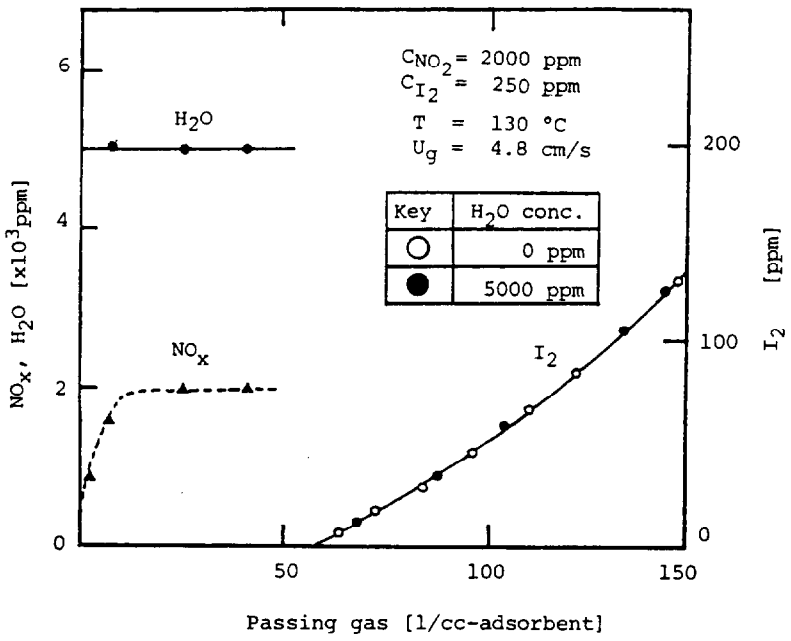

Fig.5 Effect of the presence of water vapor on the breakthrough curve of iodine.

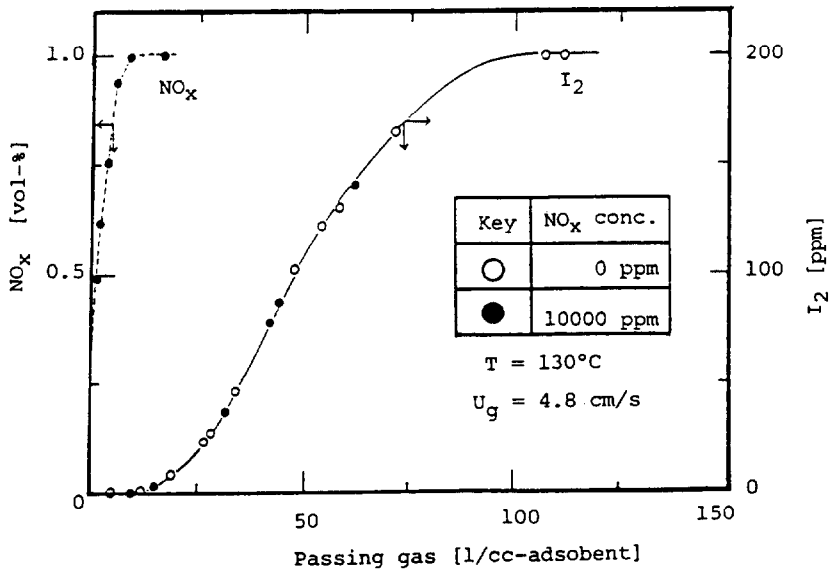

Fig.6 Effect of the presence of NO_x on the breakthrough curve of iodine.

2. Recovery of NO_x by Zeolite

2.1 Selection of zeolite

In order to find an adsorbent with a high adsorption capacity for nitrogen oxides, we have tested various natural zeolites produced in Japan and those modified by ion exchange with H^+, Na^+ and K^+. The grain size of zeolites tested lies between the sieve number 10 and 20 mesh. The experimental method and condition are the same as in the previous section.

The natural zeolite produced at Itado and Iwami had the highest adsorption capacity of 30 cm^3-NO_x/g, while the zeolite produced in Futatsui showed a low capacity of almost zero. Here the capacity means that for 10% breakthrough.

Mineral compositions determined by the powder X-ray diffraction suggest that the adsorption capacity of NO_x is controlled primarily by the content of mordenite. The zeolite from Futatsui consisted mostly of klinoptilorite.

The hydrogenation of zeolites had an effect to increase the NO_x adsorption capacity. The H-type Itado zeolite showed the capacity of 37.5 cm^3-NO_x/g and the H-type Futatsui did 15 cm^3-NO_x/g. No appreciable effect was attained by the ion exchange with Na^+ and K^+. Thus, the H-type Itado zeolite had the highest NOx adsorption capacity.

2.2 Recovery of NO_x from simulated DOG

Desorption was carried out by raising the temperature of the adsorption column up to 450°C in a dry air stream. The effluent gas was passed through an ice-cooled condenser in which HNO_3 and H_2O were recovered and a 3% H_2O_2 bubbling column in which NO and NO_2 were adsorbed.

Figure 7 shows the breakthrough curves of I_2, NO_x and H_2O for the H-type Itado zeolite. For desorption experiments, we prepared three different columns that had been allowed for adsorption to proceed by the times designated by signs (A), (B) and (C) as shown in Figure 7, respectively. Sign (A) means a point where the breakthrough of NO_x has just started, at (B) the breakthrough of H_2O has started and at (C) it has finished.

Table 2 shows the recovery of NO_x by desorption of each column. It is found that the recovery of NO_x as HNO_3 increases in the order of (A), (B) and (C) suggesting that it

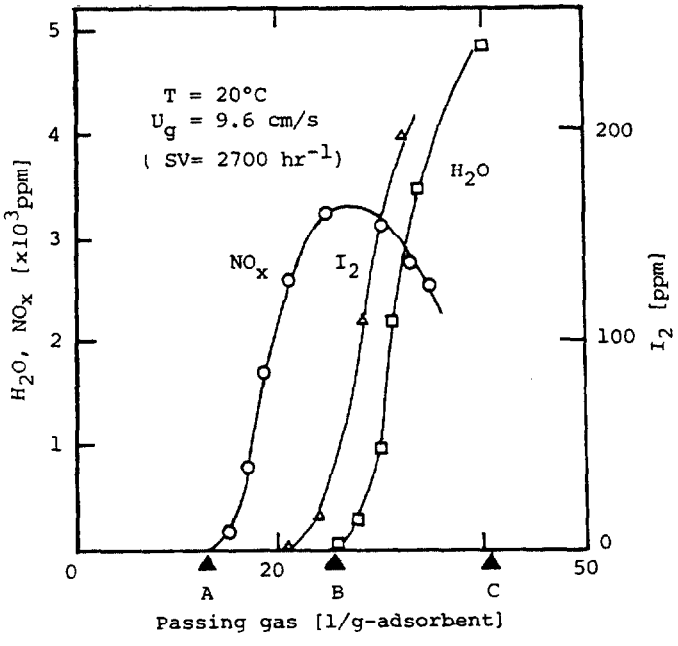

Fig.7 Breakthrough curves of iodine, NO_x and H_2O by the H-type Itado zeolite.

depends on the amount of water vapor that had adsorbed on the zeolite. For the practical purpose of NO_x removal, however, switch from adsorption to desorption has to be done at point (A) which corresponds to the lowest recovery of HNO_3.

Table 2 Relation between the amounts of NO_x and H_2O adsorbed and the recovery of NO_x

desorption point	amount of NO_x adsorbed (cc/g-STP)	amount of H_2O adsorbed (cc/g-STP)	recovery of NO_x (%)
A	33.1	67.0	48.3
B	40.0	124.	76.1
C	36.5	152.	93.5

2.3 Continuous recovery of NO_x by thermal swing adsorption

For demonstration of this process, we have constructed a bench-scale experimental plant with a treatment capacity of 1 Nm^3/h, as shown schematically in Figure 8. This consists of two pairs of zeolite columns and condensers with a recycle loop. Adsorption and desorption were repeated at a time interval of 4 hours.

Table 3 shows the experimental conditions and results of several runs, the total time of which was about 1000 hours. When the desorption gas was not recycled to the feed, the recovery of NO_x was lower than 50% (Run 1). This corresponds to the case(A) in Table 2. When recycled, the recovery of NO_x increased to 95-100% (Run 2 to 4).

The concentration of HNO_3 which is controlled primarily by the concentration ratio of NO_x and H_2O in DOG, reached up to 65%, the azeotropic concentration of HNO_3. Analysis of trace elements in the recovered acid showed that no elutriation occurred from the H-type zeolite. Also no appreciable change in the mineral structure of the zeolite was detected by the powder X-ray diffraction analysis. The adsorption capacity of NO_x and abrasion resistance were not reduced after use.

Then, we carried out an experiment in which a small amount of iodine (2ppm) was added to the feed off-gas, on the supposition that the preceding iodine removal process was reduced in its ability by some trouble (Run 4). The result showed that the iodine was almost completely adsorbed onto the zeolite with no adverse effect on the NO_x adsorption capacity. The iodine was desorbed on heating, recycled to the inlet of the system and eventually removed by the hydrophobic adsorbent. Thus, the zeolite column has a function of back-up for the iodine adsorption column.

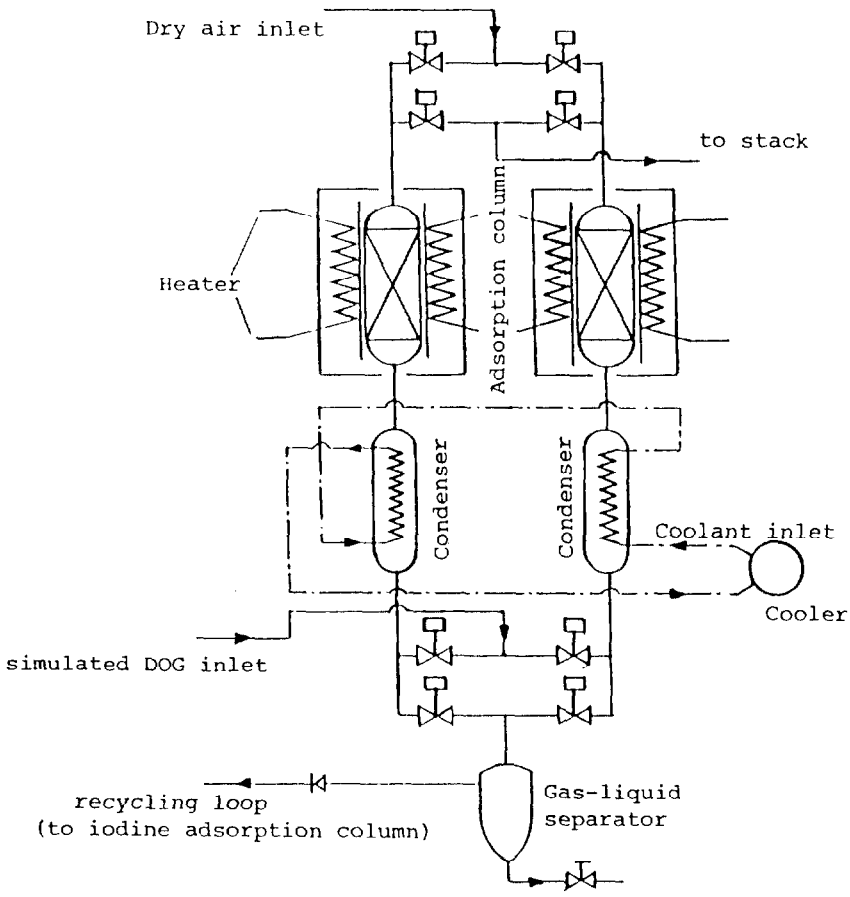

Fig.8 Schematic diagram of thermal swing adsorption process.

Table 3 Continuous recovery of NOx by thermal swing adsorption process

Run No.	total time(hr)	operating conditions			conc.of HNO_3 (%)	Recovery of NO_x (%)
		recycling of desorption gas	conc. of NOx(ppm)	conc. of H_2O (ppm)		
1	80	no	2500	5800	62.8	48.0
2	212	yes	1500	10000	51.5	97.1
3	720	yes	1800	5800	63.1	92.2
4	1000	yes	1800	5800	63.2	96.1

Concluding remarks

1) A new treatment process for removal of iodine and NO_x in DOG was developed. This system consists of two adsorption processes, and is characterized by the selective recovery of iodine and NO_x, the reduction of waste volume, the high decontamination factor for iodine and NO_x, and easy operation.

2) The adsorbent impregnated with silver or silver salt on hydrophobic support was used for removal of iodine. For impregnating silver effectively on the support, it was important to use an organic solvent such as ethanol, dioxan or amine. The adsorbent prepared by the amine-complex method showed the highest silver content and uniform distribution of silver.

3) The adsorption of iodine onto the hydrophobic adsorbent was not influenced by the presence of NO_x and water vapor.

4) NO_x was recovered continuously by thermal swing adsorption process with hydrogenated zeolite. The recovery of NO_x was 95-100% when the desorption gas was recycled. No deterioration of zeolite was found after 1000 hours of use.

Acknowledgment

The authors express appreciation to Mr.A.Kawai (Saitama Univ.) and Mr.M.Shinoda (Kitazato Univ.) for their assistance in the experiments.

Reference

1) M. Benedict et.al.:"Nuclear Chemical Engineering", Mc-Grow Hill, New York, 1981

2) S. Matsumoto et.al.: Preprints of The 50th annual meeting of The Soc. of Chem. Engrs. Japan, E-204 (1985)

3) S. Matuoka et.al.: J.Atomic Energy Soc. Japan, 28, 701 (1986)

4) H. Yamamoto :"Genshiryoku Kagaku Kogaku (in Japanese)", Nikkan Kogyo Shinbunsha, 1976

DISCUSSION

JUBIN: What is the method for long term storage or disposal for iodine-loaded adsorbent? Has the long-term stability of this organic adsorbent been studied? Of particular concern is the breakdown of the polymer into benzene, etc. due to radiation damage and the subsequent release of the AgI.

TAKESHITA: The hydrophobic adsorbent can be volume-reduced by dry distillation. As to results, the organic part of the adsorbent is decomposed completely and only silver iodide, AgI, remains. Silver iodide is a very stable compound. AgI would be disposed of in stable form by solidification with plastics or glass.

HYDER: By what mechanism is the silver fixed to the solid polymer?

TAKESHITA: In the amine-complex method, the silver-amine complex that is impregnated on the SDB support is decomposed to metallic silver completely by drying at a temperature more than 130°C. In the ethanol or dioxin method, impregnated silver salt remains as it is by drying at 130°C and reduced to metallic silver in the hydrogen stream at 150°C for ten hours.

SMITH, M.: What is the DVB level in your copolymer adsorbent? What is the surface area of your adsorbent before and after loading silver?

TAKESHITA: The DVB concentration of the polymer used in the experiments is 10%, and its surface area is 220 m^2/g. When 30 wt% silver is impregnated in the polymer particle, the surface area is reduced to 120 m^2/g.

PERFORMANCE OF SOME SILVER SORBENTS FOR CONTROL OF RADIOIODINE FROM NUCLEAR FUEL OPERATIONS*

R. D. Scheele, L. L. Burger, and B. T. Halko
Pacific Northwest Laboratory**, Richland, Washington
E. D. Waters and R. M. Orme
Westinghouse Hanford Operations, Richland, Washington

Abstract

The Process Facility Modification (PFM) proposed for the Hanford PUREX plant includes control of gaseous radioiodine. In support of the Westinghouse Hanford Company (WHC) design effort for the PFM, the Pacific Northwest Laboratory (PNL) has evaluated caustic scrubbing and the use of silver-containing solid sorbents to remove iodine from the dissolver offgas (DOG) stream.

The present report describes the behavior of several silver-containing zeolites and silver nitrate-impregnated silicic acid tested under conditions simulating normal and standby operation of the PFM.

These studies found that the silver zeolites, Norton silver mordenite (NAgZ), Linde silver mordenite (LAgZ), and partially silver-exchanged Linde silver faujasite (PAgX), can routinely reduce the gaseous iodine concentration in a simulated PFM DOG to $<10^{-5}$ μmol I/L, while a commercially produced silver nitrate-impregnated silicic acid ($AgNO_3Si$) could not at these test conditions. Tests simulating standby operation of beds loaded up to 0.25 μmol I/g sorbent indicate that standby operation will not result in effluent concentrations above 10^{-5} μmol I/L. At higher loadings standby operation initially caused iodine to migrate from NAgZ. There were indications that the iodine tends to stabilize with time, but insufficient information is available to fully characterize these reactions.

I. Introduction

In support of Westinghouse Hanford Company's (WHC) search for a method to control gaseous radioiodine releases from the proposed PUREX Process Facility Modification (PFM), the Pacific Northwest Laboratory (PNL) evaluated caustic scrubbing and silver-containing solid sorbents on their ability to remove iodine from simulated dissolver offgas (DOG) streams. These studies included determining the effect of the concentrations of nitric oxide and nitrogen dioxide, operating temperature, and exposure of partially

---

* Work Supported by the U.S. Department of Energy under Contract DE-AC06-76RLO 1830.
** Pacific Northwest Laboratory is operated for the U.S. Department of Energy by Battelle Memorial Institute.

loaded and fully loaded silver sorbent beds to iodine-free air at the beds' operating temperature (standby conditions).

This report describes some of PNL's most recent work on several state-of-the-art solid sorbents for radioiodine in a nuclear fuels reprocessing environment. The materials tested were silver mordenite prepared from Norton mordenite (NAgZ), silver mordenite prepared from Linde mordenite (LAgZ), partially exchanged silver faujasite (PAgX) prepared from Linde 13X zeolite, and silver nitrate-impregnated silicic acid ($AgNO_3Si$).

II. Experimental Design, Apparatus, Analytical Methods, and Procedure

This report describes two different sets of experiments. The objective of the first, the **extended standby test**, was to measure NAgZ's ability to control the effluent iodine concentration, its loading capacity, and its ability to retain trapped iodine. The objective of the second set of experiments, the **parallel comparison tests**, was to determine whether several state-of-the-art, silver-containing iodine traps could 1) reduce the gaseous iodine concentration in a simulated DOG to $<10^{-5}$ μmol I/L at normal expected PFM process conditions, 2) be resistant to shutdown/startup cycling, and 3) effectively retain trapped iodine during standby operations. This section describes the experimental approach, apparatus, analytical procedures, and test procedure.

Experimental Approach

In the first experiment, the objective was to determine how well NAgZ performed at simulated normal PFM operating conditions and determine how well, after breakthrough occurred (effluent iodine concentration $>10^{-3}$ μmol I/L), the NAgZ bed retained the trapped iodine at standby conditions. To accomplish this a bed of NAgZ was tested at normal expected process conditions and, after the trapping cycle, was tested at standby conditions for an extended period of time, followed by passing air through portions of the loaded bed at elevated temperature.

In the trapping portion of the extended standby experiment, the input gas contained 10.5 μmol CH_3I/L even though the expected concentration and predominant species is 0.05 μmol I_2/L. The iodine species used for this test was CH_3I since it is expected to be the predominant organic iodide present in the DOG and since organic iodides are believed to be more difficult to trap than elemental iodine. The higher than expected iodine concentration was selected to reduce the trapping portion of the experiment to a reasonable time period of about a week.

After this work, reported by Scheele and Burger[1], the next set of planned experiments was to compare the performance of three state-of-the-art silver-containing sorbents at expected PFM operating conditions and procedures. In the original design NAgZ, PAgX and $AgNO_3Si$ were to be tested in triplicate and in parallel

using the expected iodine concentration, 0.05 μmol I_2/L, and normal PFM operating conditions. These conditions include NO and NO_2 concentrations of 1 vol% each, a gaseous water concentration of 6 vol%, an operating temperature of 150°C, cycling through shutdown and startup, and standby. Due to budget and time constraints, this second set of experiments ended after loading the 20-cm beds to approximately 0.25 mmol I/g sorbent, or 15% of theoretical silver utilization based on a maximum iodine to silver ratio of 1:1.

After establishing the original experimental design and beginning construction of the experimental apparatus, we learned that Norton no longer manufactured mordenite and therefore decided to replace one bed of PAgX with LAgZ. One bed of PAgX was replaced since the chemical resistance of faujasite to an acidic environment such as that found in the PFM DOG was suspect[2].

The materials selected for testing were based on the experience of Scheele and Burger[1] with NAgZ and fully exchanged (36 wt% silver) silver faujasite (AgX), the work of Thomas et al.[3] on AgX and NAgZ, and the work of Wilhelm, Fürrer, and others on $AgNO_3Si$ as summarized by McKay, Miquel, and White[2]. The silver content of the silver faujasite used was reduced to 18 wt% silver to allow for a more equal comparison of sorbents. (The other zeolites were also 18 wt% silver.) Figure 1 presents a picture of the four as-received sorbent materials tested and the AgX used for an analytical trap.

In the extended standby test the NAgZ was -10+16 mesh. In the parallel comparison tests the NAgZ, LAgZ, PAgX, and AgX sorbents were -20+40 mesh and the $AgNO_3Si$ was at its manufactured size of

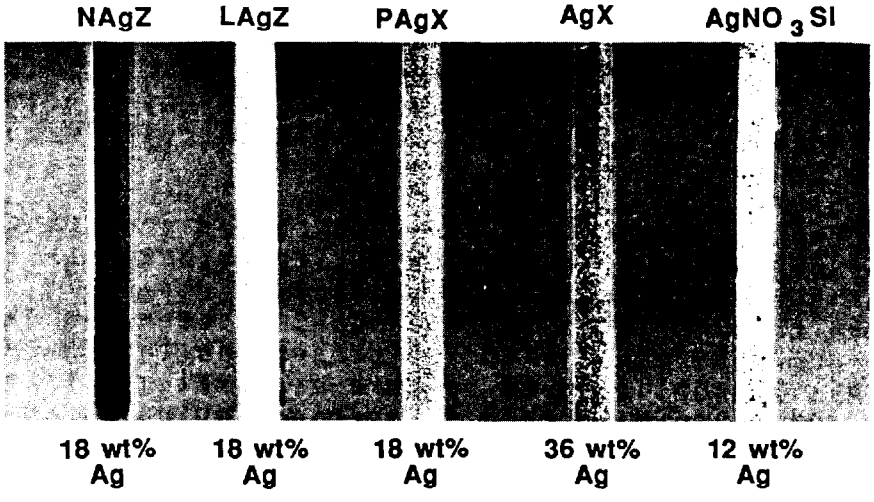

FIGURE 1. Silver Sorbents Used in the Parallel Comparison Tests

1.6 mm dia beads. This particle size was selected based on the work of Scheele and Burger[1] which showed acceptable pressure drops across beds of -20+40 mesh NAgZ, and that of Scheele, Burger, and Matsuzaki[4] which showed that trapping efficiency increased with a decrease in particle size. Ionex Corporation supplied the presized NAgZ, LAgZ, PAgX, and AgX while Dr. J. Fürrer of Karlsruhe kindly supplied the $AgNO_3Si$. The $AgNO_3Si$ was not commercially available in the small quantities needed for our experimental work.

The experimental conditions used to simulate normal and standby PFM operating conditions are presented in Table 1 and the operating procedures for the two sets of experiments are discussed in the following.

In the extended standby test, CH_3I input began at the start of the working day, and analytical traps were changed on an hourly basis until the end of the working day. At this time simulated standby operation began and ended the next working day morning, about 16 h later. These trapping and standby cycles were repeated

TABLE 1. Experimental Operating Conditions

Operating Parameter	Extended Standby Test Level		Parallel Comparison Test Level	
	Normal Operation	Standby Operation	Normal Operation	Standby Operation
Gas Composition				
NO, Vol%	1	0	1	0
NO_2, Vol%	1	0	1	0
H_2O, Vol%	6	6	6	6
I_2, μmol I_2/L	0	0	0.05	0
CH_3I, μmol CH_3I/L	10.5	0	0	0
Air, Vol%	92	94	92	94
Bed Parameter				
Length, cm	16	16	20	20
Diameter, cm	1	1	1	1
Face Velocity, m/min	5.6	5.6	5	5
Flow Rate, L/min	0.44	0.44	0.4	0.4
Temperature, °C	150	150	150	150

until the effluent concentration exceeded 10^{-3} μmol I/L, which was indicated by the analytical trap, AgX, turning yellow. The experiment then continued with extended standby testing. During standby operation there was no iodine or NO_x present, the bed temperature was at the operating temperature of 150°C or higher, and moist air (6 vol% H_2O) passed through the bed.

In the parallel comparison tests, after the beds reached the operating temperature of 150°C, iodine flow began and continued 24 h/d until a shutdown/startup cycle or until the trapping portion of the experiments ended. The shutdown/startup cycles occured approximately every 4 weeks. After the trapping phase was completed, standby operation of the beds began and lasted 7 days. The analytical traps were removed on a biweekly basis during the trapping phase and at the end of standby operation.

During normal operation of the PFM, a bed of silver sorbent (18 wt% silver) will be in place for about one year and may be exposed to one or more shutdown/startup cycles. During shutdown, gas will not flow through the beds and the bed heaters will be turned off. In our test, the shutdown and startup cycles were accomplished in an 8 h day. For shutdown, the iodine and NO_x flows were stopped, the bed heater turned off, and the bed cooled to 40°C (the dew point of the carrier gas) before stopping the moist air flow. For startup, when the bed temperature reached 40°C, the moist air flow was begun. Once at 150°C, the iodine and NO_x flows were started.

Apparatus

The experimental apparatus were designed to allow simulation of the expected normal conditions in the PFM in terms of superficial face velocity, sorbent particle size, water content in the gas stream, NO and NO_2 concentrations, and temperature. Each experimental apparatus consisted of a gas delivery and flow control system; a gaseous iodine supply; and the test bed(s), including temperature control. Figure 2 presents a schematic of the laboratory apparatus for the parallel comparison tests. The apparatus used for the extended standby test differed mainly in there was only one bed and the iodine source was a gas bottle of CH_3I/N_2.

The gas delivery and flow control system consisted of gas bottles, an oil-free air pump, mass flow controllers, rotameters, a gas holdup and mixing bulb for generation of NO_2, a gaseous water generator, and a gas manifold to distribute the iodine-containing gas to each sorbent bed; the extended standby test used a single bed of NAgZ. Commercially produced gas bottles supplied purified grades of O_2 and N_2 and a technical grade (>99% purity) of NO. The oil-free air pump provided air flow. During operation, a ballast tank eliminated variations in air pressure to the mass flow controller. Electronic mass flow controllers controlled the gas flows and rotameters verified the flows. The NO_2 was prepared by mixing a stoichiometric amount of O_2 with the

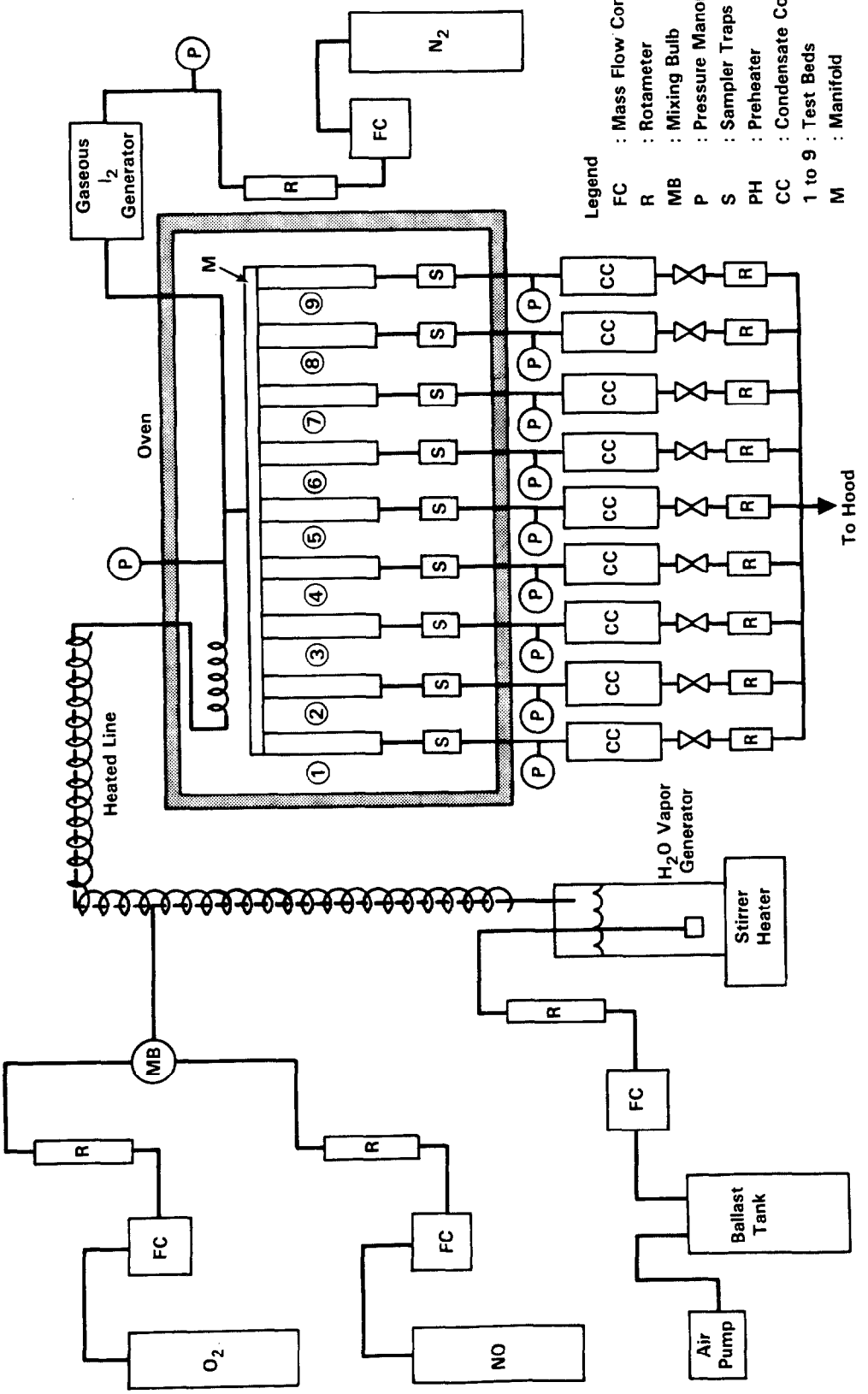

FIGURE 2. Schematic of Experimental Apparatus Used in Parallel Comparison Tests

NO in a 100-mL Pyrex bulb, thus providing a 50% NO/50% NO_2 mixture. The glass bulb provided sufficient residence time for ensuring conversion of the desired amount of NO to NO_2.

A dew point of about 35 to 40°C [5.5 to 6 vol% $H_2O_{(g)}$] for the input gas was obtained by bubbling the air stream through a bottle of 40°C water. The water temperature was controlled with a stirrer/heater plate.

The water-containing air and the NO_x were combined and delivered through a heated stainless steel line to the preheater assembly, which was contained within the oven. The preheater was a coil of 0.25-in.-O.D. stainless steel tubing. This gas stream was mixed with the gaseous iodine-containing stream and then passed into the gas manifold for distribution to each of the test beds. The gas flowed downward through the test beds to prevent fluidization of the bed material. In the parallel comparison tests, the gas flow through each bed was controlled using identical rotameters on the exit lines from each bed. For the extended standby test, the total flow passed through the bed and was not monitored at the exit.

To determine any remaining iodine in the gas stream, the gas leaving each test bed flowed downward through a 150°C, 5-cm-deep by 1-cm-dia bed of AgX. The iodine-free gas stream then left the oven and passed through condensed-liquid collection traps before passing through the exit rotameters.

The gas delivery lines for the air, N_2, NO, and O_2 were plastic, and the exit line from the NO_2 generator bulb was Teflon and glass. The gas lines between the water generator and the manifold were stainless steel. The bed containers and AgX sampler containers were borosilicate glass. The beds were joined to the manifold by butting the borosilicate tube to the manifold and using a Teflon sleeve and worm gear clamps to ensure a leak-free system. The beds were connected to the sampler tubes using ball and socket joints and silicone grease was used to seal the joints. The system was periodically pressure tested to verify that the apparatus was leak-free.

Elemental iodine is expected to be the predominant iodine species in the PFM DOG and was used in the parallel bed tests, while CH_3I was the species used in the extended standby test for reasons discussed earlier. To provide gaseous elemental iodine to the beds, we passed a measured flow of N_2 though a 22°C, aqueous, radioiodine-traced triiodide/elemental iodine suspension. The selected temperature provided the necessary iodine vapor pressure and thus the desired gaseous iodine concentration. For the extended standby test a gas tank of ^{125}I radiotraced CH_3I/N_2 was purchased from New England Nuclear.

To radiotrace the elemental iodine a mixture of solid I_2, water, iodide ion (0.01 mole I^-/mole I), and ^{125}I tracer as iodide ion was prepared and allowed to equilibrate for more than 4 weeks.

Elemental iodine reacts rapidly with I^- to form the triiodide ion, which presumably improves the isotopic exchange rate. Samples of the aqueous phase, plus gas samples from the bubbler described below, verified that exchange had occurred.

Preliminary testing demonstrated that the gaseous I_2 generator, if operated at room temperature (22°C), could consistently deliver the needed concentration of I_2 to the manifold. The transfer line from the I_2 generator was constructed of glass and stainless steel, and was as short as possible to limit I_2 deposition. Preliminary testing indicated that I_2 would pass quantitatively through 50 cm of 6.4-mm-O.D. stainless steel tubing heated to 150°C.

Analytical Methods

To evaluate the performance of the iodine sorbents, the iodine concentration was periodically measured in the effluent, the I_2-laden gas from the I_2 generator in the parallel comparison tests, and the influent in the extended standby test. Chemical and radioanalytical methods were used for the analyses.

To chemically analyze the iodine in solutions of interest, we used an iodide ion Specific Ion Electrode (SIE). The method was applicable to determining the amount of iodine present in the caustic traps used to collect gaseous I_2 and in the I_2 generator itself. In this method hydroxylamine nitrate or sulfate was added to reduce the higher oxidation states (I_2 and IO_3^-) present in solution to iodide. Nitric acid was used to adjust the pH to 2 and sodium nitrate was used to adjust the ionic strength of the solution.

This method was used in the developmental stages of the I_2 generator and later during the experiments to determine that the generator consistently delivered the desired amount of iodine to the test beds. A controlled flow of nitrogen was bubbled through the I_2 generator, then passed through a 1 M caustic scrubber to remove the gaseous halogen. The caustic solution containing iodine was then analyzed to chemically determine the iodine content. Aliquots of the aqueous radiotraced iodine/triiodide slurry/solution were also analyzed to determine total iodine. The radioiodine content was then determined and the specific activity of the iodine was calculated.

The iodine was radiotraced with ^{125}I at a nominal specific activity of 2 Ci/mol I (1 Ci/mol CH_3I for the extended standby test). We analyzed for radioiodine using NaI(Tl) scintillation detectors. We used a well crystal to measure radioiodine in the effluent traps, samples of the iodine generator slurry, caustic traps, and the bed segments from the extended standby test. Segmented bed counts for the parallel comparison tests were performed using a right circular cylindrical NaI(Tl) crystal. A lead shield with a 3.6-cm-high, 3.0-cm-wide, 10-cm deep slit was placed between the crystal and the bed, thus permitting the bed to be counted in six slightly overlapping 33-mm segments.

A standardized solution of ^{125}I was used to prepare ^{125}I standards on AgX. These standards were prepared by adding known amounts (20 to 500 μL) of standard solution, or dilutions of the solution, to the amount of AgX used in the iodine effluent sample traps. A few drops of standard solution were added to a layer of AgX, adding only enough to wet that layer without allowing the solution to contact the counting tube. A second layer of AgX was added and the process repeated until the standard aliquot was added to the AgX. The samples were air dried or dried in a vacuum oven at 70°C. Replicate samples and standards were prepared by several people using different volumes of standardized solution.

III. Results

In general the results of the experiments are positive for the three zeolites NAgZ, LAgZ, and PAgX, but not for $AgNO_3Si$. These experiments showed that 16- or 20-cm beds of the three zeolites could consistently reduce the effluent iodine concentration in a simulated normal PFM DOG to $<10^{-5}$ μmol I/L while 20-cm beds of $AgNO_3Si$ could not. Simulated standby operation for 7 days of sorbent beds loaded to 0.25 mmol I/g sorbent caused no increase in the effluent concentration; however, at an iodine loading of 0.6 mmol I/g NAgZ, standby conditions caused the effluent concentration to exceed 10^{-5} μmol I/L immediately.

The results of the extended standby test for NAgZ will be discussed first followed by a discussion on the results of the parallel comparison tests on NAgZ, LAgZ, PAgX, and $AgNO_3Si$.

Effect of Standby Operations on Fully Loaded NAgZ

The extended standby test was performed to determine whether long-term standby operation of a fully loaded bed of NAgZ would cause long-term release of iodine at levels $>10^{-5}$ μmol I/L or whether the iodine would eventually become fixed. The early work reported by Scheele and Burger[1] showed at least short-term iodine mobility. The current test also simulated the scenario in which the PFM dissolver is not operated and a fully or nearly fully loaded NAgZ bed is maintained at standby for an extended period of time before being removed.

This experiment was performed in three stages. The results of the first two stages of trapping and standby testing at 150 and 200°C are shown in Figure 3. In Figures 3 and 4 (Figure 4 is presented later), the ordinates are the time-based iodine loading calculated based on input concentration, flow rate, time, and the iodine which passed through or migrated from the bed. In the third stage the bed was divided into three equal portions and the upper portion was exposed to 180 to 200°C and flowing air for several days.

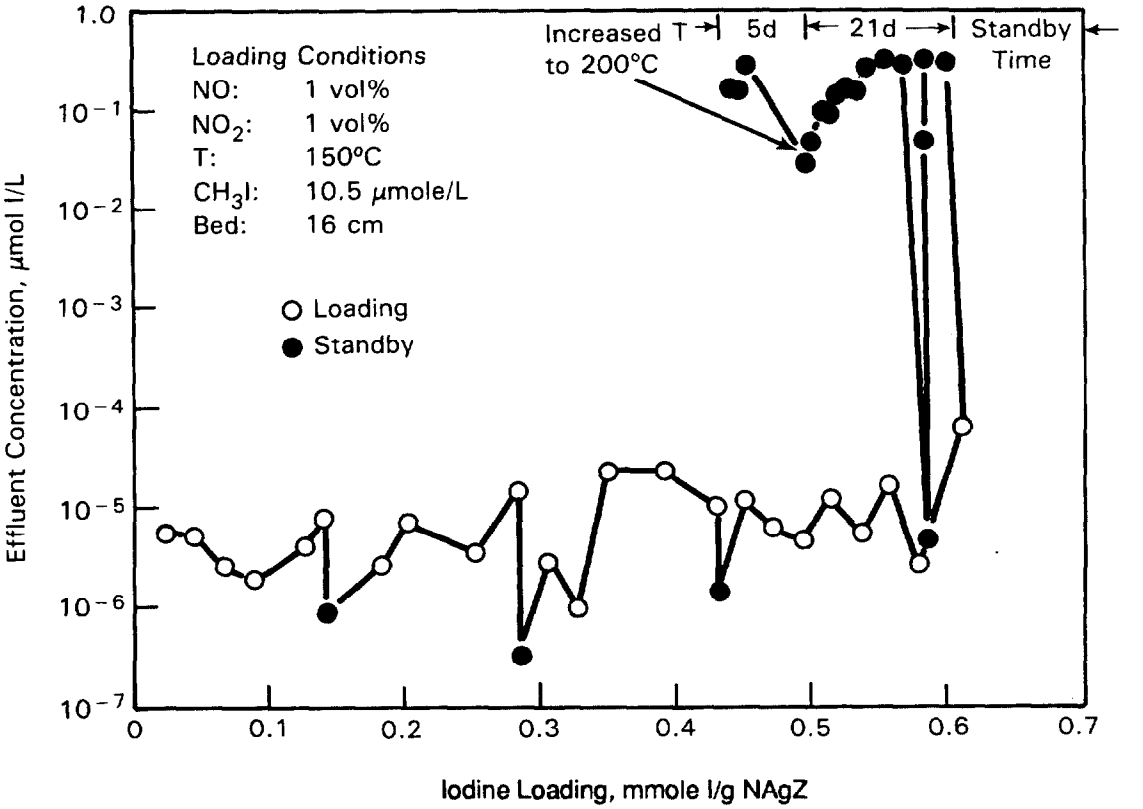

FIGURE 3. Effluent Concentration vs Iodine Loading on NAgZ for the Extended Standby Test

During trapping and the 16-h standby tests before breakthrough, the 16-cm bed loaded to 0.62 mmol I/g NAgZ while maintaining a nominal effluent concentration of 10^{-5} μmol I/L before breakthrough. This performance met the target effluent concentration established for the PFM while providing a fair loading (36% of the theoretical 1.7 mmol I/g NAgZ assuming a 1:1 I to Ag ratio at full silver utilization).

During the first stage of standby testing, the effluent concentration was monitored for 20 days with the bed temperature at 150°C followed by 5 days at 200°C. With time, the effluent concentration at 150°C began to decrease with respect to the loading level. Extrapolating these standby data suggests that the bed might have stabilized at a loading of 0.5 mmol I/g NAgZ while maintaining the standby release at $<10^{-5}$ μmol I/L. Increasing the temperature to 200°C increased the standby release level to 0.1 μmol I/L, which suggested an increase in the iodine vapor pressure. This stage of the standby testing had reduced the iodine loading by about 20%.

In the third stage of the extended standby testing, the bed was removed and divided into three parts of 4.93 g (inlet), 4.38 g (middle), and 3.81 g (outlet). The iodine loadings based on

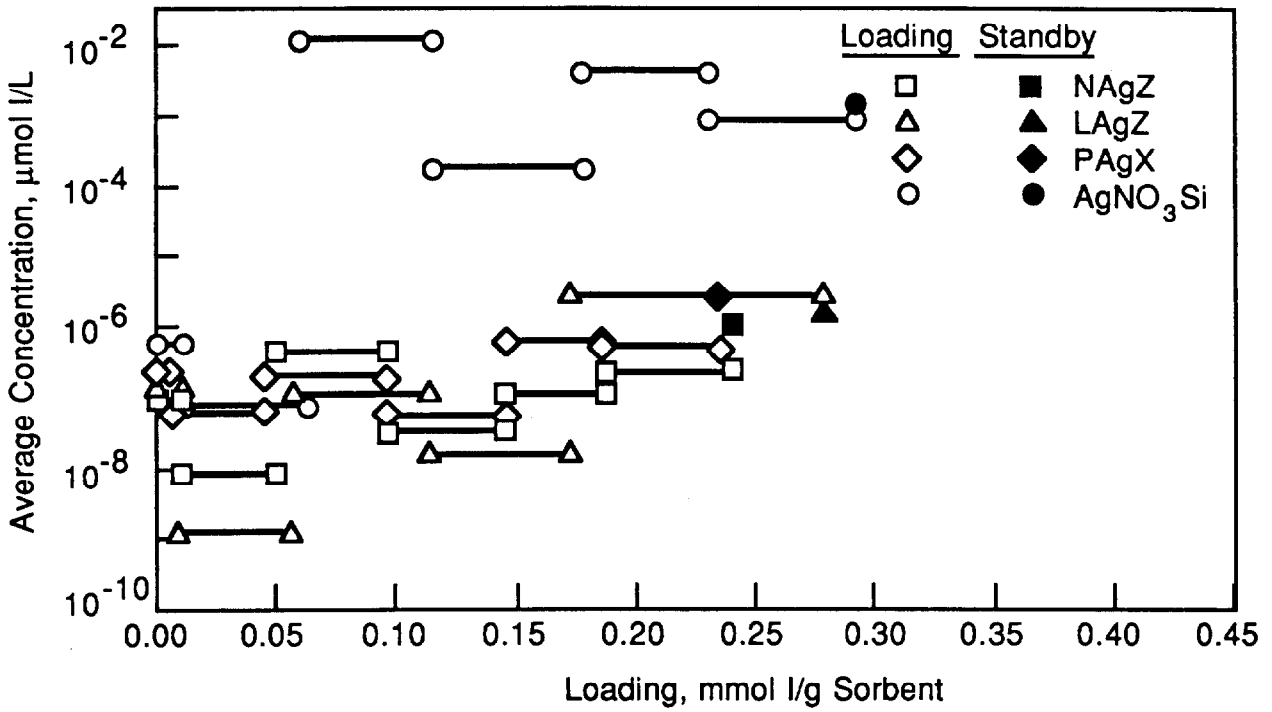

FIGURE 4. Average Effluent Concentrations from Beds of NAgZ, LAgZ, AgX, $AgNO_3Si$ (Shutdown/Startup Cycles performed at nominal loadings of 0.01, 0.05, and 0.15 mmol I/g Sorbent)

gamma count were 0.57, 0.44, and 0.35 mmol I/g NAgZ, respectively, for the three bed portions. After passing 200 mL/min air through the inlet third for 11 days at 180 to 200°C, the effluent dropped to the target release level of 10^{-5} µmol I/L. This treatment reduced the inlet bed loading to 0.43 mmol I/g NAgZ. This test suggested that if a 16-cm bed is loaded to a maximum of 0.43 mmol I/g NAgZ, the iodine loaded onto the bed might be fixed on the NAgZ and a continued effluent concentration of $<10^{-5}$ µmol I/L might be realized.

This experiment showed that a 16-cm bed of NAgZ could effectively control the effluent iodine concentration to about 10^{-5} µmol I/L when the inlet gas was representative of a normal PFM DOG containing 10.5 µmol CH_3I/L and during standby operations when loaded to <0.62 mmol I/g NAgZ. The extended standby testing portion of the experiment showed that not all of the trapped iodine is firmly fixed on the NAgZ and can be removed by passing iodine-free air through the bed at temperature. These tests suggested that, with time, the iodine bed loading will stabilize near 0.5 mmol I/g NAgZ at 150°C or near 0.4 mmol I/g NAgZ at 200°C.

We have no explanation at this time why the trapped iodine is labile at standby conditions and may become fixed with time. The possibilities include slow diffusion and reaction rates, equilibrium considerations, and the iodine species or concentration

in the inlet gas. This experiment and others discussed by Scheele and Burger[1] indicate there is a need for fundamental mechanistic studies on iodine trapping by silver sorbents.

Trapping Performance of NAgZ, LAgZ, PAgX, and $AgNO_3Si$

This section discusses the results of the parallel comparison tests of NAgZ, LAgZ, PAgX, and $AgNO_3Si$ during simulated normal operation of the PFM. These experiments measured the effluent concentration with an inlet iodine concentration at the expected process level (0.05 μmol I_2/L), after three shutdown/startup cycles, and during 7 days of standby after loading to 0.25 mmol I/g sorbent. The shutdown/startup cycles were performed at nominal loadings of 0.01, 0.05, and 0.15 mmol I/g sorbent.

As shown in Figure 4 the three silver zeolites consistently reduced the iodine concentration to $<10^{-5}$ μmol I/L in the bed effluent during trapping while the average effluent concentration from the three $AgNO_3Si$ beds was $>10^{-4}$ μmol I/L after the second shutdown/startup cycle. The performance of the zeolites met the performance criteria established by the WHC for the PFM while the effluent concentration from the $AgNO_3Si$ beds was higher than the target concentration for PFM operation after the second shutdown/startup cycle.

Shutdown/startup cycling did not hurt the performance of the silver zeolites; however, after the second and third shutdown/startups, the concentration from the $AgNO_3Si$ beds increased to levels much higher than the target concentration for the PFM. Why shutdown/startup cycling would impact the trapping performance of $AgNO_3Si$ is unknown. In a problem unrelated to shutdown which might provide a clue, the center NAgZ bed was accidentally flooded with water prior to the second shutdown, but no condensed water was seen in any other bed at any time. This flooding did not significantly affect the NAgZ bed's performance.

We do not know why the performance of the zeolites and $AgNO_3Si$ differ in these experiments. Even though the parent species of the active silver differs in the two materials, calculations show that silver nitrite and nitrate are likely to be present in the zeolites because of reactions with the humid, NO_x-containing stream. Past work on the effects of NO_x on iodine trapping by NAgZ by Scheele and Burger[1] and as reported by McKay, Miquel and White[2] for the silver nitrate-impregnated silicic acid, AC 6120, indicate that both perform well in the presence of NO_x.

The distribution of the trapped iodine varied for each of the different materials. As shown in Figure 5 and Table 2, PAgX had the shortest mass transfer zone after the trapping cycle. Essentially all of the iodine was on the first 3.3 cm of the PAgX bed. The LAgZ had a shorter mass transfer zone than NAgZ, 6.6 versus 9.9 cm. The bulk of the iodine was in the first 3.3 cm for each mordenite. The iodine was distributed throughout the $AgNO_3Si$ beds with 50% found on the top 3.3 cm.

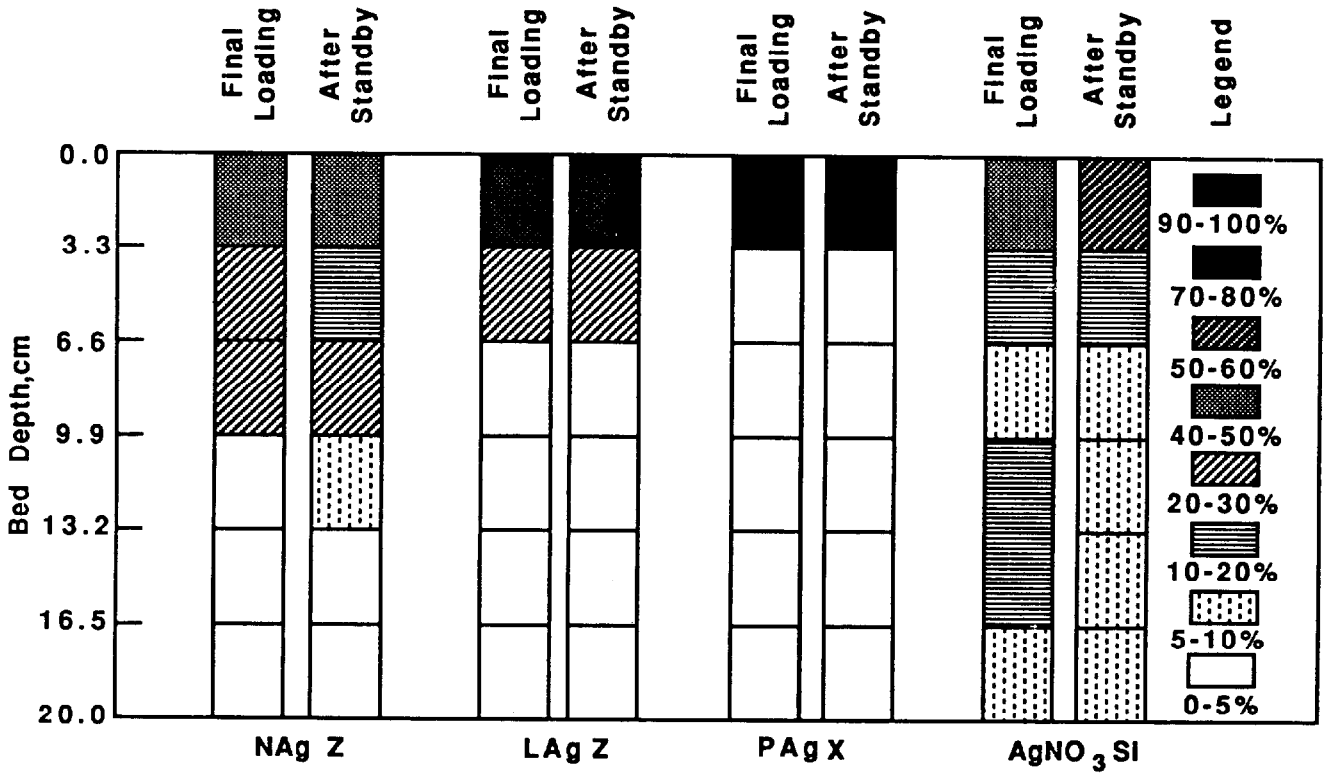

FIGURE 5. Iodine Distribution on Sorbents After Trapping and After Standby

The trapping portion of the experiments indicates that NAgZ, LAgZ, and PAgX can reduce a simulated PFM DOG iodine concentration from 0.1 to $<10^{-5}$ μmol I/L up to an iodine loading of 0.25 mmol I/g sorbent. This set of experiments also indicates that $AgNO_3Si$ can not routinely, under the same conditions, reduce the influent concentration to the desired level of 10^{-5} μmol I/L. We did not determine the breakthrough loading capacity of these materials with an influent concentration of 0.05 μmol I_2/L.

Effect of Standby on Partially Loaded NAgZ, LAgZ, PAgX, and $AgNO_3Si$

During standby operations (see Figure 4) after being loaded to 0.25 mmol I/g sorbent, the average effluent concentration from all the beds for 7 days was near the concentration just prior to standby operation. Figure 5 shows little change in the trapped iodine distribution on the different bed materials before and after standby. It appears that some migration occured on the NAgZ and on the $AgNO_3Si$. Some of the variability present in the distribution data is due to bed placement during counting.

This standby test indicates that the effluent from the silver zeolite beds during 7 days of standby operation for a bed loaded to 0.25 mmol I/g sorbent from a gas stream containing the PFM process iodine concentration will not exceed 10^{-5} μmol I/L.

TABLE 2. Iodine Distribution After Trapping and Standby Operation

Segment, cm from top	NAgZ		LAgZ		PAgX		$AgNO_3Si$	
	Final Loading, %I	After Standby, %I	Final Loading, %I	After Standby, %I	Final Loading, %I	After Standby, %I	Final Loading, %I	After Standby, %I
0-3.3	45.5	46.8	79.4	73.0	97.5	99.2	46.8	54.6
3.3-6.6	23.5	19.8	20.5	26.8	2.3	0.5	14.5	14.2
6.6-9.9	27.1	26.0	0.04	0.05	0.05	0.08	9.3	8.2
9.9-13.2	3.8	7.1	0.03	0.05	0.05	0.07	10.4	8.4
13.2-16.5	0.05	0.2	0.03	0.05	0.05	0.07	11.7	8.7
16.5-20.0	0.04	0.06	0.03	0.05	0.05	0.07	7.3	5.9

IV. Conclusions

These two sets of experiments have shown that the silver zeolites NAgZ, LAgZ, and PAgX can routinely reduce the influent iodine concentration in a simulated nuclear fuels reprocessing plant dissolver offgas stream to less than 10^{-5} μmol I/L. The extended standby experiment showed that the trapped iodine on NAgZ loaded to 0.6 mmol I/g NAgZ becomes mobile during standby operation but with time becomes less mobile. The experiments with $AgNO_3Si$ indicate that the sorbent can not routinely guarantee an effluent concentration at the desired level in a simulated PFM DOG when it is cycled through several shutdown/startup cycles.

Standby operation of a 20-cm bed of a tested silver zeolite loaded to 0.25 mmol I/g sorbent should not cause the effluent concentration after 7 days to increase to $>10^{-5}$ μmol I/L. Standby operation did not change the iodine concentration in the effluent from a 20-cm bed of $AgNO_3Si$; however, the effluent concentration was higher than the target concentration.

These tests indicate that studies are needed to determine the mechanism of iodine trapping by silver-containing sorbents. The surprising mobility of trapped iodine on NAgZ loaded to breakthrough and the relatively poor performance of the silver nitrate-impregnated silicic acid compared to the zeolites point to this lack of basic information. Possible studies include thermoanalyses of the sorption reaction to determine the energetics and possibly kinetics, sorption on short beds to determine the kinetics, and utilization of surface analytical techniques to investigate the chemical speciation of the trapped iodine. There are many questions to be answered and several approaches that could yield significant results.

References

(1) Scheele, R. D., and L. L. Burger. 1987. Evaluation of Silver Mordenite for Radioiodine Retention at the PUREX Process Facility Modification. PNL-6261, Pacific Northwest Laboratory, Richland, Washington.

(2) McKay, H. A. C., P. Miquel, and I. F. White. 1982. "Management Modes for Iodine-129." In Management Modes for Iodine-129, eds. W. Hebel and G. Cottone. Harwood Academic Publishers, New York, New York.

(3) Thomas, T. R., L. P. Murphy, B. A. Staples, and J. T. Nichols. 1977. Airborne Elemental Iodine Loading Capacities of Metal Zeolites and A Method for Recycling Silver Zeolite. ICP-1119, Idaho National Engineering Laboratory, Idaho Falls, Idaho.

(4) Scheele, R. D., L. L. Burger, and C. L. Matsuzaki. 1983. Methyl Iodide Sorption by Reduced Silver Mordenite. PNL-4489, Pacific Northwest Laboratory, Richland, Washington.

DISCUSSION

HERRMANN: Active operation with iodine filters in the dissolver offgas of the WAK reprocessing plant shows iodine concentrations downstream of the iodine filters to be less that 10^{-11} mole I/L. So, I cannot understand the results you obtained with $AgNO_3Si$. Maybe the material was wet or exposed to high humidity? Have you considered that high concentrations of NO may influence the sorption behavior?

SCHEELE: The performance of $AgNo_3Si$ is also baffling to us, particularly considering the excellent performance of AC6120 observed by you in the WAK plant. Of the sorbents tested, $AgNO_3$ should have the most straightforward and predictable chemistry.

In a gas stream containing 1 vol% NO_2, and assuming that the sorption product is AgI, the equilibrium iodine concentration should be about 10^{-5} μmol I/L, yet we observed an iodine concentration a factor of 100 greater in the effluent after the second shutdown/startup cycle. We would not predict this performance considering that there is an ample supply of $AgNO_3$ available for reaction with the iodine. This suggests to me that something occurred to the matrix during the shutdown/startup cycle to limit the access of iodine to the active chemical, $AgNo_3$. Maybe water condensed in the pores of the material, dissolving the soluble $AgNO_3$, and the pores became blocked when the material was reheated to 150°C. Though we observed condensed water in one of the Norton silver mordenite beds prior to the second shutdown/startup cycle, we did not observe any in any other bed including the three $AgNO_3Si$ beds. It is worth noting that the silver mordenite bed was still able to reduce the iodine concentration to less that 10^{-5} μmol I/L.

In this experiment we used only 1 vol% NO, which I would not consider high. We have not done a complete thermodynamic analysis on the effects of NO_x on iodine trapping by $AgNO_3$-containing sorbents. Most of our work has concentrated on silver zeolites.

Based on the current state of knowledge about the chemistry of silver-containing sorbent/iodine systems, any additional explanations would be sheer conjecture, as are the possible explanations already given. We just had sufficient funding to complete the trapping studies but not to study why we observed what we did. The chemistry appears to be adequate to provide the desired reduction in iodine concentration at these conditions, but in these tests the $AgNO_3Si$ did not perform as predicted. Our results show that there is much to be learned about the dynamics and mechanisms of iodine trappings by silver-containing materials. We believe that these studies should be performed to better predict the performance of these silver sorbents in a nuclear fuels reprocessing environment.

GUEST: Did you only introduce iodine as methyl iodide? Did you analyze the methyl iodide in downstream air and if so, how?

SCHEELE: In the extended standby test, we introduced the iodine as iodine-125-traced methyl iodide and in the parallel comparison tests as iodine-125-traced elemental iodine. In these tests we did not try to identify the effluent iodine chemical species. We measured the total iodine concentration by collecting the radioactively traced iodine on a fully exchanged silver faujasite

trap. In past work, we used a gas chromatograph to measure methyl iodide in the effluent down to about 0.01 μmol CH_3I/L. In that work we found that some, and occasionally all, of the introduced methyl iodide converted to elemental iodine over a bed of hydrogen-reduced silver mordenite depending on the gas composition and bed operating conditions.

FURRER: In more than several hundred tests evaluating trapping of I or CH_3I with silicic acid impregnated with $AgNO_3$ under different conditions, we found that iodine penetration as a function of bed depth was an exponential function. You found in your tests a different distribution function. I can not explain it, can you explain it for me?

SCHEELE: The iodine distribution that we observed on the three beds of $AgNO_3Si$, where the top 3.3 cm contained 50% of the trapped iodine, the second 3.3 cm contained 15% of the iodine, and the remaining five 3.3 cm segments each contained about 10% of the iodine, suggests to me that something occurred to the $AgNO_3Si$ during the second shutdown/startup cycle which prevented iodine penetration into the interior of the beads and to the active sorbent chemical, $AgNO_3$. One speculation, based on your own observations that condensed water has a negative affect on the performance of AC6120, is that during the shutdown/startup cycle, water condensed in the pores of the silicic acid as the beds were cooled to 40°C with moist air (dew point 35°C) passing through them. The condensed water dissolved some of the $AgNO_3$ and when the bed was reheated to 150°C, it resolidified, blocked the pores, and left a very limited active surface. If this blockage occurred, it could change the distribution function. We did observe condensed water prior to the first shutdown/startup cycle in one of the beds of Norton silver mordenite (NAgZ), though we did not observe any condensed water in the three beds of $AgNO_3Si$. The NAgZ bed did not appear to be affected by exposure to condensed liquid up to the loading obtained in these tests.

MURTHY: There is a real controversy on the performance of nitrate as reported by you (Scheele) and as reported by them (Karlsruhe Nuclear Research Center). I do not think we can resolve it here but I think you should both be talking.

WILHELM: Did you do something to the AC6120? I read your paper and it looks like you picked out certain particle sizes by sieving or something.

SCHEELE: We used the material as we received it.

WILHELM: Did you really reproduce the distribution of iodine shown for the left filter column of $AgNO_3Si$ in your slide? We have never seen a distribution of that type in hundreds of laboratory experiments and filters in the real dissolver offgas of the WAK, while controlling iodine for more than 11 years. That means that if the loading is evenly distributed you have a certain iodine content in the first two beds, a lower content in the third, a higher content in the fourth and fifth, and again a lower content in the sixth; and it is three times. I can not believe that you see that uneven a distribution. It is a distribution I have never seen in hundreds of experiments over eleven years of use in a real repossessing plant. I

do not know how it is possible.

SCHEELE: The iodine distribution presented for $AgNO_3Si$ after loading is the average observed for the three test beds of $AgNO_3Si$. This figure is also an example of a problem that arises when results are presented in terms of ranges. The slide indicates that the average iodine content of the fourth and fifth segments is higher than the third, however, the numerical average percentages observed for these same three sections were 9.3, 10.4, 11.7%, which for our analytical method are not statistically different. Because the values fall on both sides of the arbitrary boundary value of 10%, the iodine distributions fall in two separate ranges and are presented on the slide as such. In general the percentage of the iodine found on the third, fourth, and fifth segments was a nominal 10%. In only one of the individual test beds did the fifth segment have a statistically different iodine content of 15%. The results were in general reproducible between beds. The iodine distribution after loading the $AgNO_3Si$ beds was consistent with the trapping performance observed for $AgNO_3Si$ in our tests. Iodine was observed throughout the bed indicating partial trapping of the iodine.

MURTHY: Obviously, there is a very strong concern about your nitrate results. I think it was a good discussion between the German investigators and you. After this meeting you might look at your results.

WILHELM: I suggest that we will send you our material and that you send your material to us. We will both reproduce the experiments and then we will have a discussion.

TESTING AN IODINE FILTER FOR THE VESSEL OFFGAS OF THE GERMAN INDUSTRIAL-SCALE REPROCESSING PLANT

F.J. Herrmann, V. Motoi, H. Fies, B. Stojanik
Wiederaufarbeitungsanlage Karlsruhe

J. Furrer, R. Kaempffer
Kernforschungszentrum Karlsruhe,
Federal Republic of Germany

Abstract

An extensive retention of the iodine (iodine 129 and iodine 131) is required in the German industrial-scale reprocessing plant to be erected at Wackersdorf. This calls for iodine retention both in the dissolver offgas and in the vessel offgas.

Various sorption materials have been tested under realistic conditions in the Karlsruhe Reprocessing Plant (WAK) in cooperation with The Karlsruhe Nuclear Research Center. The good laboratory results achieved with the AC 6120 material justified construction of an iodine filter for the vessel offgas. The filter has been operated since October 1987 and exposed to a 10 % side stream (10 % iodine filter); the decontamination factor (DF) obtained is > 50.

Based on this experience, it is envisaged to equip the WAK vessel offgas cleaning systems as from 1989 with iodine filters. From this measure and from iodine filtration in the dissolver offgas applied since 1975, an iodine decontamination factor exceeding 500 for the total offgas discharged is expected.

I. Introduction

The flowsheet for iodine in a reprocessing plant is determined largely by the process management during fuel dissolution.

After the fuel has been dissolved, most of the fission iodine is present in the volatile elemental form. On account of its distribution coefficient, it occurs in the fuel solution, in the dissolver offgas, and in the scrubber solutions of the dissolver offgas section. The fraction left in the fuel solution is distributed in the subsequent liquid streams and the dissolver offgas of the plant without needing special measures to be taken.

If the completest possible retention of iodine-129 is to be guaranteed, most of the iodine should be transferred into the dissolver offgas where it is fixed on suitable sorption materials. At WAK, about 99 % of the iodine inventory is expelled into the dissolver offgas and removed by iodine filters.

The iodine sorption material used is a silver nitrate impregnated porous catalyst carrier (amorphous SiO_2). The material is termed AC 6120. The filter technique relying on AC 6120 in the dissolver offgas has proved its value at WAK since 1975.

The minor iodine fraction not expelled from the fuel solution gets into the PUREX process.

II. Requirements on Iodine Retention in the German Industrial-Scale Reprocessing Plant

Almost complete retention of the iodine-129 isotope is required in the Federal Republic of Germany to be achieved by an industrial-scale reprocessing plant.

The maximum admissible value for I-129 release via the offgas pathway for the Wackersdorf site is 1.85 GBq/a /1/.

At a 500 t/a throughput this means that only about 0.2 % of the iodine input may be emitted via the offgas. This corresponds to a DF $\geq$ 460 for I-129 retention in the offgas.

It will be exemplified for two cases (Figure 1) how a DF of approx. 500 can be attained for I-129 during the cleaning process.

Case 1: Iodine filtration in the dissolver offgas with a DF $\geq$ 1000 is adequate if it is ensured, at the same time, that during dissolution 99.9 % of iodine is expelled from the dissolver and thus removed by the iodine filter. In this case no iodine filter must be installed in the vessel offgas system.

Case 2: Studies performed at WAK have shown that under the present operating conditions 99.9 % of iodine can not be expelled. Assuming that 99 % of iodine is expelled /2, 3/, it must be anticipated that some of the 1 % residual iodine is emitted together with the vessel offgas. This means that iodine in the vessel offgas will also have to be retained.

Only little technical experience has been accumulated so far in the application of iodine filters in the vessel offgas system of a reprocessing plant /4/.

Consequently, it may be asked whether the iodine sorption material, which has been used in the WAK dissolver offgas since 1975, will be equally suited for application in the vessel offgas.

First laboratory experiments have shown that after exposure of more than 40 days the efficiency of the filter material is clearly reduced. This has been attributed to poisoning of the sorption material by the organic impurities contained in the vessel offgas /5/. For this reason, testing of an iodine filter in the vessel offgas became an urgent necessity.

The objectives pursued in the present investigations were the following:

- study of different iodine sorption materials in a bypass-stream of the WAK vessel offgas system
- test of a technical iodine filter in a larger side-stream of the vessel offgas

III. Special Conditions for Iodine Filtering in the Vessel Offgas

Iodine, entering the extraction process, can be emitted with the vessel offgas.

The conditions for iodine retention in the vessel offgas are less favorable than in the dissolver offgas, for the following reasons stated below:

- The iodine concentrations in the vessel offgas are lower by the factor of 10^5 (10 to 30 Bq/m^3 instead of 10^6 Bq/m^3 in the dissolver offgas).
- The offgas stream is 5 to 20 times higher.
- The vessel offgas contains organic compounds which may poison the AC 6120 iodine sorption material (e.g. dodecane and organic radiolytic products).

On account of potential poisoning by organic compounds, the efficiency of iodine sorption materials in the vessel offgas must be investigated under realistic conditions for long service life.

IV. Investigation of the Iodine Sorption Material in the Vessel Offgas

The investigation of the AC 6120 iodine sorption material was performed at WAK using the experimental facility constructed by the Karlsruhe Nuclear Research Center.

This testloop is presently connected with the WAK vessel offgas system (Figure 2). The sampling point is located downstream of the HEPA filters and is shown schematically in figure 3.

The gas flows through six absorption columns connected in parallel which are installed in a heating cabinet. The internal diameter of the columns is 0.025 m. The total flow rate through the six columns is 2.4 m^3/h. The heating cabinet can be operated up to 150 ^{o}C.

Each column contains six successive beds consisting of the AC 6120 sorption material and two beds consisting of SS 207 B charcoal. The charcoal beds are located behind the AC 6120 beds. They have been foreseen to remove the iodine species which are not retained by AC 6120. The SS 207 B charcoal has been impregnated with 1.5 % potassium iodide. Each bed is 0.025 m deep. At 0.4

m^3/h (STP) flow rate the calculated gas residence time is 0.1 s per bed. After different exposure times the columns were removed. The beds were emptied individually and a representative 1 g sample was measured on an Intrinsic Germanium Planar Detector to determine its I-129 content. The concentration profiles and decontamination factors for the various beds are presented as graphs on figure 4 for an exposure of about 50 days and 100 days.

It can be seen that for 10 cm bed depths, 0.4 s gas residence time, and 50 days exposure time a decontamination factor of more than 100 is achieved provided that the operating temperature of the iodine sorption material is 140 °C.

At an operating temperature of 100 °C and with the other conditions remaining unchanged, the DF is smaller than 100 /6/.

For exposure times up to 220 days no significant decrease in the DF has been observed.

V. Testing an Iodine Filter in the WAK Vessel Offgas

Based on the experience gained with the experimental filters a prototype iodine filter was constructed for use in the WAK vessel offgas system. The filter has been operated since October 1987 and the results derived from the laboratory-scale investigations have been validated.

1. Description of the iodine filter

As indicated in the figure 2 this iodine filter is connected to a side stream of the vessel offgas. The point of connection is located downstream the HEPA filters. Two iodine sampling points (S6 and S7) are arranged upstream and downstream the iodine filter, respectively.

The gas flow chosen for these iodine filters is a 10 % side stream of the vessel offgas. The flow rate is 35 m^3/h. The first filter has been permanently operated since October 1987. It contains AC 6120 with 12 % silver content. The filter operating temperature is 140 °C. The gas is preheated in an electric heater.

2. Results

Regular measuring (for half a year) of the iodine activity in the offgas upstream and downstream the 10 % iodine filter results in a DF greater than 100. After that time a slight decrease has been observed.

When the DF decreases to about 20, the filter will be regenerated by a treatment with NO_2 proposed by Furrer /7/.

The iodine in the vessel offgas (sampling points S6 and S7) is sampled with heated filter beds consisting of AC 6120/12 % Ag, with one charcoal bed (SS 207 B) in series.

VI. Investigations of the Iodine Compounds in the Vessel Offgas

As already indicated above, organic iodine compounds are formed during the extraction process which, depending on their vapor pressure, are released via the vessel offgas system.

This type of compound has been isolated and analyzed using a cooling trap installed in a bypass of the vessel offgas system /8/.

It appears from the results of gas chromatographic analyses that mainly iodated dodecane is formed. In addition all straight-chain iodated alkanes from C-1 to C-11 have been detected.

The investigations have shown that the iodine of these organic compounds is retained by the iodine sorption materials investigated.

VII. Future Activities

The WAK began to install iodine filters in the other vessel offgas systems. After installation of these filters an overall iodine retention factor related to the original input of more than 500 is expected for the total offgas.

References

/1/ Deutsche Gesellschaft für Wiederaufarbeitung
"Kurzbeschreibung für die Wiederaufarbeitungsanlage Wackersdorf"
Hannover, January 1988

/2/ R. Berg, H. Schüttelkopf
"Die Messung der Verteilung in und die Abgabe aus der Wiederaufarbeitungsanlage Karlsruhe"
Seminar on Radioactive Effluents from Nuclear Fuel Reprocessing Plants, Karlsruhe, November 1977

/3/ B. Lorrain, D. Saundray, M. Tarnero
"Dissolveur continu rotatif pour combustibles eau légère"
RECOD 87, Paris, August 1987

/4/ M. Fukushima, K. Miyahara, K. Matsumoto
"Iodine Removal from the Vessel Off Gas in Tokai Reprocessing Plant"
IAEA-SR-72/25, 1972

/5/ J.G. Wilhelm, H.G. Dillmann, J. Furrer
"Entwicklung von Iodfiltern und Adsorbermaterialien für Wiederaufarbeitungsanlagen"
KFK 1818, 1972

/6/ F.J. Herrmann, J. Furrer, C. Berger-Wittmar,
R. Kaempffer, V. Motoi, B.J. Nemes
"Erprobung des Iod-Sorptionsmaterials AC 6120
im Behälterabgas der WAK"
Jahrestagung Kerntechnik 1988, Travemünde, May 1988

/7/ J. Furrer, J.G. Wilhelm
"Jodfilterung aus der Abluft von Wiederaufarbeitungsanlagen"
Seminar on Iodine Filter Testing, Karlsruhe, 1973

/8/ L. Stieglitz et al.
"Organo-Iodverbindungen im Abgas einer
Wiederaufarbeitungsanlage"
Atomwirtschaft, to be published

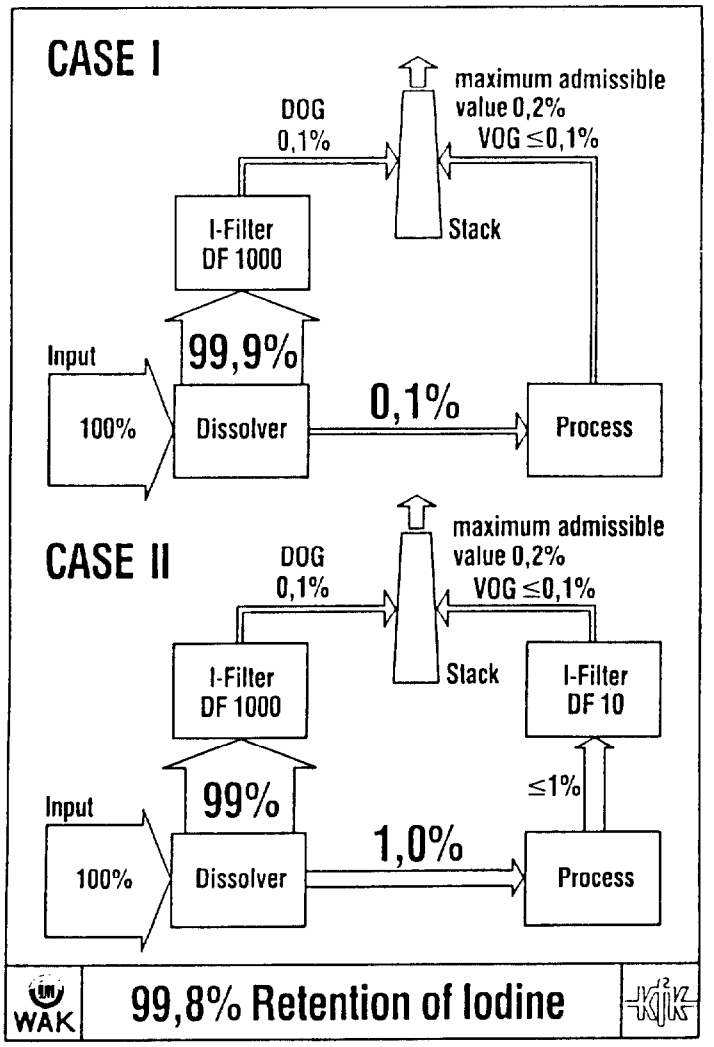

Figure 1

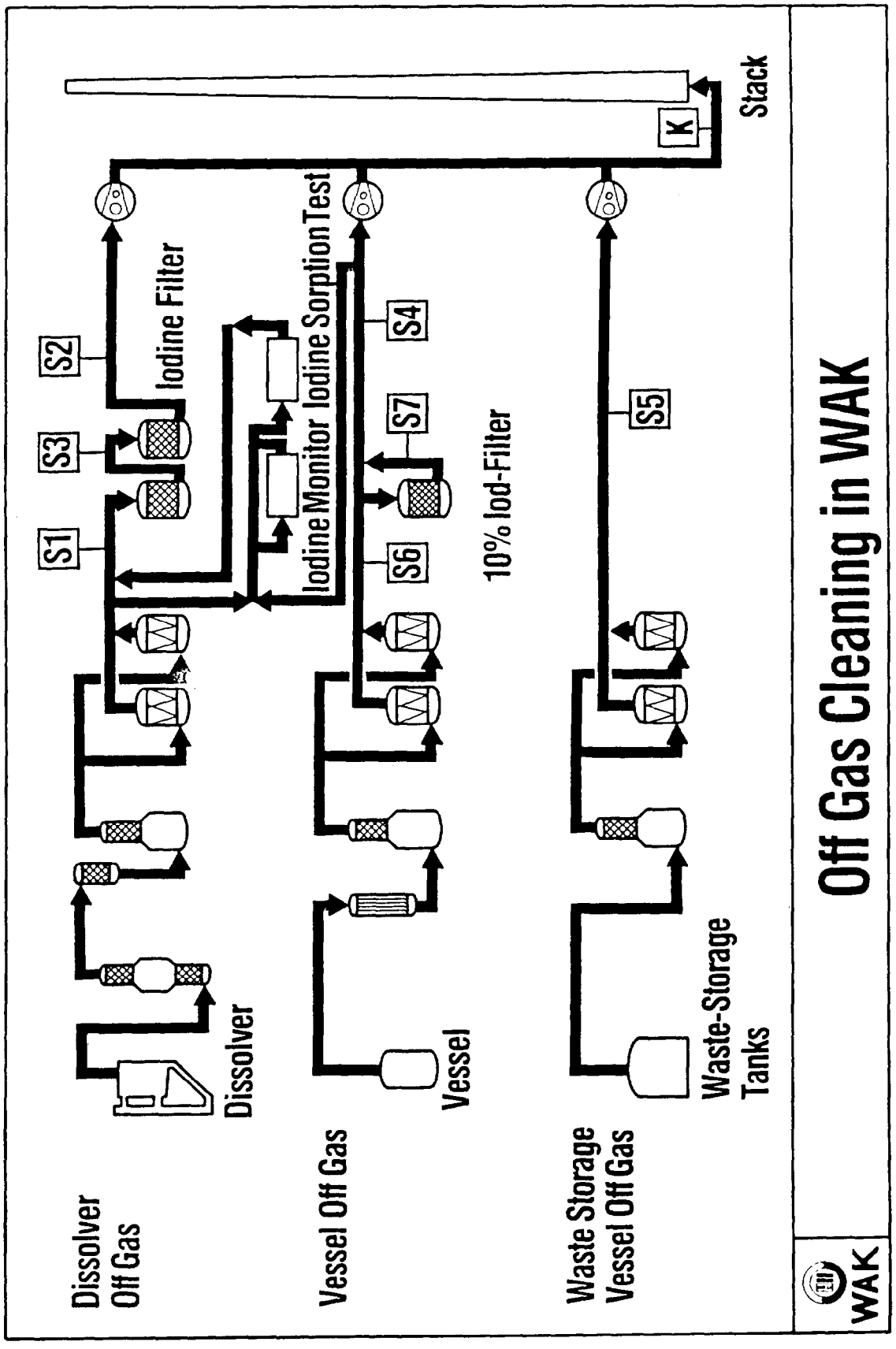
Off Gas Cleaning in WAK
WAK
Dissolver Off Gas
Dissolver
Vessel Off Gas
Vessel
Waste Storage Vessel Off Gas
Waste-Storage Tanks
S1
S2
S3
Iodine Filter
Iodine Monitor
Iodine Sorption Test
S4
S6
S7
10% Iod-Filter
S5
K
Stack

Figure 2

Test of Materials for Iodine Sorption in the Vessel Off Gas

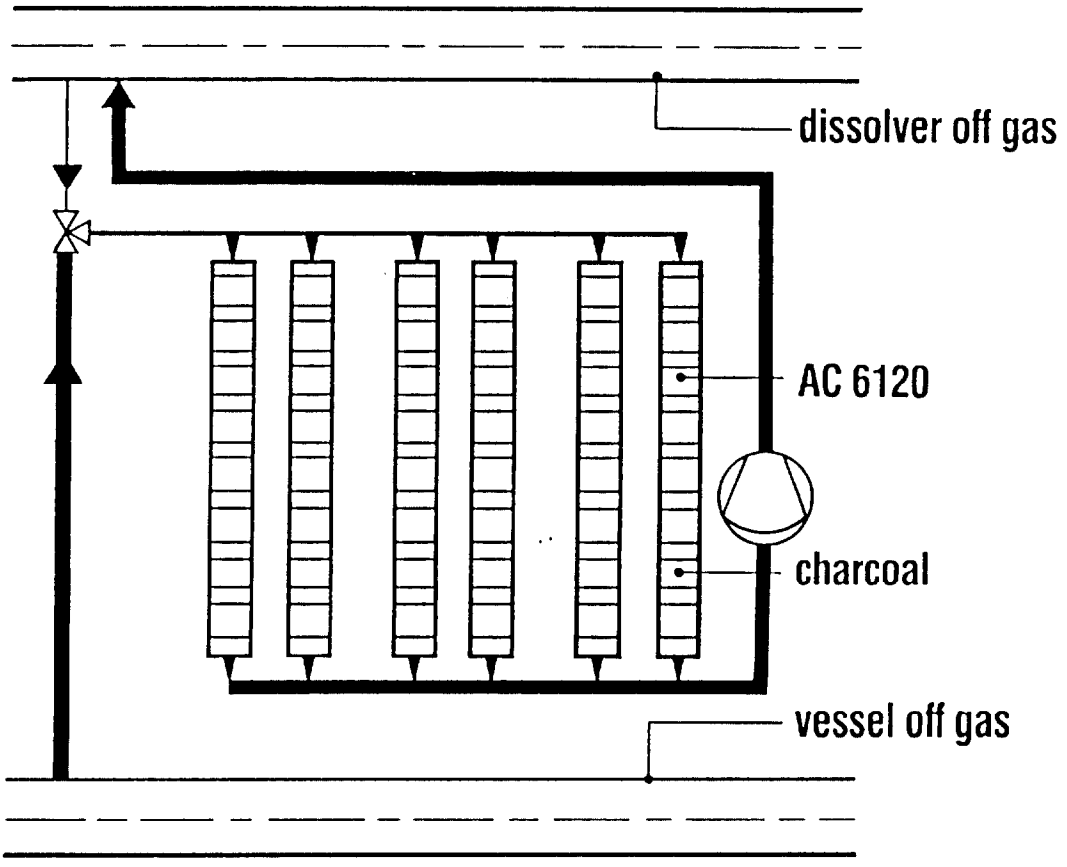

The long-term testing of sorption materials demonstrate the efficiency of iodine retention

WAK | Iodine Retention by Absorption | KfK

Figure 3

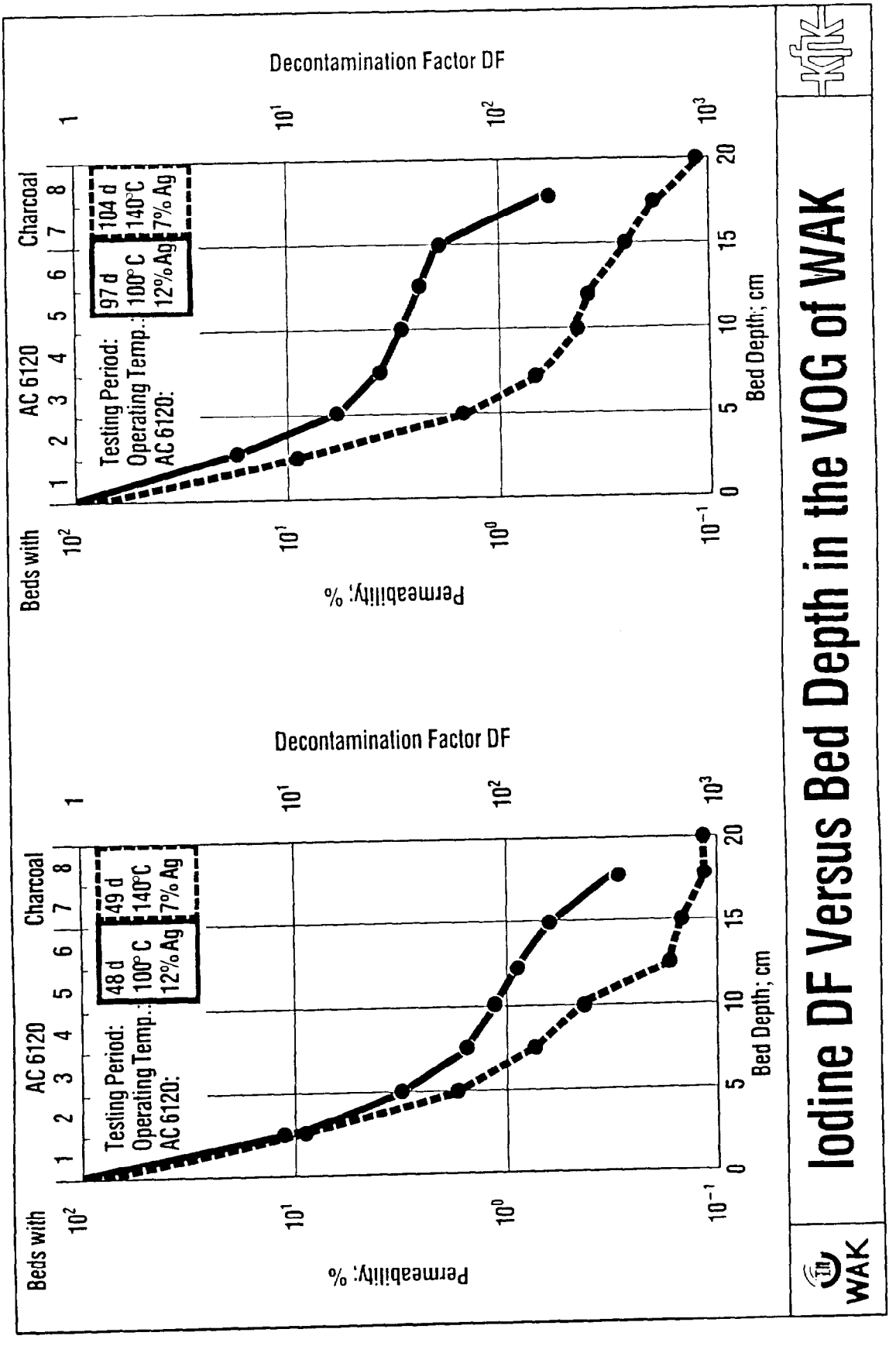
Iodine DF Versus Bed Depth in the VOG of WAK
WAK
KfK
Beds with AC 6120 Charcoal
Testing Period: 48 d 49 d
Operating Temp.: 100°C 140°C
AC 6120: 12% Ag 7% Ag
Permeability; %
Decontamination Factor DF
Bed Depth; cm
Beds with AC 6120 Charcoal
Testing Period: 97 d 104 d
Operating Temp.: 100°C 140°C
AC 6120: 12% Ag 7% Ag
Permeability; %
Decontamination Factor DF
Bed Depth; cm

Figure 4

DISCUSSION

KOVACH, J. L.: I have some difficulty with the linearity between your concentration and the decontamination factor (DF) curve that you are showing because, if it is really linear, your activity deposition curve in the column would look different then what it does.

HERRMANN: I agree with you as that is the scientific conclusion. We have plotted all the points we obtained in our dissolver offgas. We had the sampling points before the first iodine filter, behind the first iodine filter, and behind the second iodine filter. With all these points we have plotted this curve. We compare concentrations which go from 0.01 to 10^5 B_q per cubic meter.

KOVACH, J. L.: I do not believe that there is a linearity in the relationship between iodine concentration and DF, unless there is a species change. If other parameters than concentration change phase, indicate these also.

HERRMANN: I don't insist on linearity. In any case, there must be a relationship between iodine-DF and iodine-concentration at low iodine concentrations (without species change). This is clear and understandable by chemical thermodynamics and kinetics, because iodine filtering with silver-impregnated silica is a chemical reaction.

We have observed the influence of I-concentration on DF by sampling iodine at different sampling points in the dissolver offgas line in the WAK Reprocessing Plant. These results are not from laboratory tests but have been obtained during several years of plant operation.

KOVACH, J. L.: Maybe you are getting past the detectable limit and that is why it is seemingly linear.

HERRMANN: We have no difficulty measuring DF at low iodine concentrations: our sampling periods are long enough to collect an iodine amount which is clearly higher than the detection limit, even downstream.

WILHELM: I completely agree that when we always have the same compounds in the offgases we will not have a linear function between concentration and contamination factor. What really occurs is that the composition of the offgases changes in the course of filtering. When we have higher iodine concentrations, we have a larger amount of elemental iodine which is easier to trap; when we have extremely low concentrations, there are compounds which are more difficult to trap. When only one compound is present, no dependency can be observed of the removal efficiency on concentration for a large range of concentrations.

HERRMANN: Do you agree with me that at low concentrations it is difficult to obtain a high DF, or do you believe that a DF of 1000 is always attainable?

KOVACH, J. L.: I am not convinced that there is a linearity between concentration and DF.

HERRMANN: I do not insist on linearity. I would only point out the difficulty of having a high DF at very low concentrations.

KOVACH, J. L.: I think you may even have difficulty measuring high DFs at very low concentrations; it is just impossible to measure when you have very low concentrations.

HERRMANN: No. Its not impossible to measure if you make sure your measurement intervals are long enough, that is all.

KOVACH, J. L.: Not impossible, but very difficult with good statistical reliability. I think the explanation that Mr. Wilhelm gave is reasonable but I think that all these provisos should be put on your chart. A number of people have spent 10-15 years trying to convince people that there is no such thing as a concentration effect and I don't want to spent another 10-15 years convincing them again just because slides like yours are being shown to people.

HERRMANN: I repeat, I don't insist at all on a linear relationship between DF and iodine concentration. The lower limit of iodine adsorption as a chemical process is determined by chemical kinetics and thermodynamics. So it is understandable that DF goes down when iodine concentration is very low.

THOMAS, T.: Penetration of iodine in charcoal may be due to the behavior of iodated dodecane and not due to low levels of iodine.

HERRMANN: We have no significant penetration of iodine in the charcoal-beds. The charcoal beds give us the security that no significant iodine has penetrated through the AC6120 beds. We have not observed that iodated dodecane has different sorption behavior than other iodated paraffins.

COLLINSON: As you are probably aware, British Nuclear fuels operate a reprocessing plant at Windscale. The plant produces a large amount of contaminated odorless kerosene which they want to get rid of. They plan to do this in a burner plant and pass the exhaust gas through AC6120. My section has been asked to do some QA tests on AC6120. Do you know if burning kerosene can affect the performance of the absorbent material?

HERRMANN: That will depend on the concentrations of organic compounds in the burner offgas. Maybe an afterburner at high temperature can reduce concentrations of the organic compounds considerably and give a longer service life for iodine filters in the burner offgas. I believe there has been studies done by Nukem and Wilhelm in Germany on the problem of exhaust gas cleaning when burning dodecane. Can you comment?

WILHELM: We performed the first experiments with both kinds of lab scale burners and tried AC6120 behind the burner. It works when it is fresh, but it ages very quickly. At the moment we don't think this is the solution but we have to do something so we use it. The material ages quickly. For a technical solution, that is not acceptable. So, we have to change something, and I think we know what

we have to do.

THOMAS, T.: Is the water vapor content of the gas a problem?

WILHELM: No, because the temperature on the filters is, by far, too high. The relative humidity, not the absolute humidity, is always important for adsorption processes. There is really only one thing to say: one develops a certain material for a certain purpose but when you change all the parameters, you see that the material won't work well under the new conditions. This material was developed originally for the dissolver offgas and for defined conditions of temperature. We looked at what variations we could tolerate. Now, we have to use the material for vessel offgases in another concentration range with highly aging materials in the offgas and, of course, we get lower decontamination factors, as Mr. Herrmann said, around 100. We tested the material over six orders of magnitude. It just may be that the composition of the offgas and the iodine compounds are different because of the operating conditions in the plant. By the way, since we began to use the trap at 140°C for the vessel offgas, we have obtained only a few results with a decontamination factor below 100%. And we can explain the measured values lower than 99% by pump failure and wet sorbent. The dependency of the DF on iodine concentration, measured in WAK, may be the result of the relatively higher amount of organic iodine compounds in the offgas when the total I-concentration is low, because no dissolution of fuel is performed.